Weather Research Forecast Version 3.8
Meteorological Model Evaluation
Annual 2013 12-km CONUS

Prepared for:
US EPA

Prepared by:
UNC-Chapel Hill

September 23, 2016

UNC
INSTITUTE FOR
THE ENVIRONMENT

CONTENTS

TABLES

FIGURES

1.0 INTRODUCTION

The University of North Carolina (UNC) at Chapel Hill simulated annual meteorology for the 2013 calendar year to support emissions, photochemical, and dispersion modeling applications for this year. The simulated meteorological data will be used to support assessments of ozone, $PM_{2.5}$, visibility, and a variety of toxics.

The annual meteorology was simulated using the Weather Research and Forecasting model (WRF) at a 12-km horizontal resolution for the continental United States (CONUS). The WRF meteorological fields were processed using the Meteorology Chemistry Interface Process (MCIP) to generate Community Multiscale Air Quality (CMAQ)-ready input files. Additionally, the 2013 WRF meteorological fields were processed using the Mesoscale Model Interface Tool (MMIF) to generate input files for dispersion models. This report provides technical details about the WRF model configuration and the meteorological model performance evaluation for the 2013 calendar, which includes performance evaluation of 2-m temperature, 2-m mixing ratio, 10-m wind speed and direction, accumulated monthly precipitation, and surface radiation.

2.0 WRF MODEL CONFIGURATION

We used the Weather Research and Forecasting (WRF) model with the Advanced Research dynamic solver for this meteorological modeling study.[1] WRF is a next-generation mesoscale numerical weather prediction system designed to serve both operational forecasting and atmospheric research needs. WRF contains separate modules to compute different physical processes, such as surface energy budgets and soil interactions, turbulence, cloud microphysics, and atmospheric radiation. Within WRF, the user has many options for selecting the different schemes for each type of physical process. There is a WRF Preprocessing System (WPS) that generates the initial and boundary conditions used by WRF, based on topographic datasets, land use information, and larger-scale atmospheric and oceanic models. Below, we outline the model setup, model input, and options (e.g. parameterizations) that were used for the 2013 WRF simulations. The WRF options were selected based on numerical meteorological modeling research and the experience of scientists at the U.S. Environmental Protection Agency (USEPA), within the Office of Research and Development (ORD).[2,3,4]

A summary of the WRF input data preparation procedure used for this annual modeling exercise is provided below.

Model Selection: The publicly available version of WRF (version 3.8) was used for the 2013 meteorological simulation. This was the latest version of WRF available at the time the simulation was performed. WPS version 3.8 was also used to develop the model inputs.

Horizontal Domain Definition: The WRF 12-km configuration includes a 5-grid cell buffer in all directions to minimize any potential numeric noise along WRF domain boundaries, which can affect the air quality model meteorological inputs. Such numeric noise can occur near the boundaries of the WRF domain solution as the boundary conditions come into balance with the WRF numerical algorithms. The WRF horizontal domains are presented in Figure 2-1. The grid projection was Lambert Conformal with a pole of projection of 40 degrees north, -97 degrees east and standard parallels of 33 and 45 degrees.

Vertical Domain Definition: The WRF modeling was based on 36 vertical layers with a surface layer approximately 20 meters deep. The vertical domain is presented in both sigma and approximate height coordinates in Table 2-1.

Topographic Inputs: Topographic information for the WRF model was developed using the standard WRF terrain databases. The 12-km CONUS domain was based on the latest USGS GMTED2010 data.[5] This is 30-second (~900 m) data and replaces the old topography data (GTOPO30) available in prior WRF releases.

---

[1] Skamarock, W.C. and J.B. Klemp, 2008. A time-split nonhydrostatic atmospheric model for weather research and forecasting applications. *Journal of Computation Physics*, Volume 227, pp. 3465-3485.

[2] Pleim, J.E. and R.C. Gilliam, 2009. An indirect data assimilation scheme for deep soil temperature in the Pleim-Xiu land surface model. *Journal of Applied Meteorology and Climatology*, Volume 48, pp. 1362-1376.

[3] Gilliam, R.C. and J.E. Pleim, 2010. Performance assessment of the Pleim-Xiu LSM, Pleim surface-layer and ACM PBL physics in version 3.0 of WRF-ARW. *Journal of Applied Meteorology and Climatology,* Volume 49, pp. 760-774.

[4] Gilliam, R.C., J.M. Godowitch, and S.T. Rao, 2012. Improving the horizontal transport in the lower troposphere with four dimensional data assimilation. *Atmospheric Environment*, Volume 53, pp. 186-201.

[5] Global Multi-resolution Terrain Elevation Data 2010 (GMTED2010); https://lta.cr.usgs.gov/GMTED2010

Vegetation Type and Land Use Inputs: Vegetation type and land use information were based on the National Land Cover Database (NLCD) 2011.[6] This is a 9-second, ~250 m, dataset that includes fractional land use, which is advantageous for use with the land-surface model applied (Pleim-Xiu). NLCD 2011 dataset (40-class) is only available for the CONUS and areas of Canada and Mexico are defined using the 20-class MODIS scheme.

Atmospheric Data Inputs: The initial and lateral boundary conditions were taken from the 12-km (Grid #218) North American Model (NAM) archives available from the National Climatic Data Center (NCDC) National Operational Model Archive and Distribution System (NOMADS) server.[7] Both the 6-hour analysis and 3-hour NAM forecast were used.

Time Integration: Third-order Runge-Kutta integration was used.

Diffusion Options: Horizontal Smagorinsky first-order closure with sixth-order numerical diffusion and suppressed up-gradient diffusion was used.

Water Temperature Inputs: The water temperature data were taken from the Group for High Resolution Sea Surface Temperature (GHRSST).[8] The GHRSST product used has a horizontal resolution of 1 km.

Snow Inputs: Snow height and snow water equivalent within the CONUS were taken from the National Snow and Ice Data Center. Within the CONUS, the Snow Data Assimilation System (SNODAS)[9] data product was used to provide best available estimates of snow cover and snow water equivalent. The NAM fields were applied to provide snow estimates outside of the CONUS.

Data Assimilation: The objective analysis program (OBSGRID) was run to incorporate additional observational data from the Meteorological Assimilation Data Ingest System (MADIS)[10] observation archive, including the MADIS metar, sao, and maritime observations. These data are then incorporated into the NAM boundary conditions and used within the WRF data assimilation. Specifically, the WRF model was run with analysis nudging (i.e., Four Dimensional Data assimilation [FDDA]). For winds and temperature, an analysis nudging coefficient of $1\text{x}10^{-4}$ was applied to the 12-km domain. For mixing ratio, an analysis nudging coefficient of $1.0\text{x}10^{-5}$ was applied to the 12-km domain. Analysis nudging for winds, temperature, and mixing ratio were applied above the planetary boundary layer.

An indirect data assimilation scheme was applied with the Pleim-Xiu land surface model, which uses the surface fields from the OBSGRID program. The first indirect data assimilation is a technique in which soil moisture is nudged according to the biases in 2-m air temperature and relative humidity between the

---

[6] National Land Cover Database 2011, http://www.mrlc.gov/nlcd2011.php

[7] North American Model Analysis-Only, http://nomads.ncdc.noaa.gov/data.php ; download from ftp://nomads.ncdc.noaa.gov/NAM/analysis_only/

[8] Global High Resolution SST (GHRSST) analysis, https://www.ghrsst.org/ ; download from ftp://podaac-ftp.jpl.nasa.gov/allData/ghrsst/data/L4/GLOB/JPL/MUR/

[9] National Operational Hydrologic Remote Sensing Center. 2004. *Snow Data Assimilation System (SNODAS) Data Products at NSIDC*, [January 2013 – December 2013]. Boulder, Colorado USA: National Snow and Ice Data Center. http://dx.doi.org/10.7265/N5TB14TC

[10] Meteorological Assimilation Data Ingest System. http://madis.noaa.gov/.

model- and observation-based analyses. The second is a technique that nudges the deep soil temperature according to the model bias in 2-m air temperature.

Physics Options: The physics options chosen for this application are presented in Table 2-2.

Application Methodology: The WRF model was executed as a continuous simulation with a 60-second integration time step. A 10-day spin-up period was applied. WRF was initialized on December 21, 2013 at 00Z and run through January 1, 2015. Model results were output every 60 minutes and output files were split at 24-hour intervals beginning at 00Z.

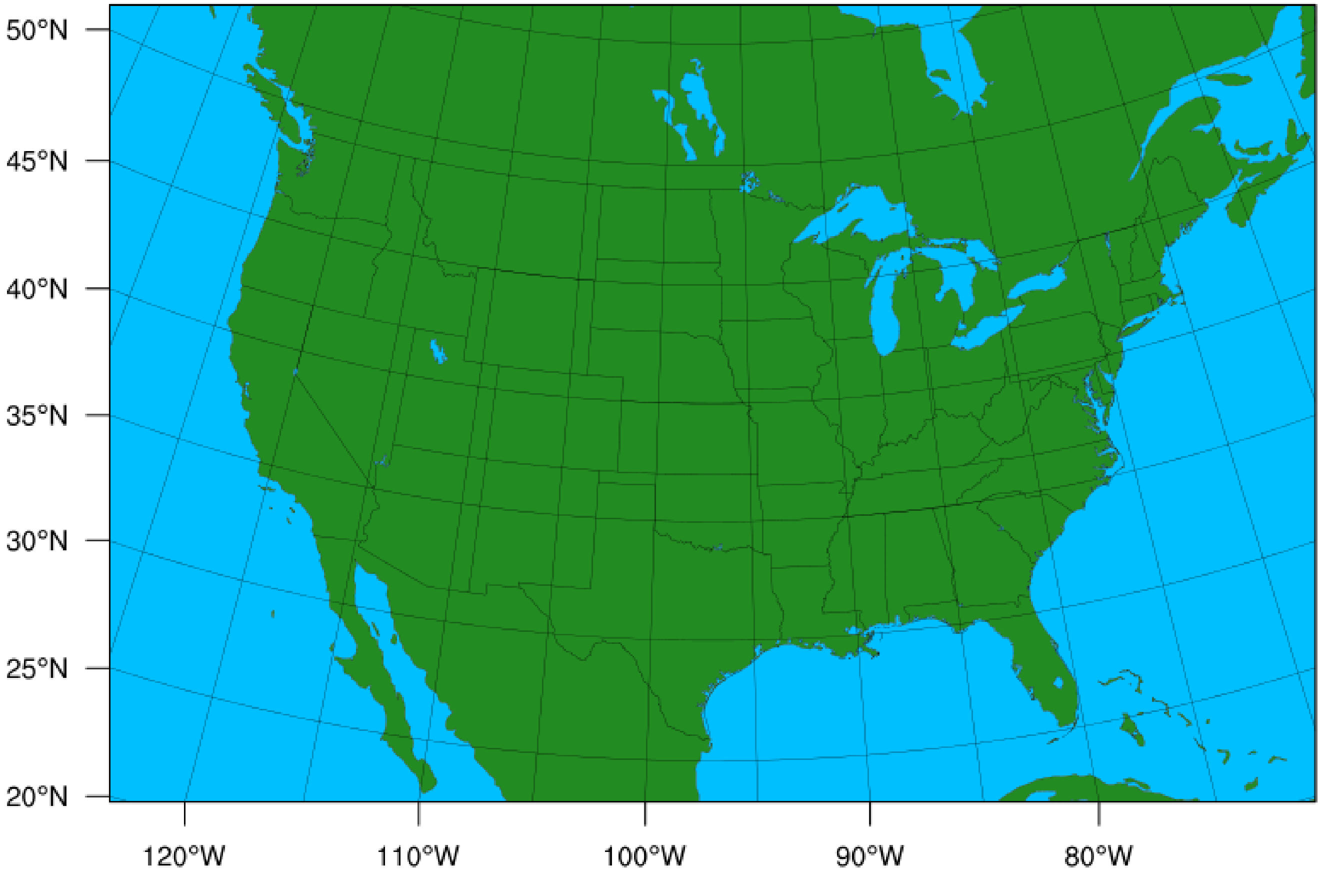

Figure 2-1. 12-km CONUS WRF modeling domain.

Table 2-1. Vertical layer definition for WRF simulations.

WRF Meteorological Model				
WRF Layer	Sigma	Pressure (mb)	Height (m)	Thickness (m)
36	0.0000	50.00	19313	3423
35	0.0500	98.15	15890	2243
34	0.1000	146.30	13648	1706
33	0.1500	194.45	11942	1392
32	0.2000	242.60	10551	1183
31	0.2500	290.75	9367	1034
30	0.3000	338.90	8333	921
29	0.3500	387.05	7412	832
28	0.4000	435.20	6580	761
27	0.4500	483.35	5820	702
26	0.5000	531.50	5117	652
25	0.5500	579.65	4465	610
24	0.6000	627.80	3856	573
23	0.6500	675.95	3283	541
22	0.7000	724.10	2742	412
21	0.7400	762.62	2330	298
20	0.7700	791.51	2032	289
19	0.8000	820.40	1742	188
18	0.8200	839.66	1554	185
17	0.8400	858.92	1369	182
16	0.8600	878.18	1188	178
15	0.8800	897.44	1010	175
14	0.9000	916.70	834	87
13	0.9100	926.33	748	86
12	0.9200	935.96	662	85
11	0.9300	945.59	577	84
10	0.9400	955.22	492	84
9	0.9500	964.85	409	83
8	0.9600	974.48	325	83
7	0.9700	984.11	243	82
6	0.9800	993.74	162	41
5	0.9850	998.56	121	40
4	0.9900	1003.37	80	40
3	0.9950	1008.19	40	20
2	0.9975	1010.59	20	20
1	1.0000	1013	0	

Table 2-2. Physics options used in the 12-km CONUS WRF Version 3.8 simulation of the 2013 calendar year.

WRF Treatment	Option Selected	Notes
Microphysics	Morrison 2-moment scheme[11]	6-class microphysics scheme that includes number concentrations for ice, snow, rain, and graupel.
Longwave Radiation	RRTMG[12]	Rapid Radiative Transfer Model (RRTM) for GCMs includes random cloud overlap and improved efficiency over RRTM.
Shortwave Radiation	RRTMG	Same as above, but for shortwave radiation.
Land Surface Model (LSM)	Pleim-Xiu[13]	Two-layer scheme with vegetation and sub-grid tiling.
Planetary Boundary Layer (PBL) scheme	ACM2[14]	Non-local upward mixing and local downward mixing.
Cumulus parameterization	Kain-Fritsch[15]	Deep and shallow convection sub-grid scheme using a mass flux approach with downdrafts and CAPE; moisture advection trigger applied.

---

[11] Morrison, H., G. Thompson, and V. Tatarskii, 2009. Impact of Cloud Microphysics on the Development of Trailing Statiform Precipitation in a Simulated Squall Line: Comparison of One- and Two-Moment Schemes. *Monthly Weather Review*, Volume 137, pp. 991-1007.

[12] Iacono, M.J., J.S. Delamere, E.J. Mlawer, M.W. Shepherd, S.A. Clough, and W.D. Collins, 2008. Radiative forcing by long-lived greenhouse gases: Calculations with AER radiative transfer models. *Journal of Geophysical Research*, Volume 113, D13103.

[13] Gilliam, R.C. and J.E. Pleim, 2010. Performance assessment of the Pleim-Xiu LSM, Pleim surface-layer and ACM PBL physics in version 3.0 of WRF-ARW. *Journal of Applied Meteorology and Climatology,* Volume 49, pp. 760-774.

[14] Pleim, Jonathan E., 2007. A Combined Local and Nonlocal Closure Model for the Atmospheric Boundary Layer. Part I: Model Description and Testing. *Journal* of *Applied Meteorology and Climatology*, Volume 46**,** pp. 1383–1395.

[15] Ma, Lei–Ming, and Zhe–Min Tan, 2009. Improving the behavior of the cumulus parameterization for tropical cyclone prediction: Convection trigger. *Atmospheric Research*, Volume 92**,** pp. 190–211.

3.0 MODEL PERFORMANCE EVALUATION APPROACH

The model evaluation approach was based on a combination of qualitative and quantitative analyses. The quantitative analysis was divided into monthly summaries of 2-m temperature, 2-m mixing ratio, and 10-m wind speed for each month to help generalize the model bias and error. The observed database for winds, temperature, and water mixing ratio used in this analysis was the National Oceanic and Atmospheric Administration (NOAA) Earth System Research Laboratory (ESRL) Meteorological Assimilation Data Ingest System (MADIS). The locations of the MADIS monitoring sites within the 12-km CONUS are shown in Figure 3-1.

The quantitative model performance evaluation of WRF using surface meteorological measurements was performed using the publicly available AMET evaluation tool.[16] AMET calculates statistical performance metrics for bias, error and correlation for surface winds, temperature and mixing ratio and can produce time series of predicted and observed meteorological variables and performance statistics. This evaluation only summarizes the meteorological model performance using bias and error model performance statistics metrics with select plots to enhance potential users' understanding of model performance. However, we provide an online source so data users can independently judge the adequacy of the model simulation. Overall, comparisons are offered herein to judge the model efficacy for 2013, but this review does not necessarily cover all potential user needs and applications.

In this report, we evaluated the model near surface temperature, mixing ratio (humidity), wind speed, and wind direction bias and error. The equations for bias and error are given below.

$$\text{Bias} = \frac{1}{N}\sum_{i=1}^{N}\left(P_i - O_i\right)$$

$$\text{Error} = \frac{1}{N}\sum_{i=1}^{N}\left|P_i - O_i\right|$$

For the wind direction difference statistics, a difference called wind displacement was applied. Wind displacement is the difference in the U and V vectors of the modeled and observed winds. The displacement is calculated as:

$$\textbf{Wind Displacment} = \textbf{abs}\left(\left(U_m - U_o + V_m - V_o\right) \text{ X } (1\text{km}/1000\text{m}) \text{ X } (3600\text{s/hr}) \text{ X } 1\text{hr}\right)$$

Where U_m and V_m are the U and V components respectively of the modeled wind vector and U_o and V_o are the U and V components of the observed wind vector.

We also evaluated the WRF spatial field of accumulated monthly precipitation against the observed monthly precipitation estimates from the Parameter-elevation Relationships on Independent Slopes Model (PRISM) interpolation procedure. The PRISM interpolation uses approximately 13,000 precipitation measurement sites across the CONUS and interpolates them to a < 1 km grid using

---

[16] AMET evaluation tool; https://www.cmascenter.org/help/documentation.cfm?MODEL=amet&VERSION=1.1&temp_id=99999

regression weights based primarily on the physiographic similarity of stations to the grid cell.[17] Factors considered are location, elevation, coastal proximity, topographic facet orientation, vertical atmospheric layer, topographic position, and orographic effectiveness of the terrain. The PRISM interpolation approach represents a significant improvement over other techniques used to spatially interpolate observed precipitation that failed to account for factors that influence precipitation away from the observations, such as orographic effects. However, it is still an interpolation technique that may not always capture all effects on precipitation and is just limited to precipitation within the CONUS. The PRISM interpolation procedure will be particularly challenged during summer convective precipitation events (thunderstorms) that can be very spotty and isolated. Such events can occur between the rainfall monitoring sites, and so would not be present in the observations, and hence, the PRISM analysis fields. In our comparison, we regrid PRISM precipitation estimates to take a difference between WRF and PRISM for each month to help illuminate the WRF precipitation errors.

Lastly, model evaluation includes comparison with shortwave downward radiation measurements. Shortwave downward radiation measurements are taken at Surface Radiation Budget Network (SURFRAD)[18] and Integrated Surface Irradiance Study (ISIS)[19] monitor locations. The SURFRAD network consists of seven sites and the ISIS network consists of nine sites across the United States. Both networks are operated by NOAA, with SURFRAD sites existing as a subset of ISIS monitors that provide higher-level radiation information not used in this evaluation.

---

[17] Daley, C., M. Halbleib, J. Smith, W. Gipson, M. Doggett, G. Taylor, J. Curtis and P. Pasteris, 2008. Physiographically sensitive mapping of the climatological temperature and precipitation across the conterminous United States. *International. Journal of Climatology*, Volume 28, pp 2031-2064.

[18] http://www.srrb.noaa.gov/surfrad

[19] http://www.esrl.noaa.gov/gmd/grad/isis/index.html

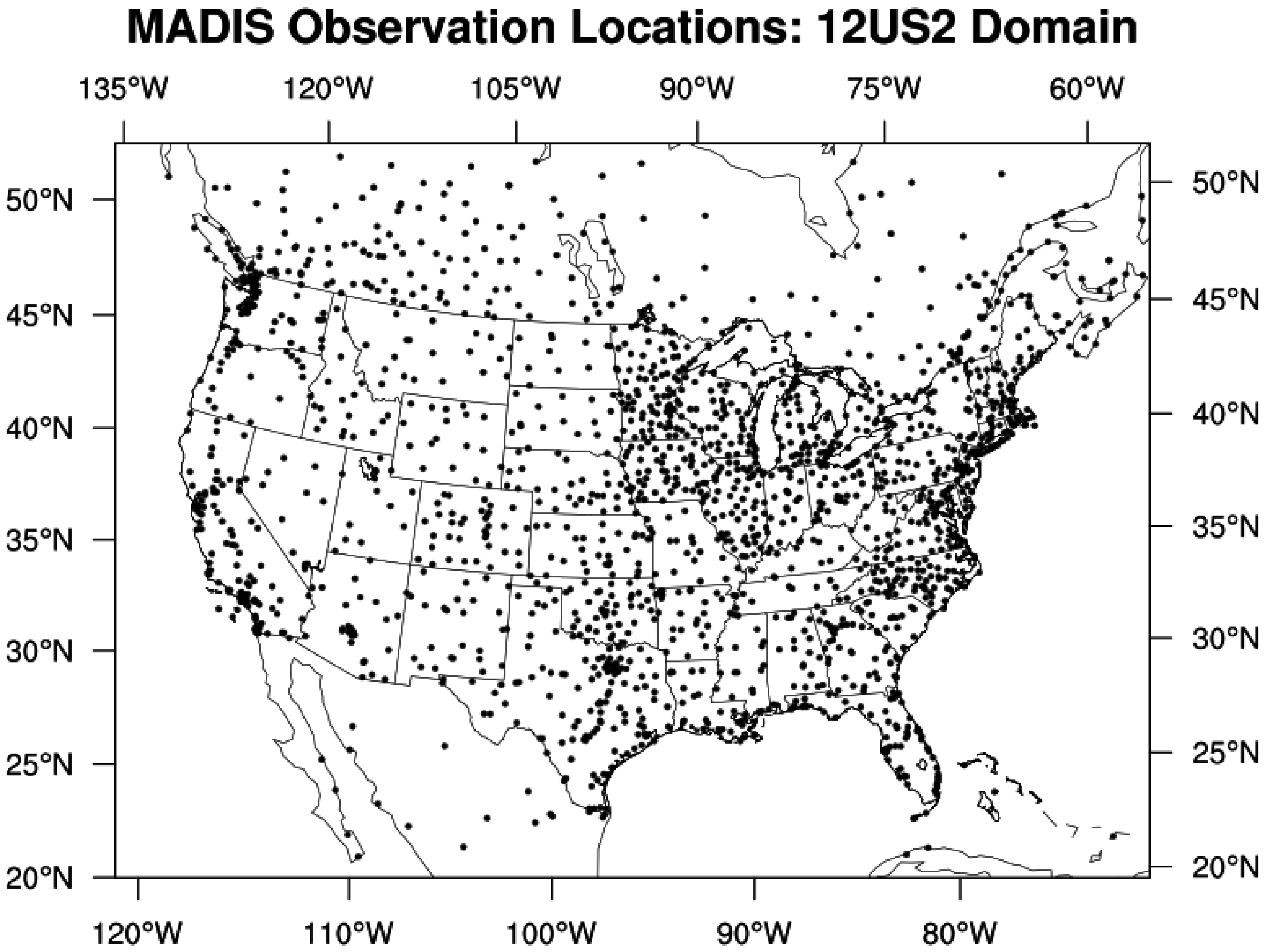

Figure 3-1. Locations of MADIS surface meteorological modeling sites with the WRF 12-km CONUS modeling domain.

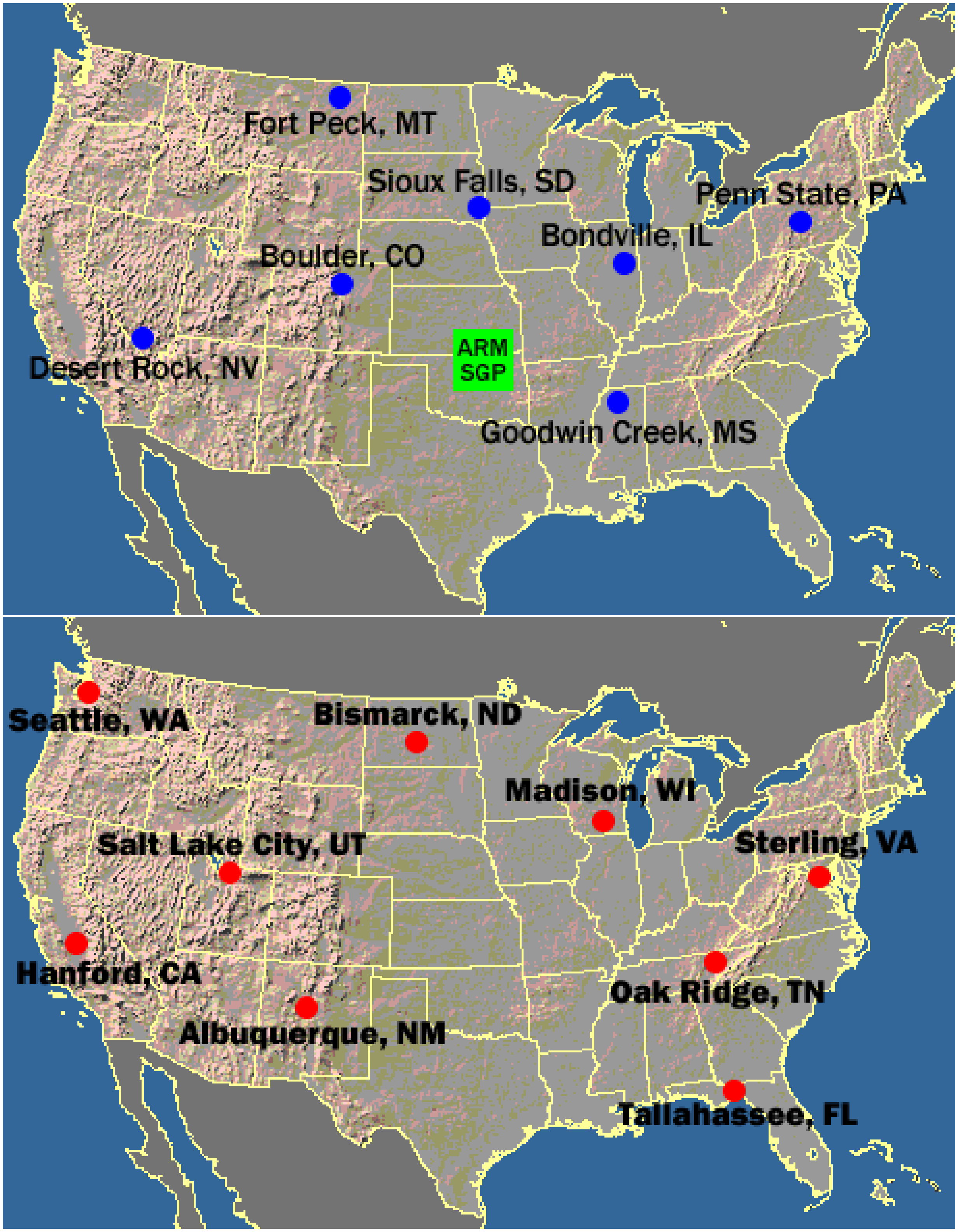

Figure 3-2. Location of SURFRAD (top) and ISIS (bottom) radiation monitors.

4.0 WRF MODEL PERFORMANCE EVALATUION RESULTS

Model Evaluation Results for 2-m Temperature

The temperature bias and error on average for the CONUS are shown in Figure 4-1. On average, there is a warm bias during the summer and fall months and a cool bias during the winter and spring months. The bias is smaller than ±1K for all months. The temperature errors for all months are between 1K and 2K and smallest during the summer.

Figure 4-2 shows the diurnal temperature statistics for January and July. The diurnal plot illustrates a cool bias in January (winter) overnight into the early morning. The bias becomes near zero in January by late afternoon and evening. The opposite is true for July (summer), with a general warm bias throughout the day. The warm bias and error for July (summer) is largest during the early morning and then again during the late afternoon/evening hours.

Figure 4-3 illustrates a cool bias 0.5°C to 1.0°C during the winter months (January and February) for many locations throughout the eastern half of the CONUS (Great Plains and eastward). However, some portions of the western CONUS (Rocky Mountains and westward) have a warm bias, especially along the Pacific West Coast. Similar spatial patterns in the bias continue into the early spring and the bias improves for many locations within the eastern half of the CONUS by late spring, as shown in Figure 4-4. During the summer, there is a transition to a warm bias in the northern half of the CONUS (Midwest towards the Northeast; however, a cool bias persists for many locations within the Southeast, especially along the Gulf Coast; seen in Figure 4-5 and Figure 4-6. The western half of the CONUS reveals a complex bias pattern during the summer, especially in the intermountain West and likely a result of the model's ability to resolve the complex terrain. An exception during the summer months is a persistent warm bias for coastal stations along the Pacific Northwest. By October, November and into December – Figure 4-7 and Figure 4-8 – the warm bias for the eastern half of the CONUS reverses back to a cool bias for many locations.

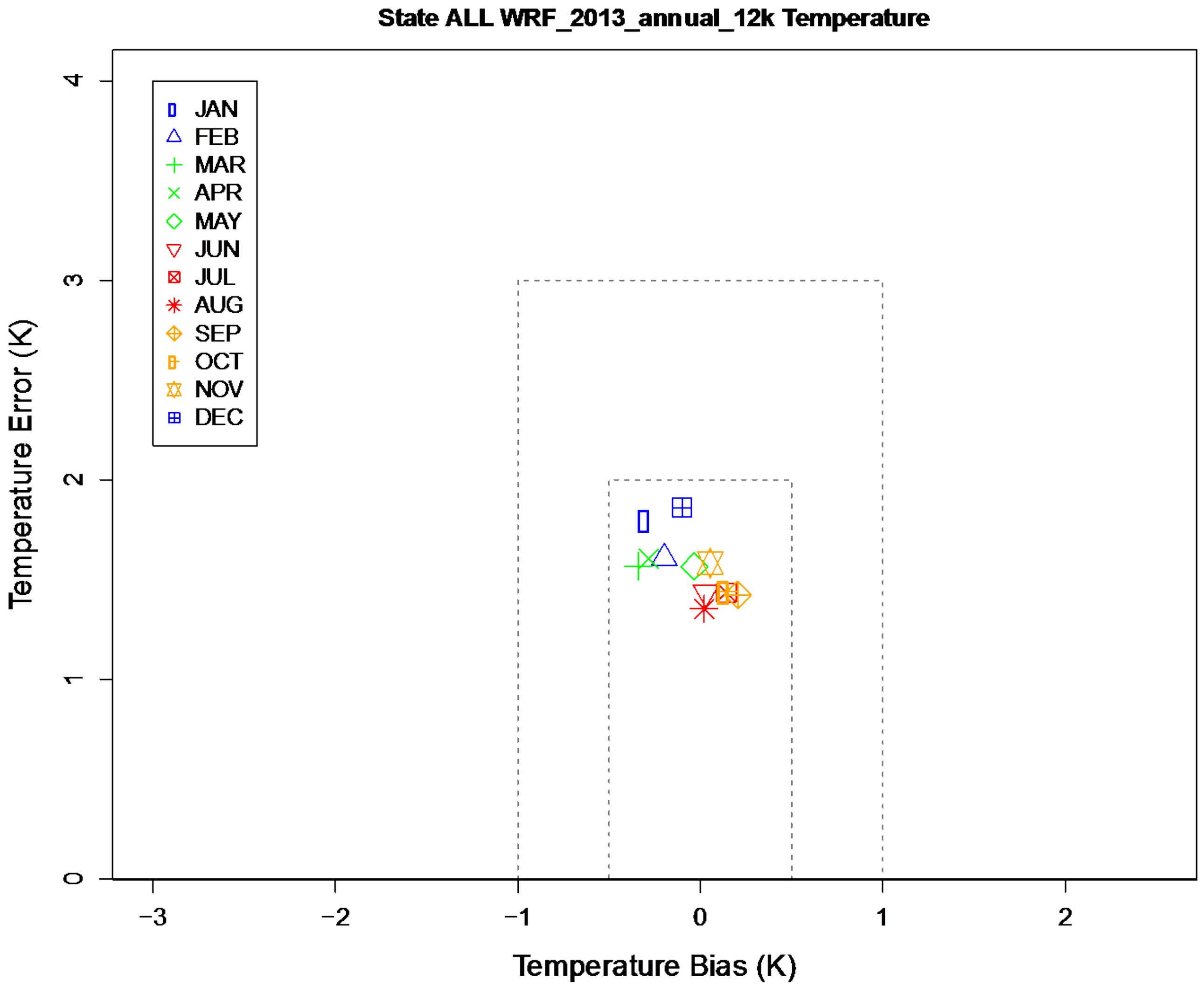

Figure 4-1. Soccer plot of monthly 2-m temperature error and bias averaged over the 12-km CONUS domain for the 2013 calendar year.

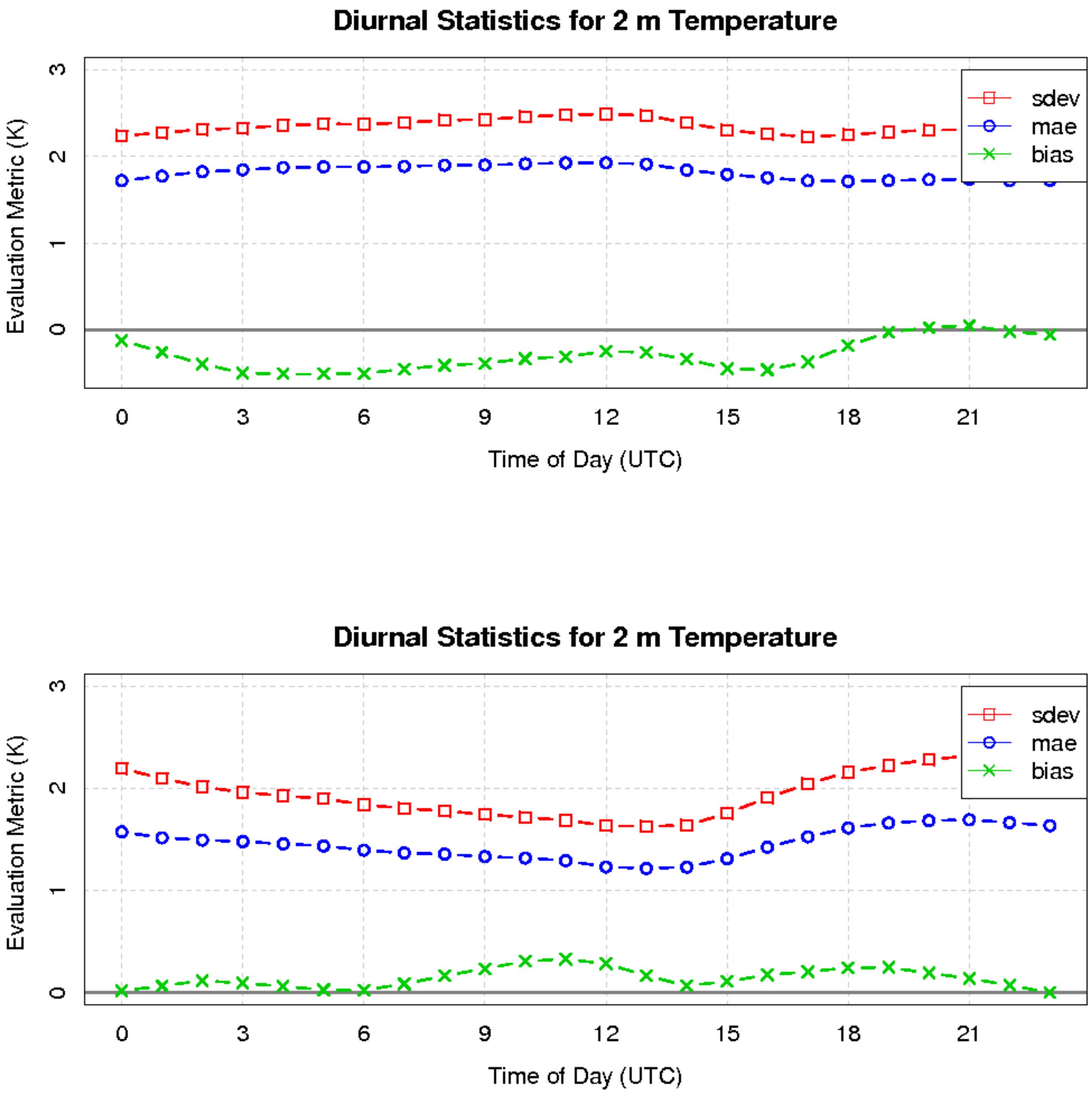

Figure 4-2. Diurnal 2-m temperature error and bias (°C) averaged over the 12-km CONUS domain for January (top) and July (bottom) 2013.

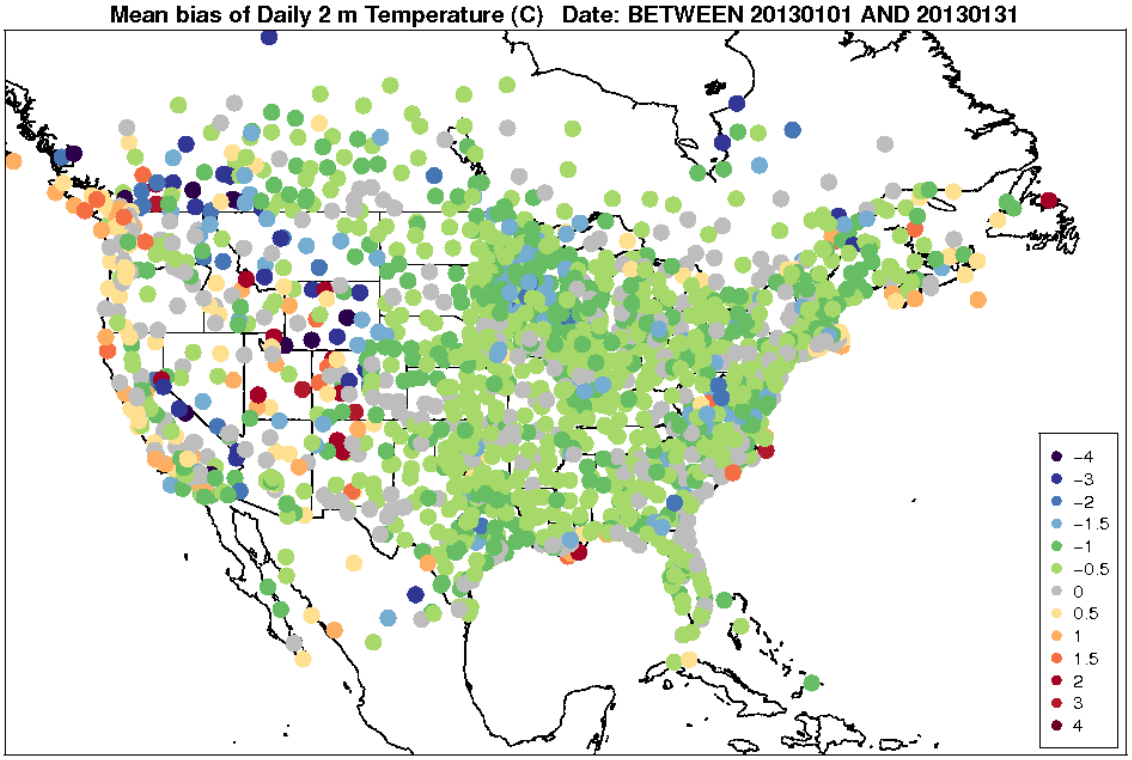

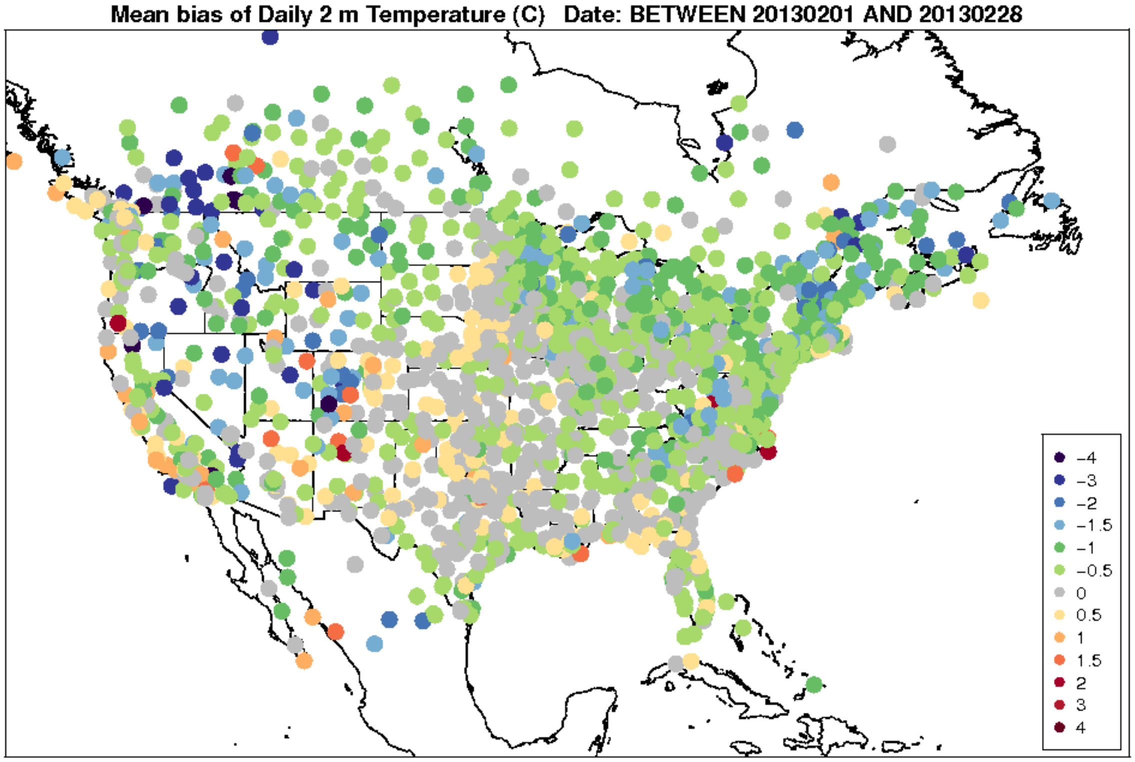

Figure 4-3. Spatial distribution of 2-m temperature bias (°C) within the 12-km CONUS domain for January (top) and February (bottom).

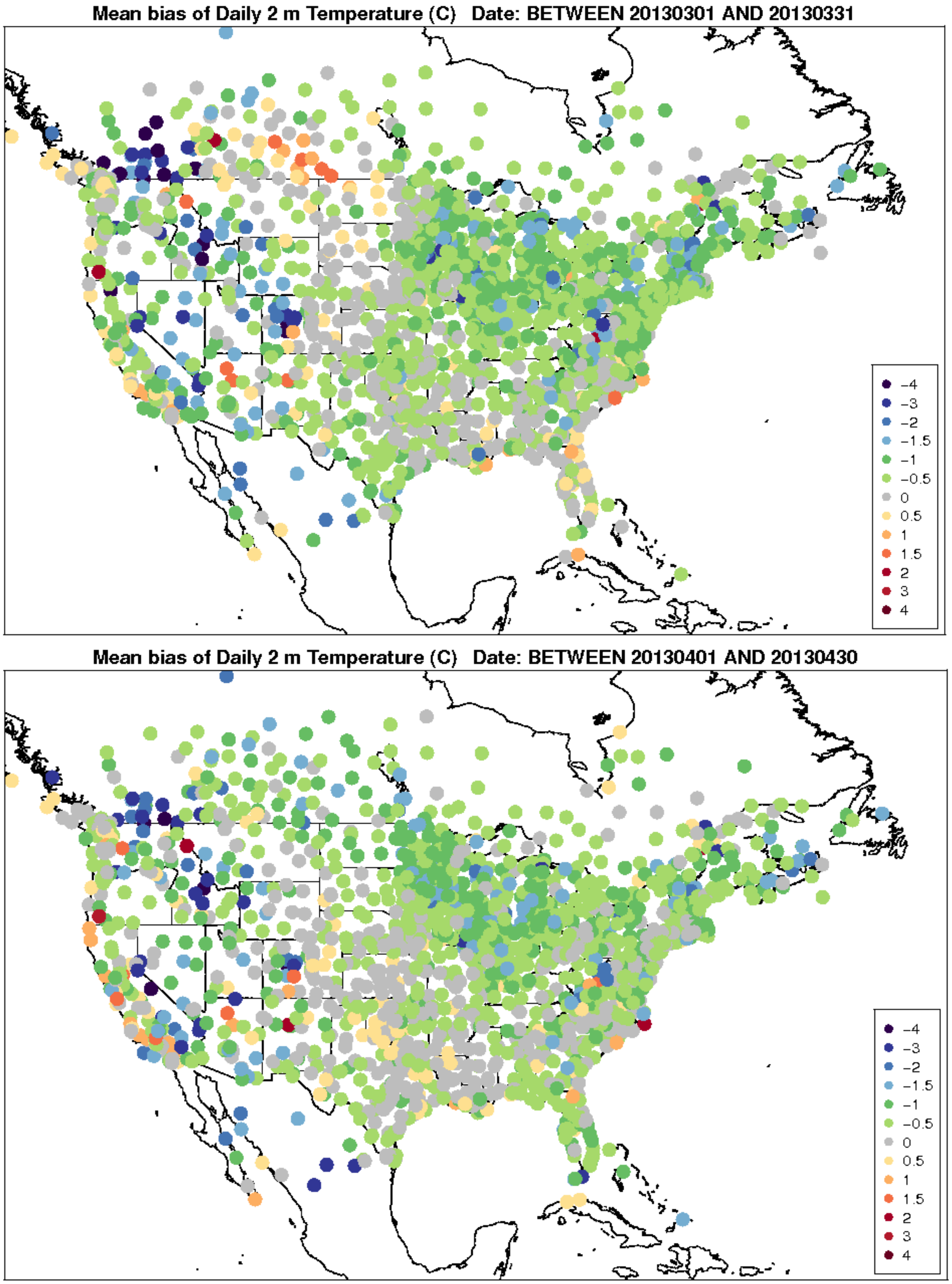

Figure 4-4. Spatial distribution of 2-m temperature bias (°C) within the 12-km CONUS domain for March (top) and April (bottom).

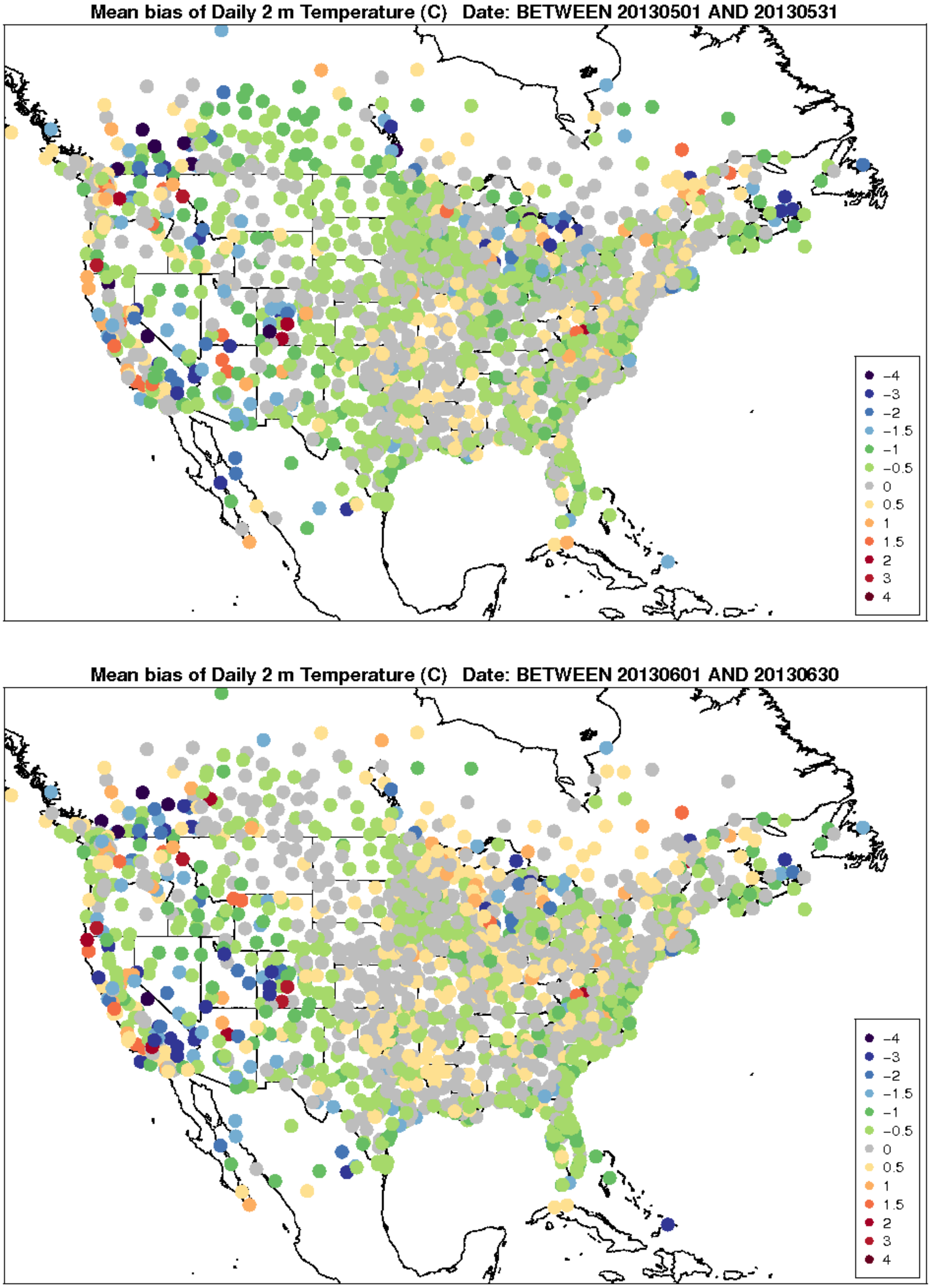

Figure 4-5. Spatial distribution of 2-m temperature bias (°C) within the 12-km CONUS domain for May (top) and June (bottom).

Mean bias of Daily 2 m Temperature (C) Date: BETWEEN 20130701 AND 20130731

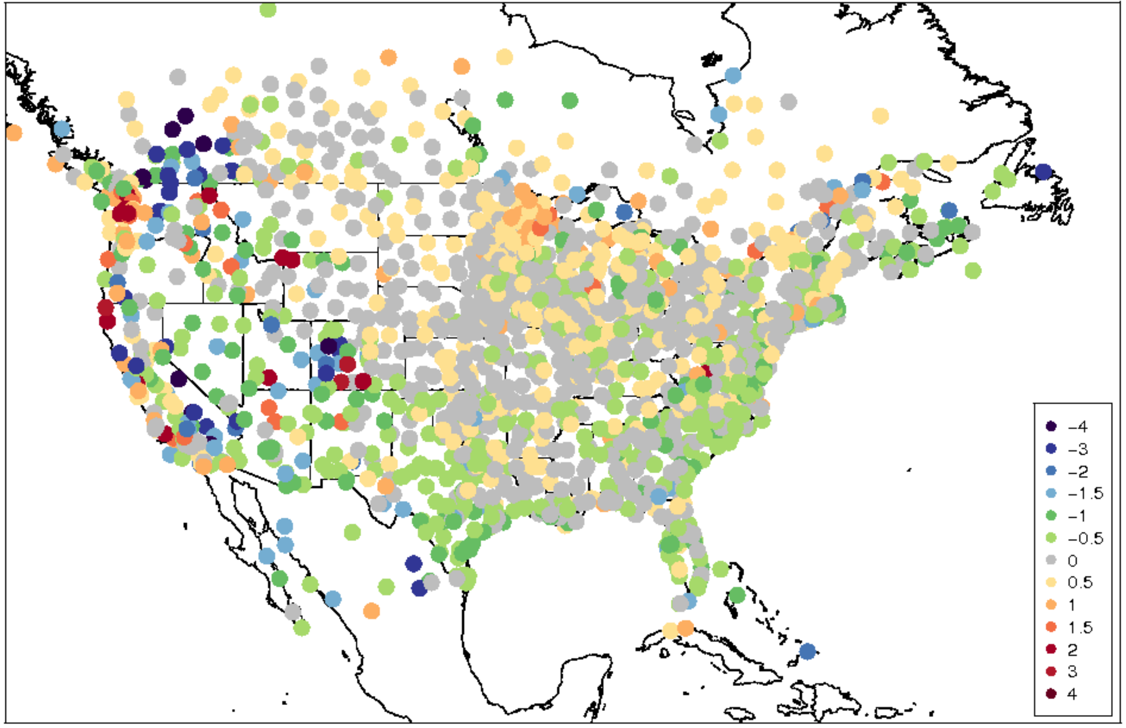

Mean bias of Daily 2 m Temperature (C) Date: BETWEEN 20130801 AND 20130831

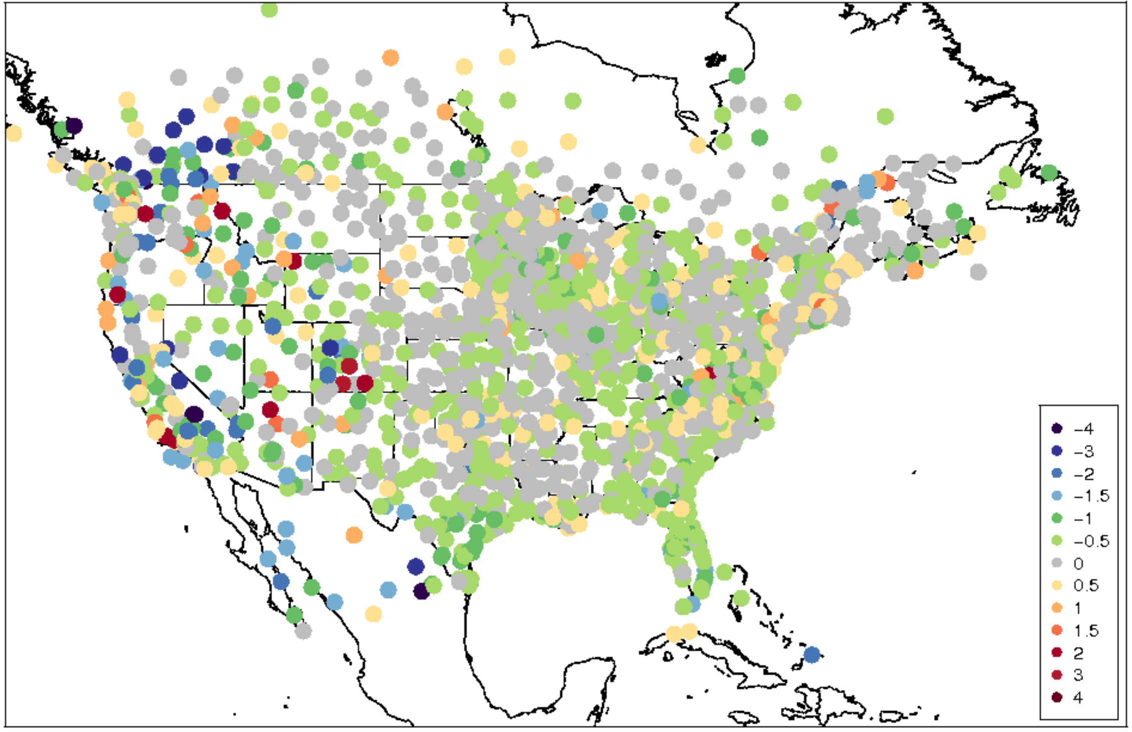

Figure 4-6. Spatial distribution of 2-m temperature bias (°C) within the 12-km CONUS domain for July (top) and August (bottom).

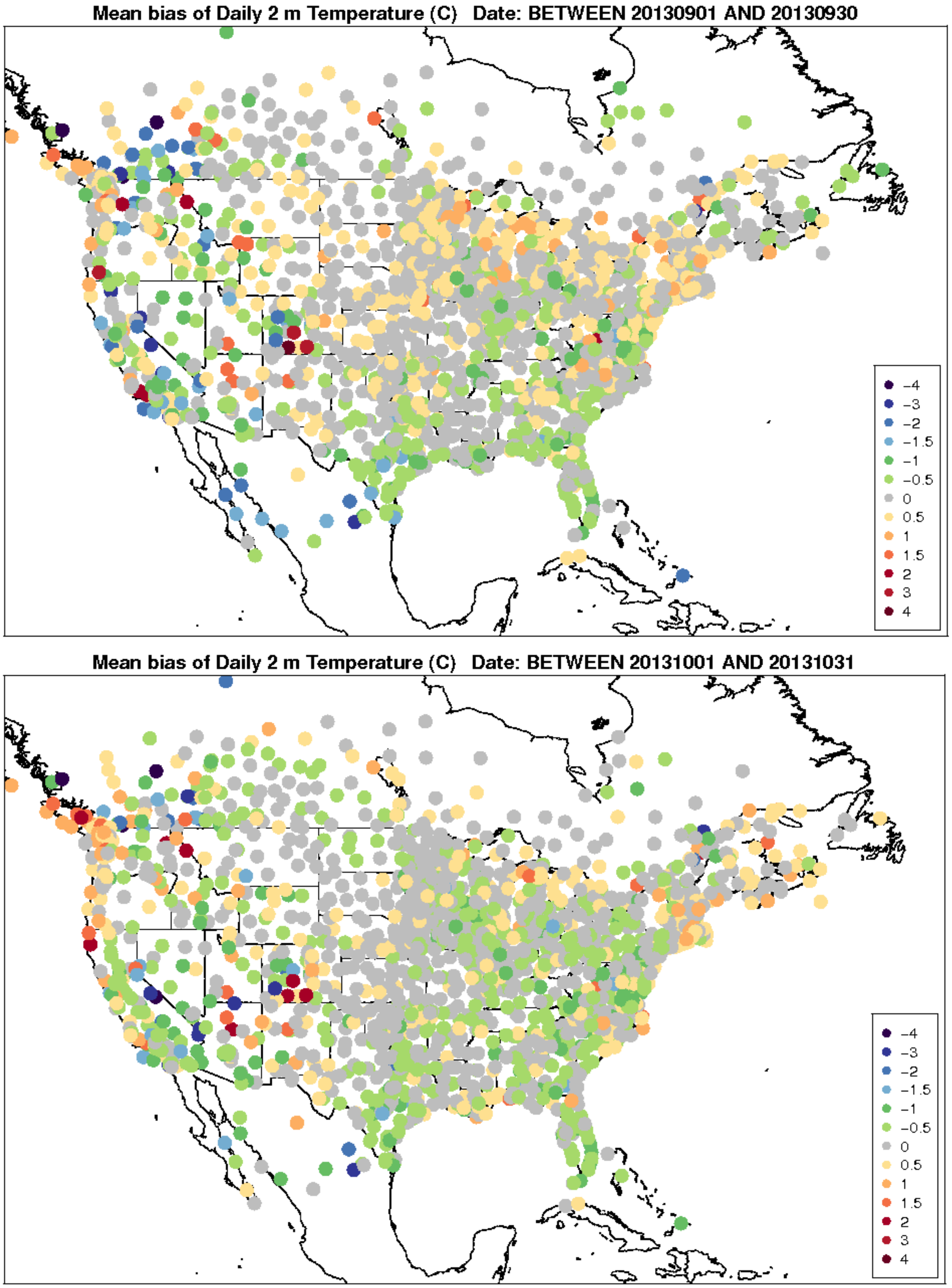

Figure 4-7. Spatial distribution of 2-m temperature bias (°C) within the 12-km CONUS domain for September (top) and October (bottom).

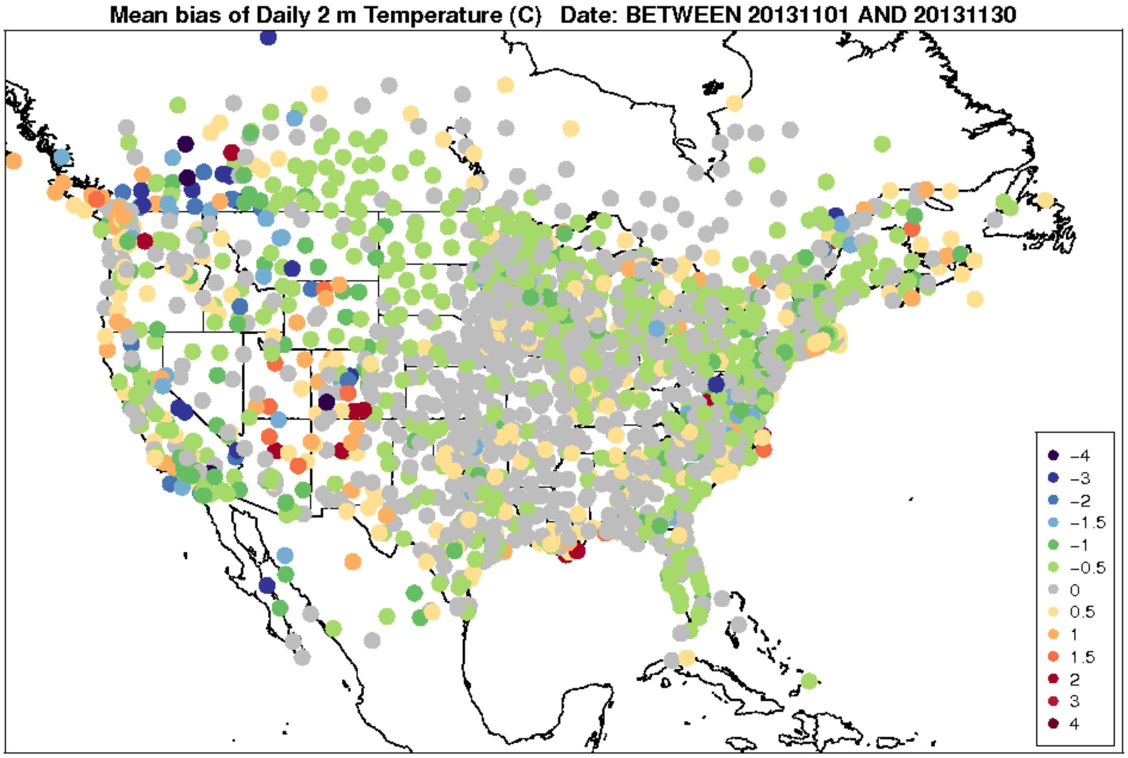

Mean bias of Daily 2 m Temperature (C) Date: BETWEEN 20131101 AND 20131130

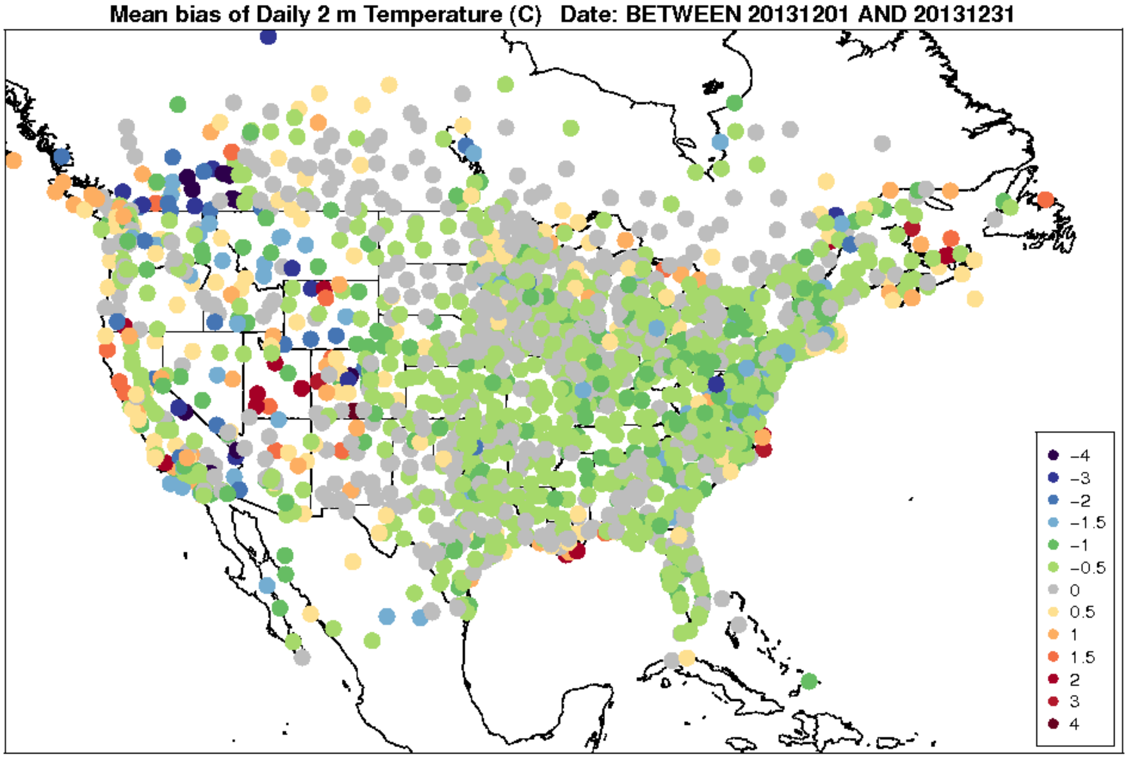

Mean bias of Daily 2 m Temperature (C) Date: BETWEEN 20131201 AND 20131231

Figure 4-8. Spatial distribution of 2-m temperature bias (°C) within the 12-km CONUS domain for November (top) and December (bottom).

Model Evaluation Results for 2-m Mixing Ratio

In general, there is a positive bias for the mixing ratio for the CONUS in 2013, Figure 4-9. The mixing ratio error is largest during the summer months (June, July, August) and smallest during the winter when the moisture capacity of the atmosphere is reduced. Overall, the mixing ratio bias is smaller than ±0.5 g/kg and errors are less than 1.0 g/kg outside of the warmest months from June - September.

The diurnal statistics of the mixing ratio illustrate some similarities in the behavior of the mixing ratio bias between January (winter) and July (summer), seen in Figure 4-10. During both months, the mixing ratio bias remains positive for almost the entire day. The bias for both months is smallest during the early afternoon hours but quickly grows and is largest by the late evening and early overnight hours. We note that the exact times of the shifts are not exact and may be related to the length of daylight hours between the two months.

During winter, there is a negative bias of ~1 g/kg in January within the Plains and Midwest for many stations that improves slightly during February, see Figure 4-11. There is also a persistent negative bias for many locations along the Pacific coast. On the other hand, the mixing ratio bias is positive within the Southeast during January that increases for February. During the spring, Figure 4-12, much of the eastern half of the CONUS has a persistent positive mixing ratio bias. The sign of the bias quickly becomes negative for stations within the Great Plains during the spring. There is also a persistent negative mixing ratio bias for stations within California during the spring. During the summer, a larger positive bias (~ 1.5 g/kg) is found for many stations within the eastern half of the CONUS, see Figure 4-13 and Figure 4-14. In particular, during the summer, the Southwest emerges as an area with a large positive bias that peaks in July, exceeding 2 g/kg. By October, the mixing ratio bias returns to a negative values for much of the CONUS, Figure 4-15. An exception is for coastal stations along the Gulf and Southeast coasts and southern coastal California. By December, the mixing ratio bias returns to positive values for coastal Mid-Atlantic while improving (bias smaller than ±0.5 g/kg) for locations within the Plains and Midwest, Figure 4-16.

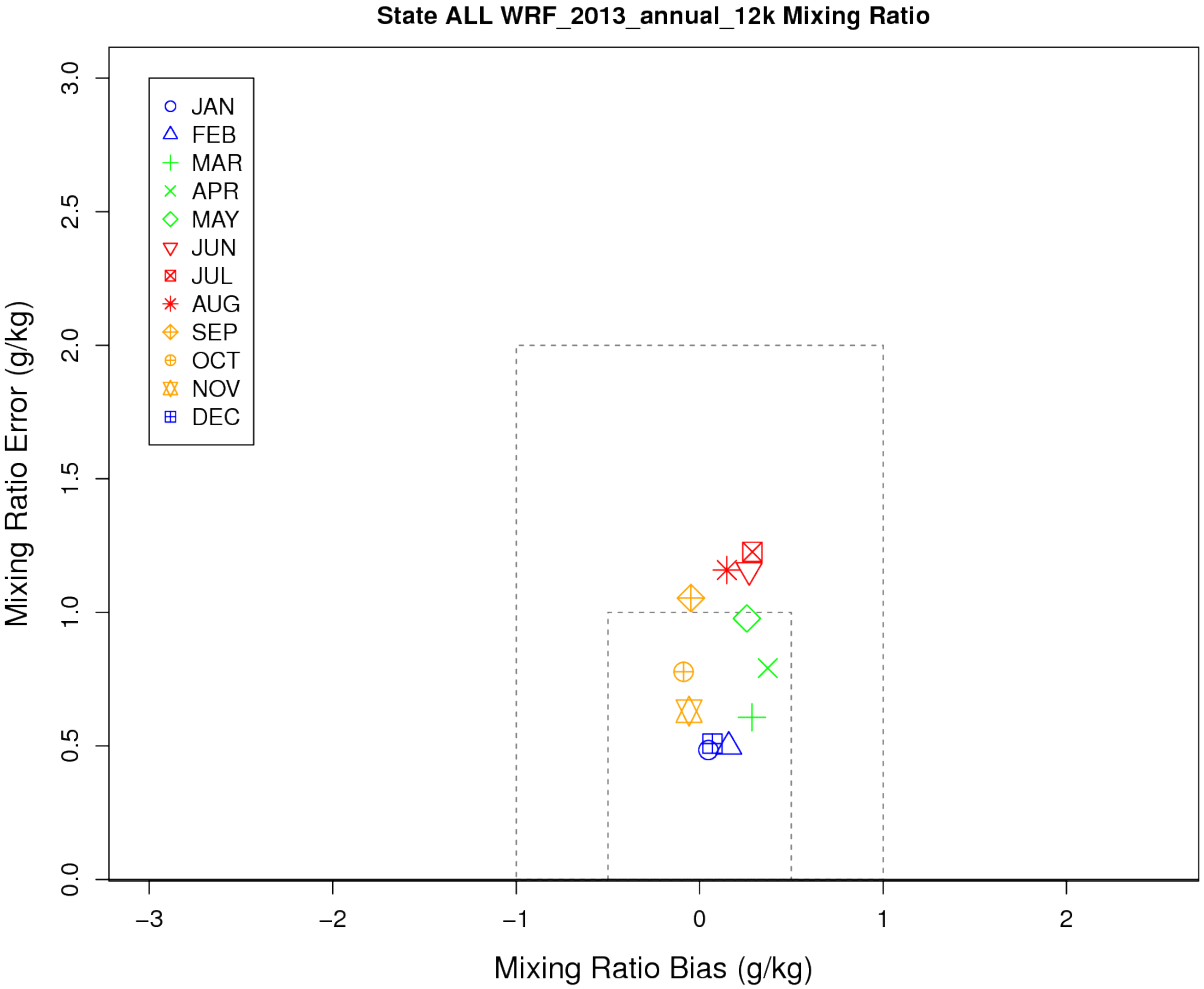

Figure 4-9. Soccer plot of monthly 2-m mixing ratio error and bias (g/kg) averaged over the 12-km CONUS domain for the 2013 calendar year.

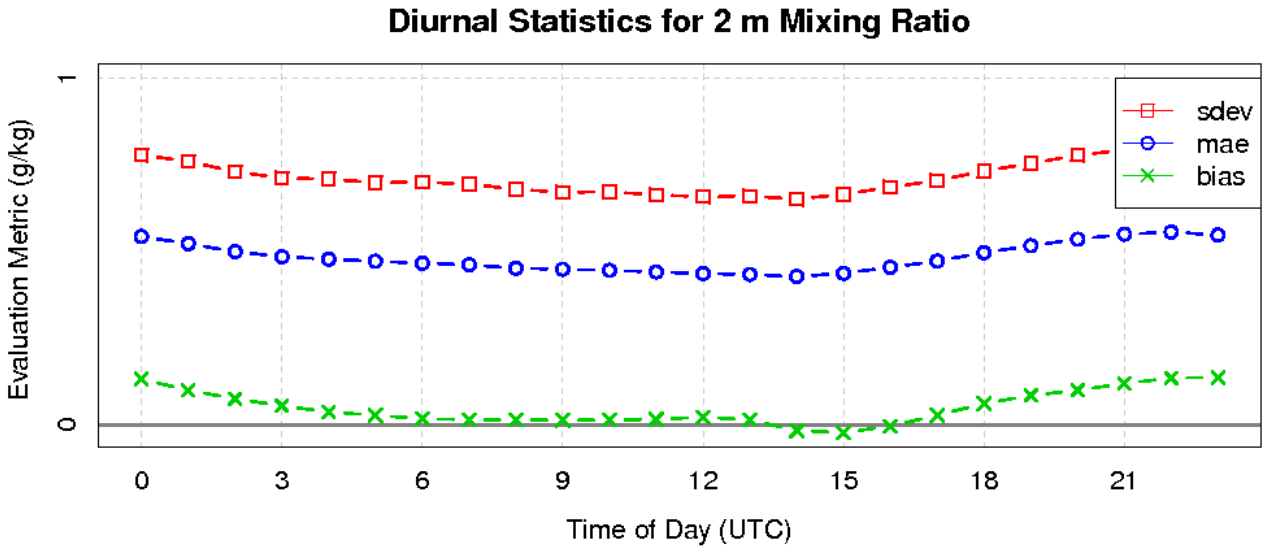

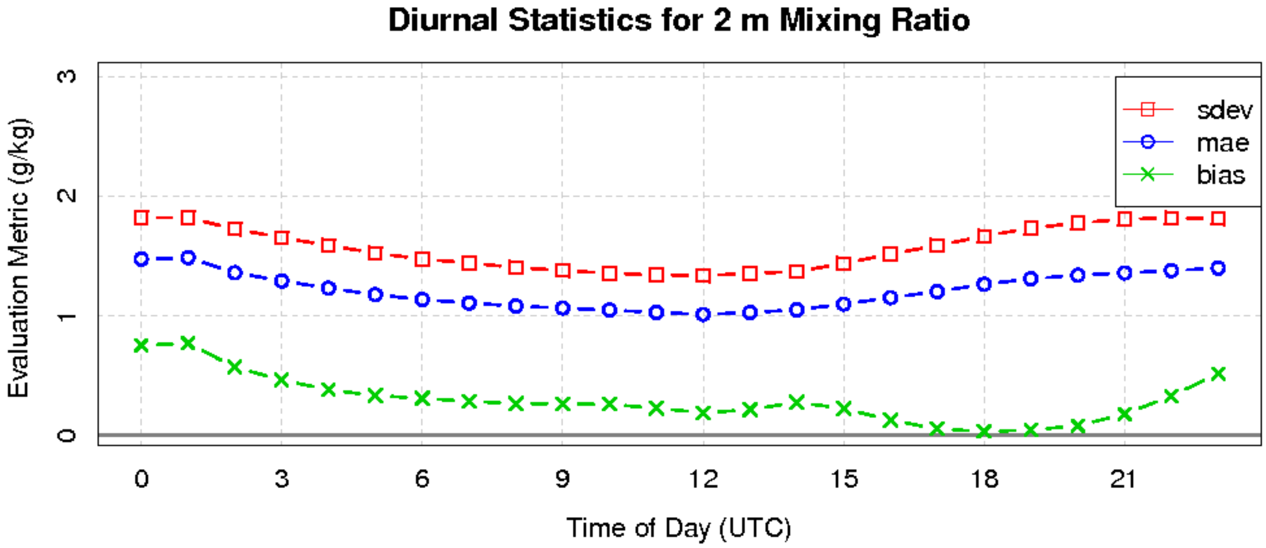

Figure 4-10. Diurnal 2-m mixing ratio error and bias (g/kg) averaged over the 12-km CONUS domain for January (top) and July (bottom) 2013.

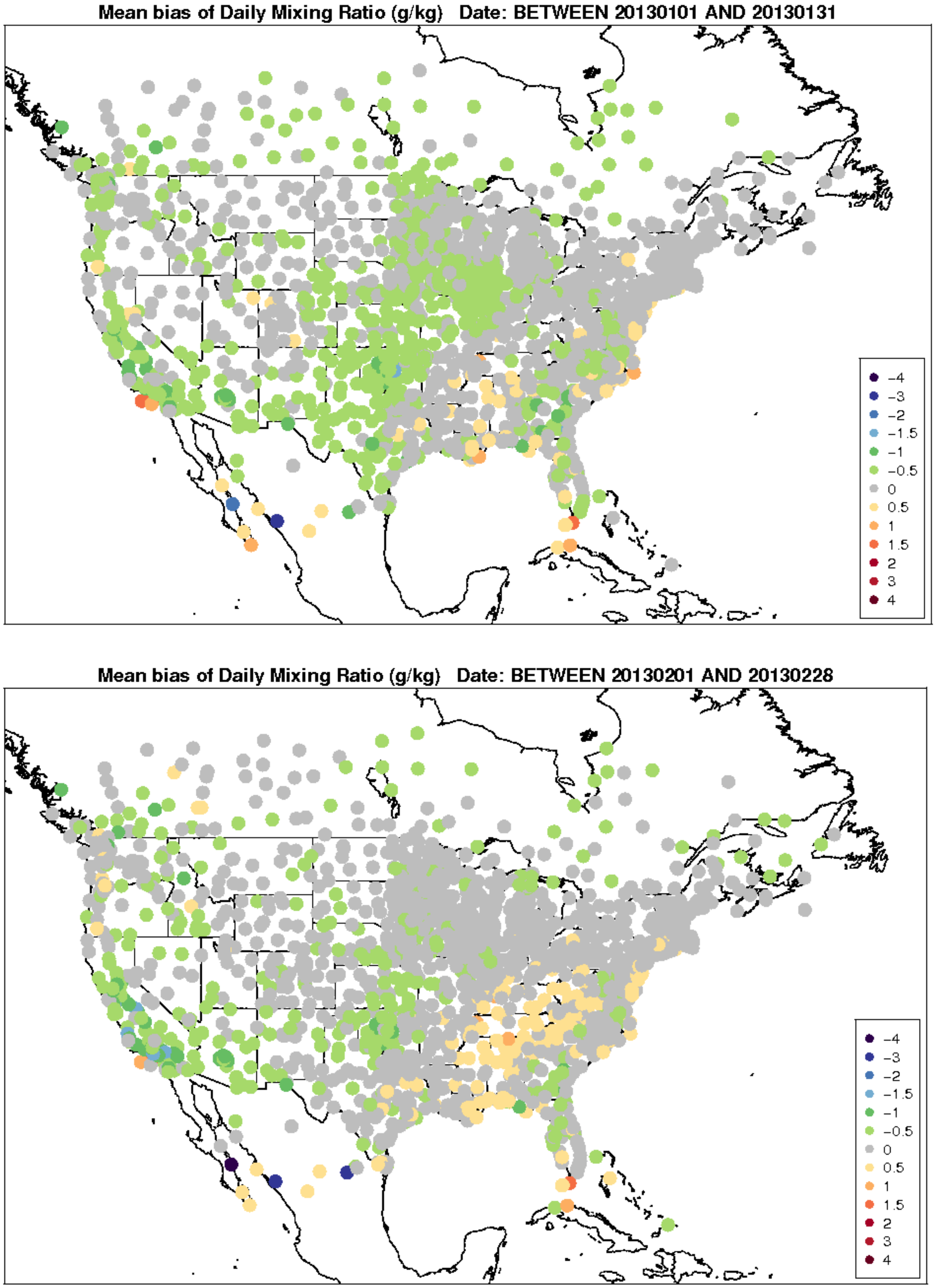

Figure 4-11. Spatial distribution of 2-m mixing ratio bias (g/kg) within the 12-km CONUS domain for January (top) and February (bottom).

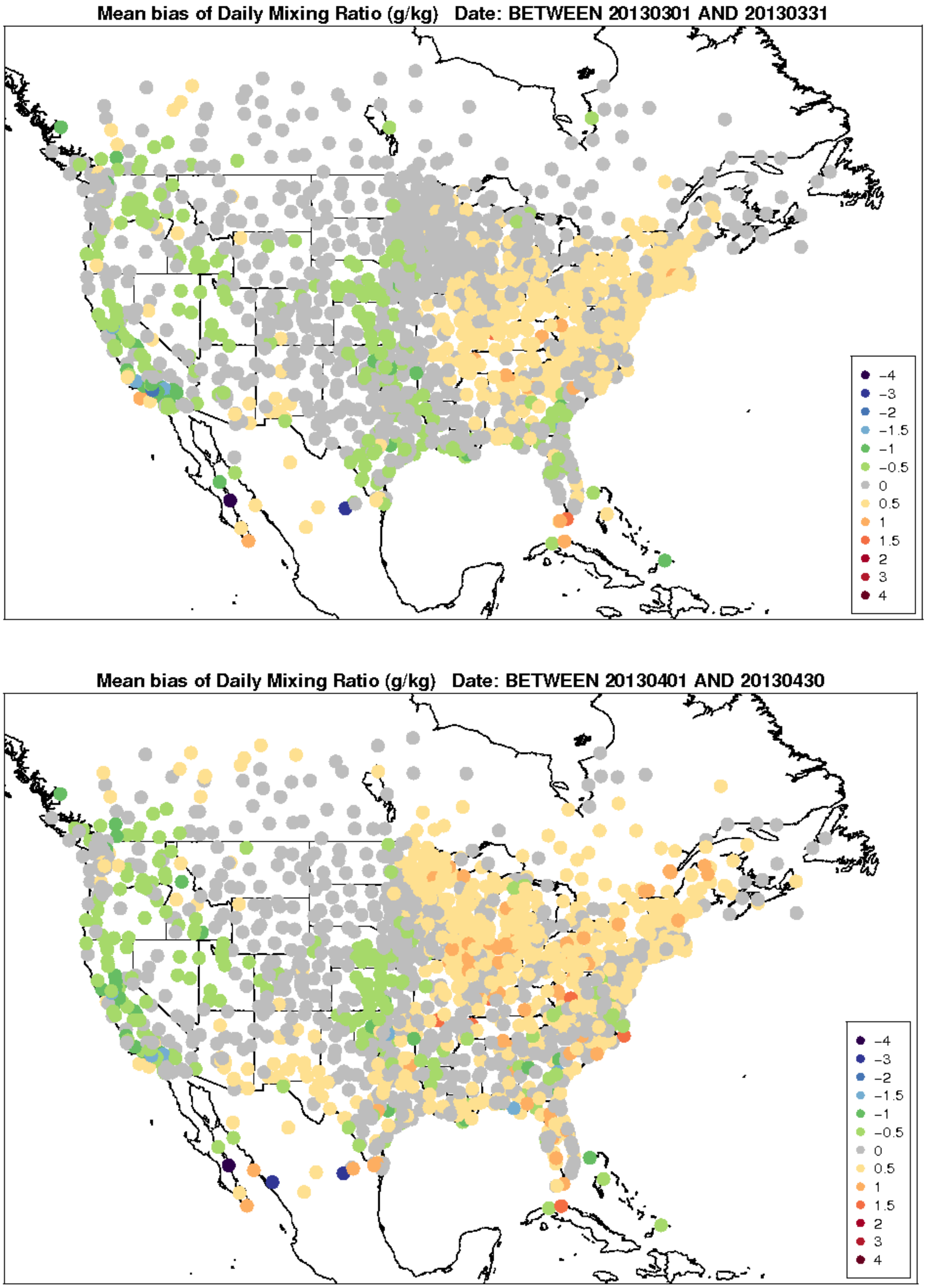

Figure 4-12. Spatial distribution of 2-m mixing ratio bias (g/kg) within the 12-km CONUS domain for March (top) and April (bottom).

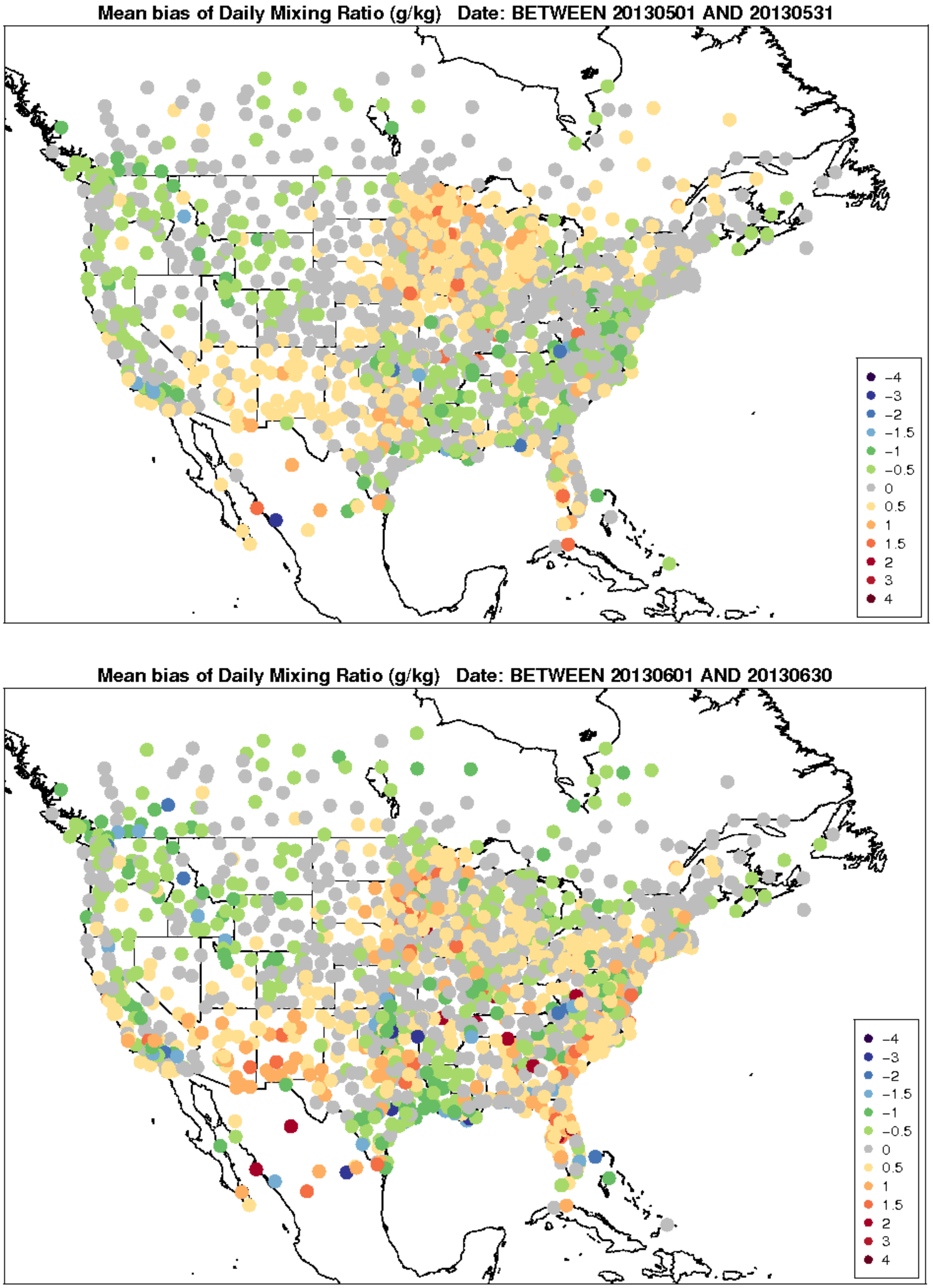

Figure 4-13. Spatial distribution of 2-m mixing ratio bias (g/kg) within the 12-km CONUS domain for May (top) and June (bottom).

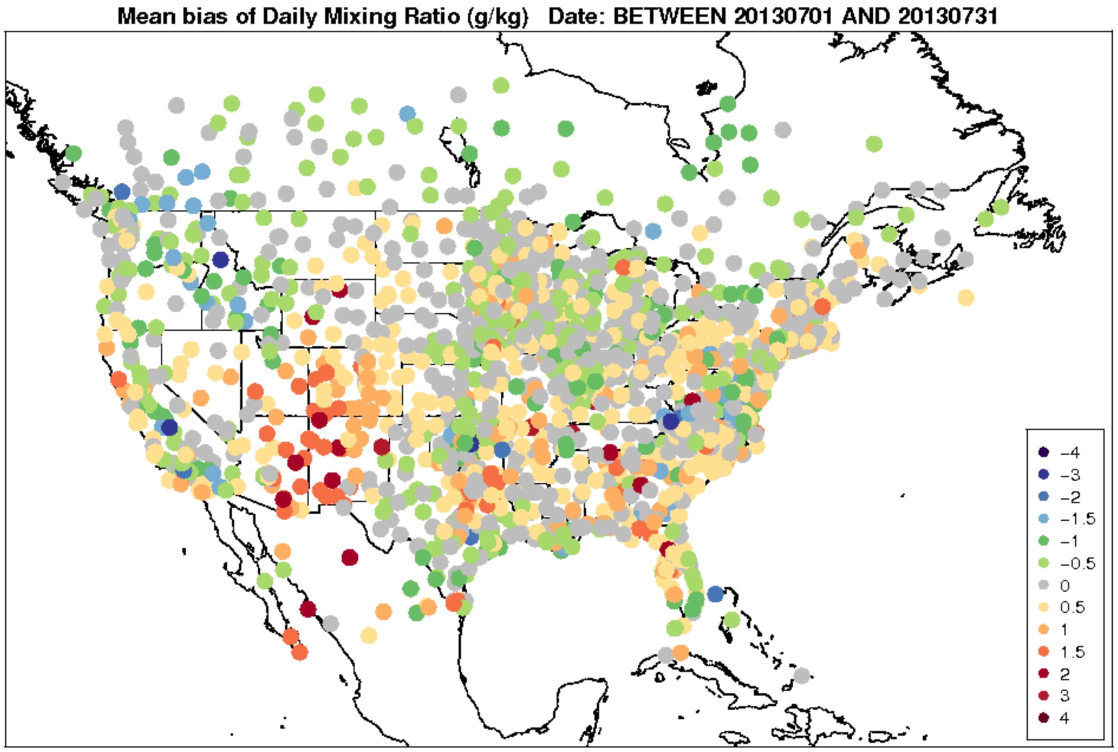

Mean bias of Daily Mixing Ratio (g/kg) Date: BETWEEN 20130701 AND 20130731

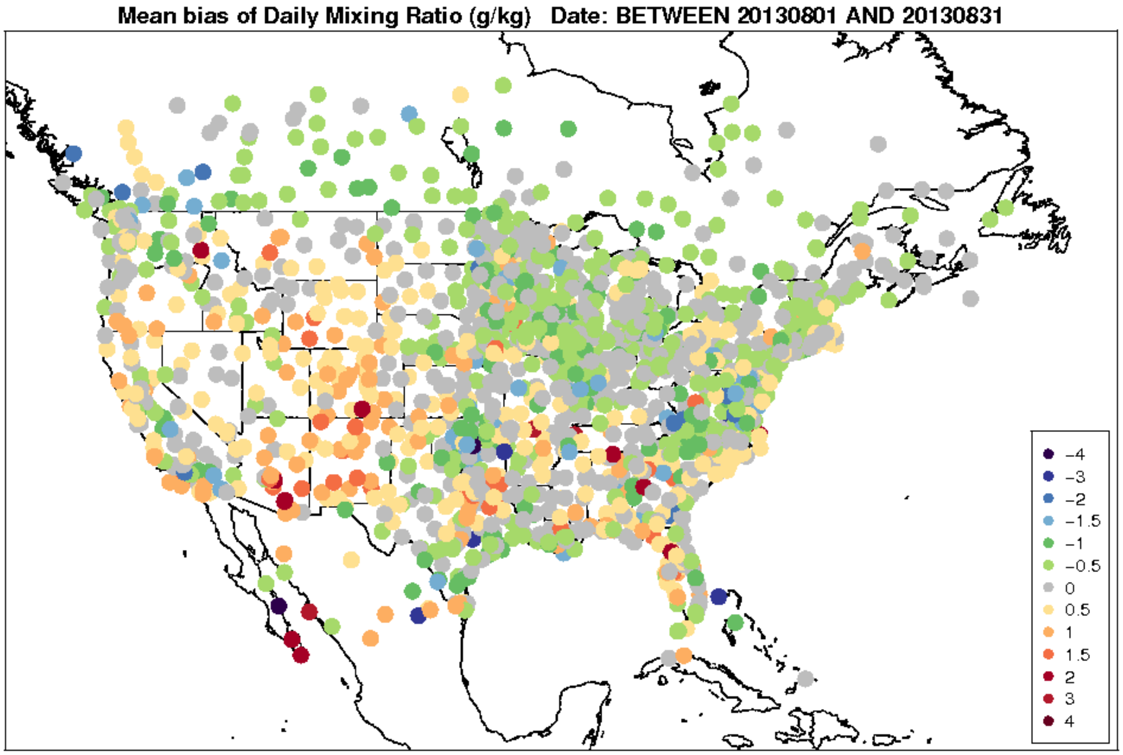

Mean bias of Daily Mixing Ratio (g/kg) Date: BETWEEN 20130801 AND 20130831

Figure 4-14. Spatial distribution of 2-m mixing ratio bias (g/kg) within the 12-km CONUS domain for July (top) and August (bottom).

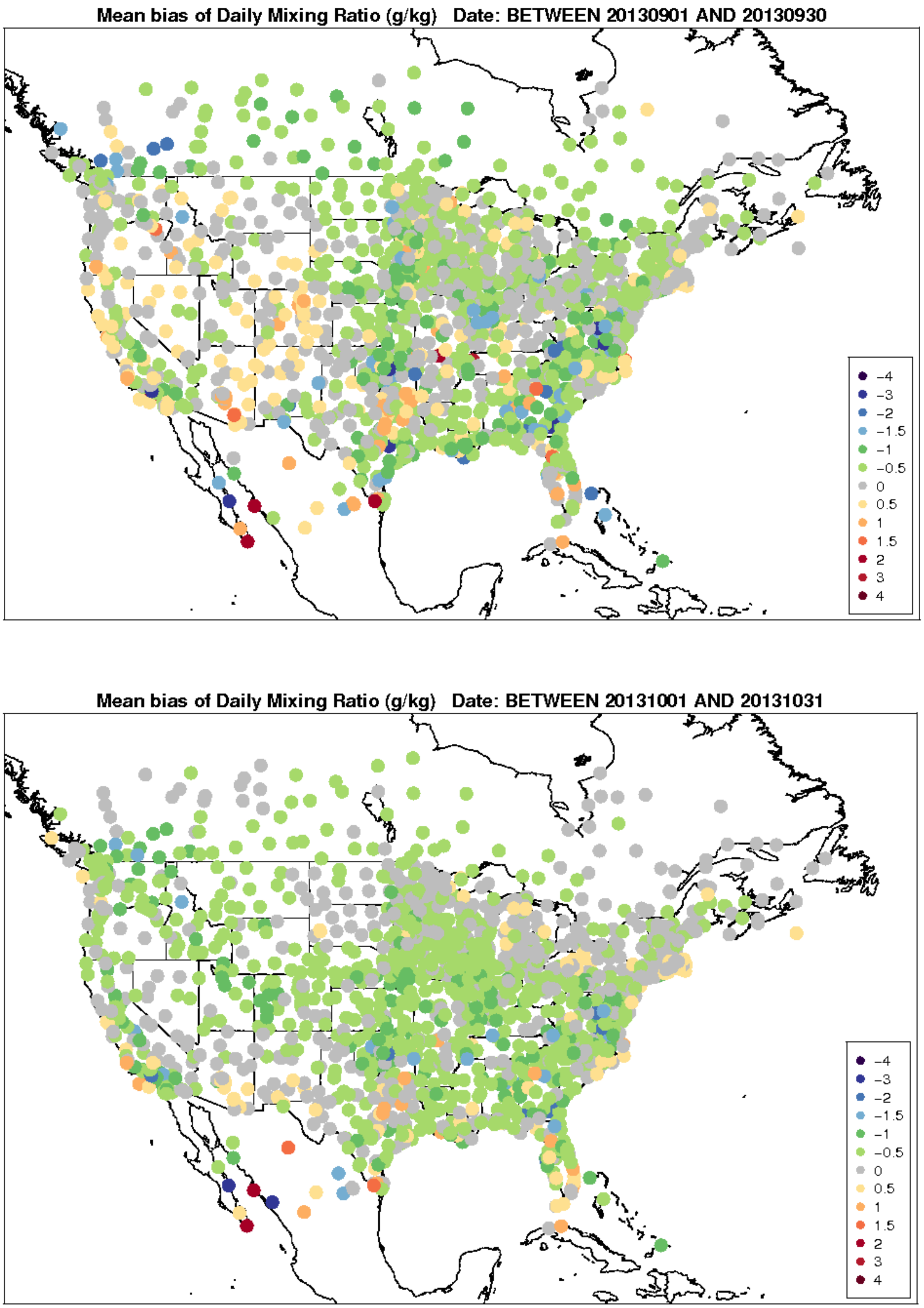

Figure 4-15. Spatial distribution of 2-m mixing ratio bias (g/kg) within the 12-km CONUS domain for September (top) and October (bottom).

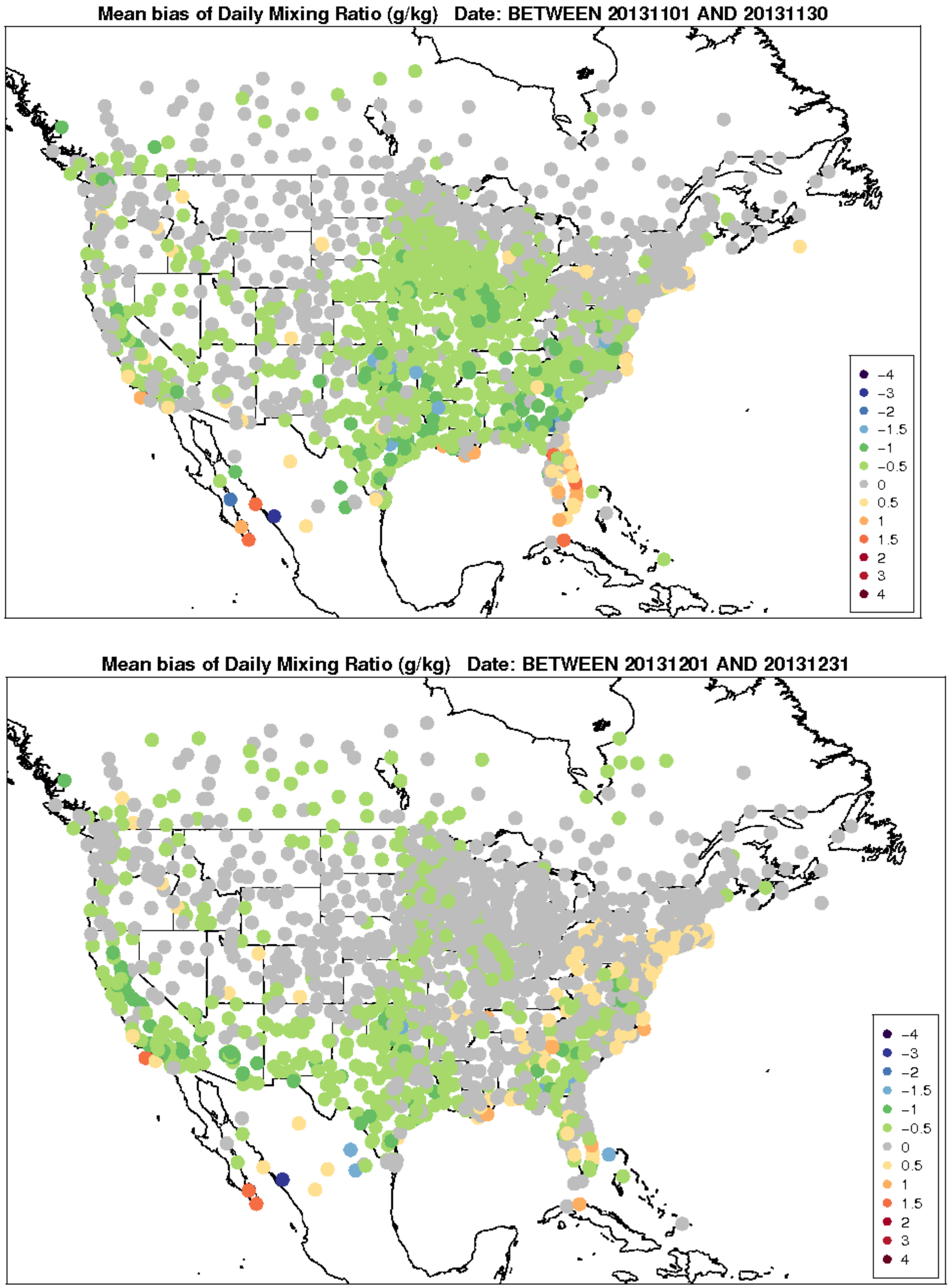

Figure 4-16. Spatial distribution of 2-m mixing ratio bias (g/kg) within the 12-km CONUS domain for November (top) and December (bottom).

Model Evaluation Results for 10-m Wind Speed

All months on average for the CONUS have a wind speed bias smaller than ±0.5 m/s and wind speed error less than 2 m/s, shown in Figure 4-17. Unlike 2-m temperature and mixing ratio, the differences in the bias between winter and summer months are similar with slightly better performance for wind speed during the summer/fall compared to the winter/spring.

The diurnal statistics illustrate the 10-m wind bias is typically larger in the afternoon and evening hours for both January (winter) and July (summer), see Figure 4-18. The bias and error is smallest for July overnight into the early morning hours. Overall, the diurnal bias is less than 0.5 m/s. There is also a persistent diurnal error, between 1 m/s to 1.3 m/s, for winter and summer months.

The spatial pattern illustrates the complexity in the wind speed bias throughout the CONUS. During the winter months (January and February), Figure 4-19, the wind speed bias is generally positive for many locations within the Mid-Atlantic, Northeast, and Great Lakes. However, from the Great Plains and westward, many locations experience a negative bias with an exception for coastal stations along the West Coast. A similar pattern continues into the spring months (March, April), Figure 4-20. By summer (June, July, August), there is an improvement in the wind speed bias for the western/eastern half of the CONUS, Figure 4-21 and Figure 4-22. However, a negative/positive bias remains for many locations within the western/eastern half of the CONUS, respectively. In addition, positive wind speed bias exists for many stations within the Northeast U.S. Some of the largest negative wind speed biases during the summer months occur for locations in the western half of the CONUS, from the Rocky Mountains, west.

We find the largest bias occurs during the fall season (October, November), Figure 4-23 and Figure 4-24. Some of the locations with the largest positive bias are found around the Great Lakes, as well as in states on the East Coast, with some of the largest positive bias found along land-water interfaces. The largest negative bias locations tend to occur over the western half of the CONUS, especially in the Rocky Mountains. The poor wind speed performances in these locations are likely related to complex processes not resolved by the 12-km horizontal resolution.

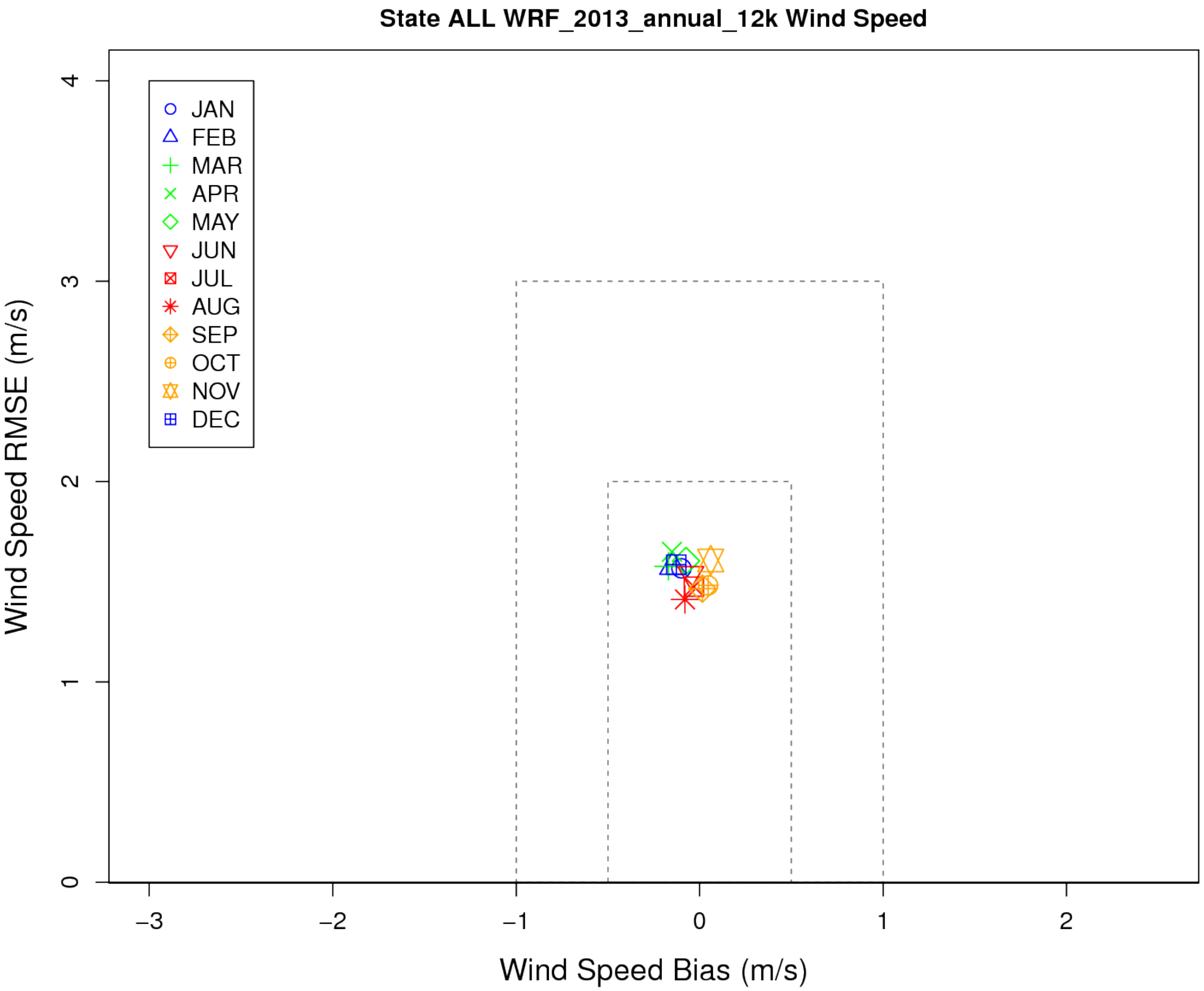

Figure 4-17. Soccer plot of monthly 10-m wind speed error and bias (m/s) averaged over the 12-km CONUS domain for the 2013 calendar year.

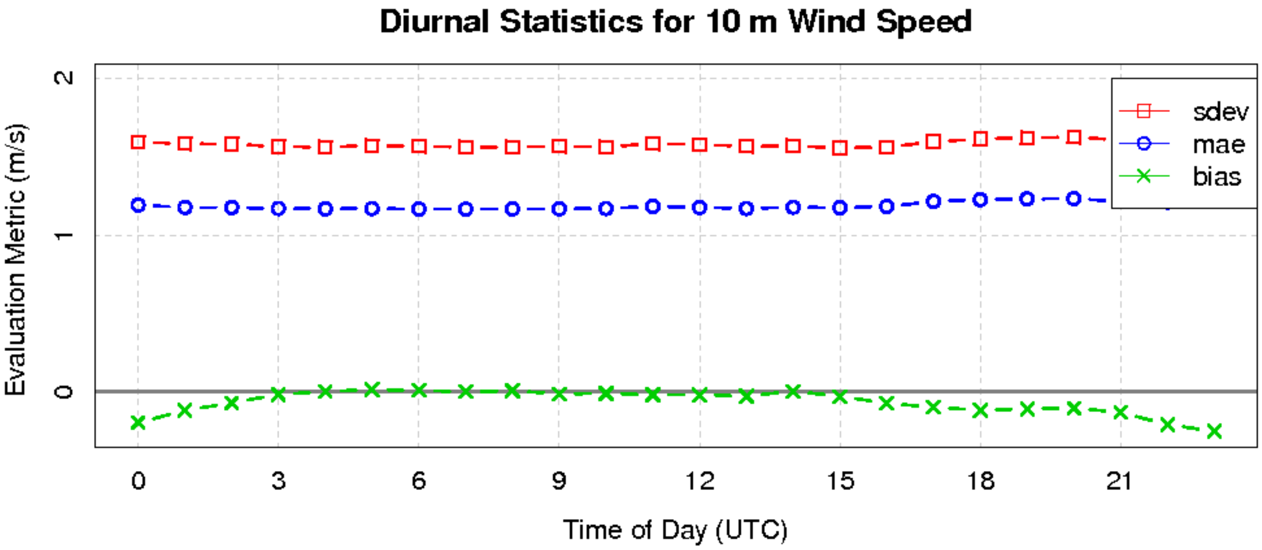

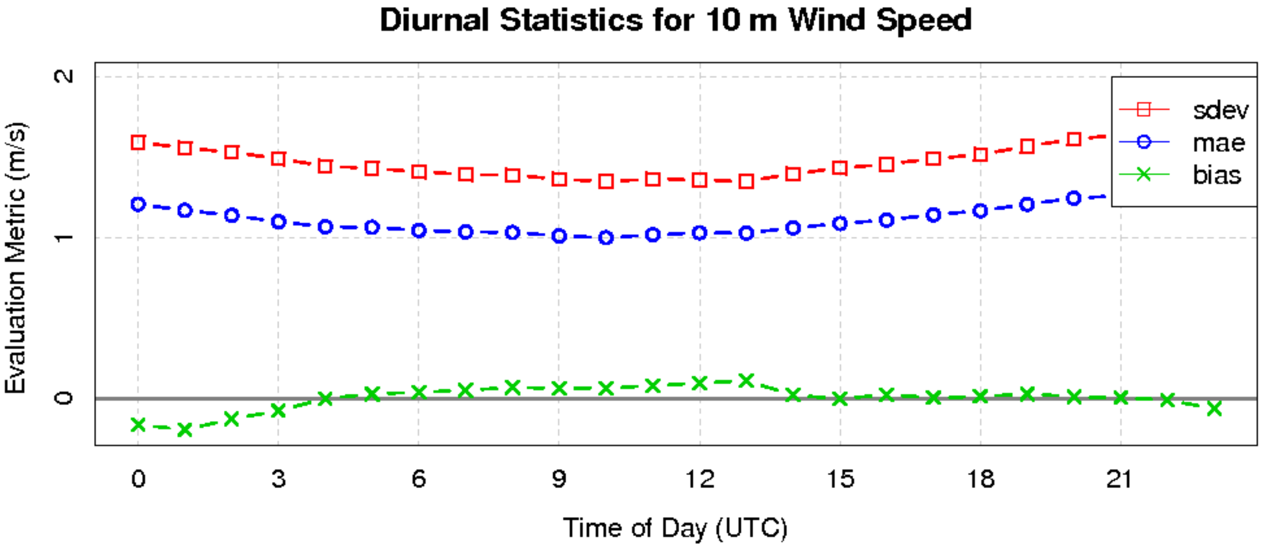

Figure 4-18. Diurnal 10-m wind speed error and bias (m/s) averaged over the 12-km CONUS domain for January (top) and July (bottom) 2013.

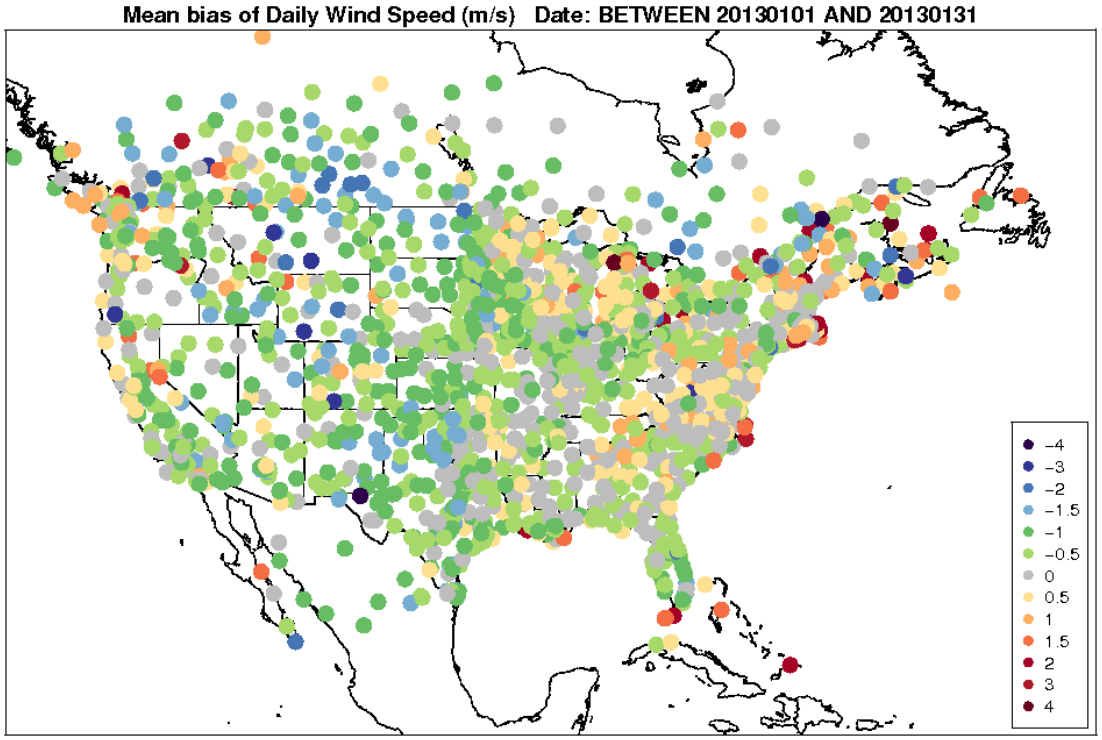

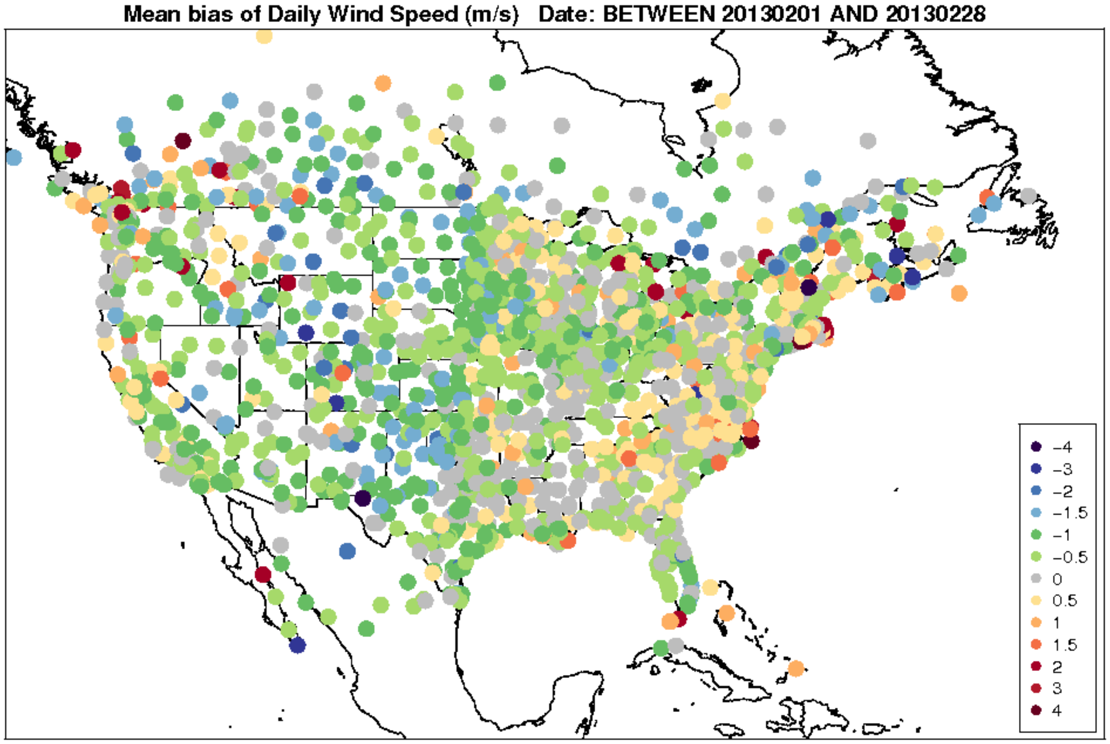

Figure 4-19. Spatial distribution of 10-m wind speed bias (m/s) within the 12-km CONUS domain for January (top) and February (bottom).

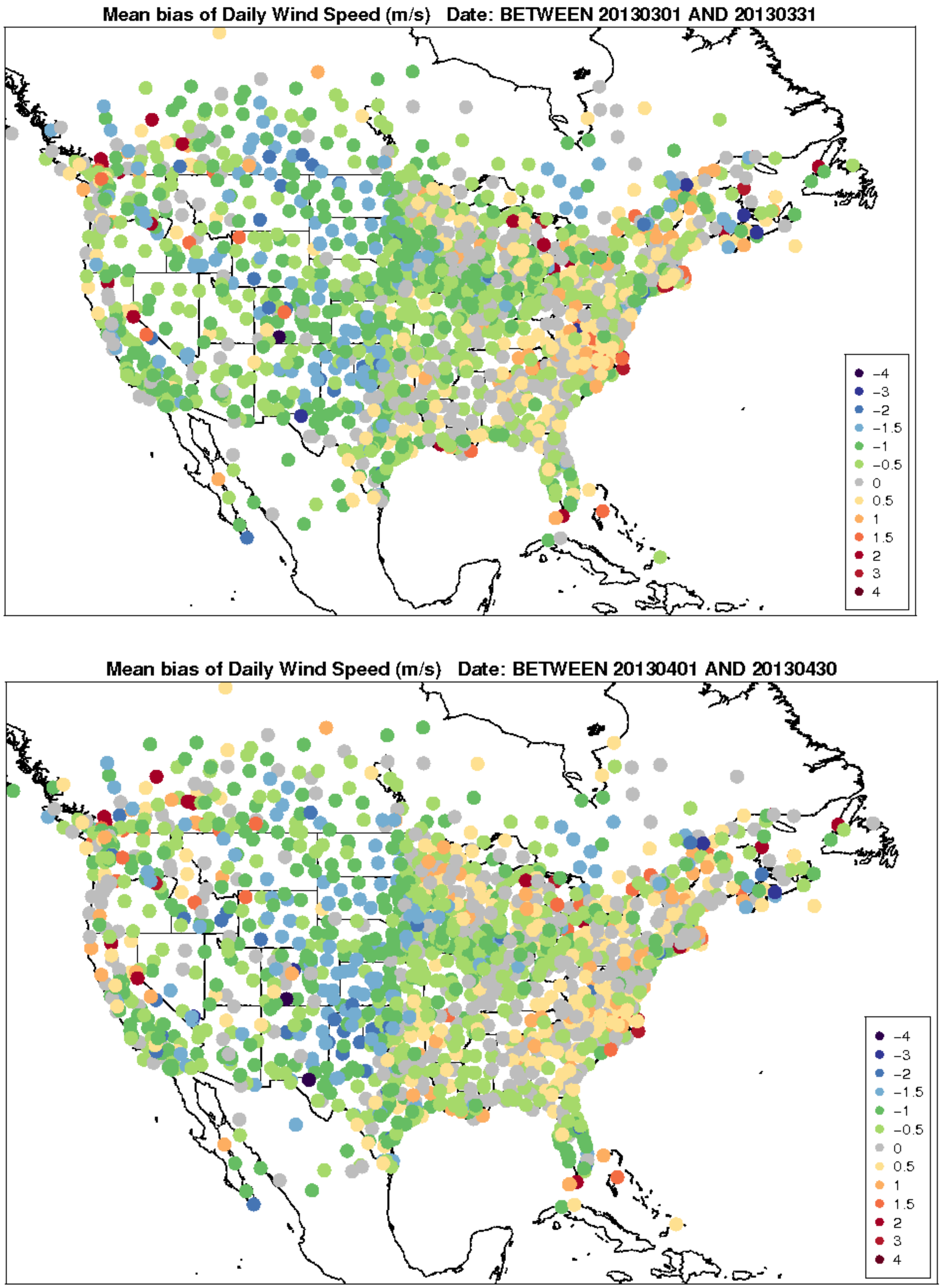

Figure 4-20. Spatial distribution of 10-m wind speed bias (m/s) within the 12-km CONUS domain for March (top) and April (bottom).

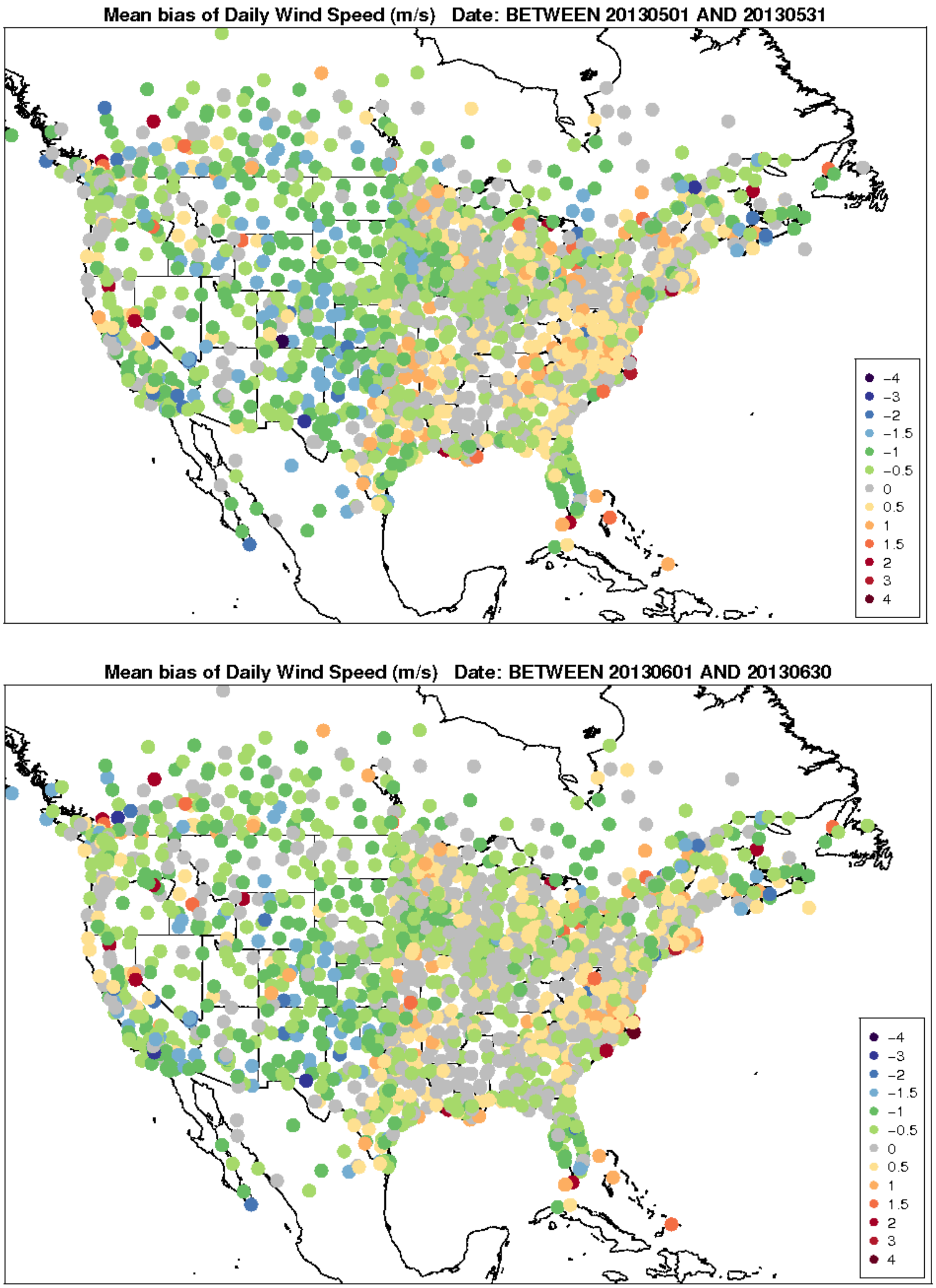

Figure 4-21. Spatial distribution of 10-m wind speed bias (m/s) within the 12-km CONUS domain for May (top) and June (bottom).

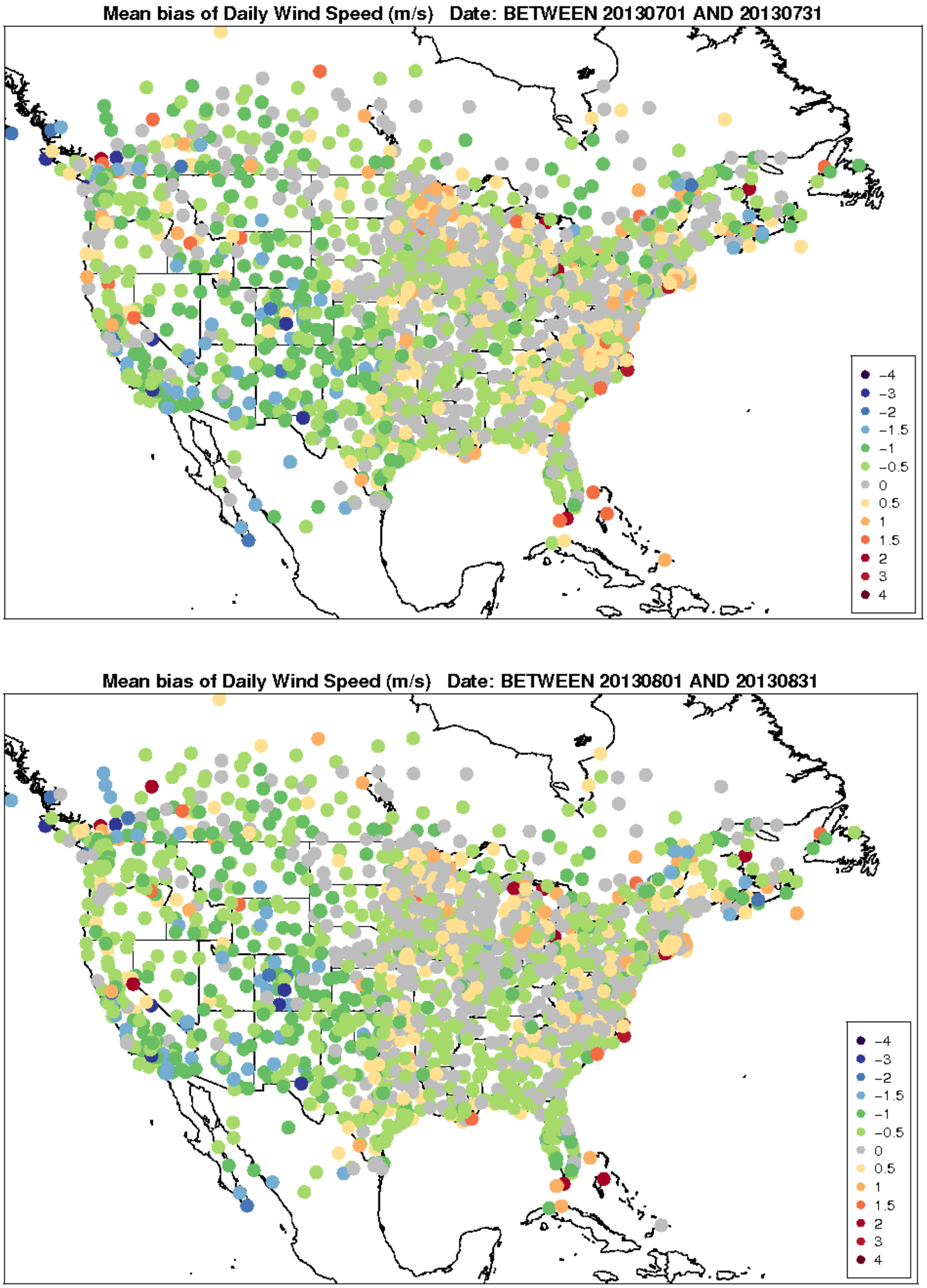

Figure 4-22. Spatial distribution of 10-m wind speed bias (m/s) within the 12-km CONUS domain for July (top) and August (bottom).

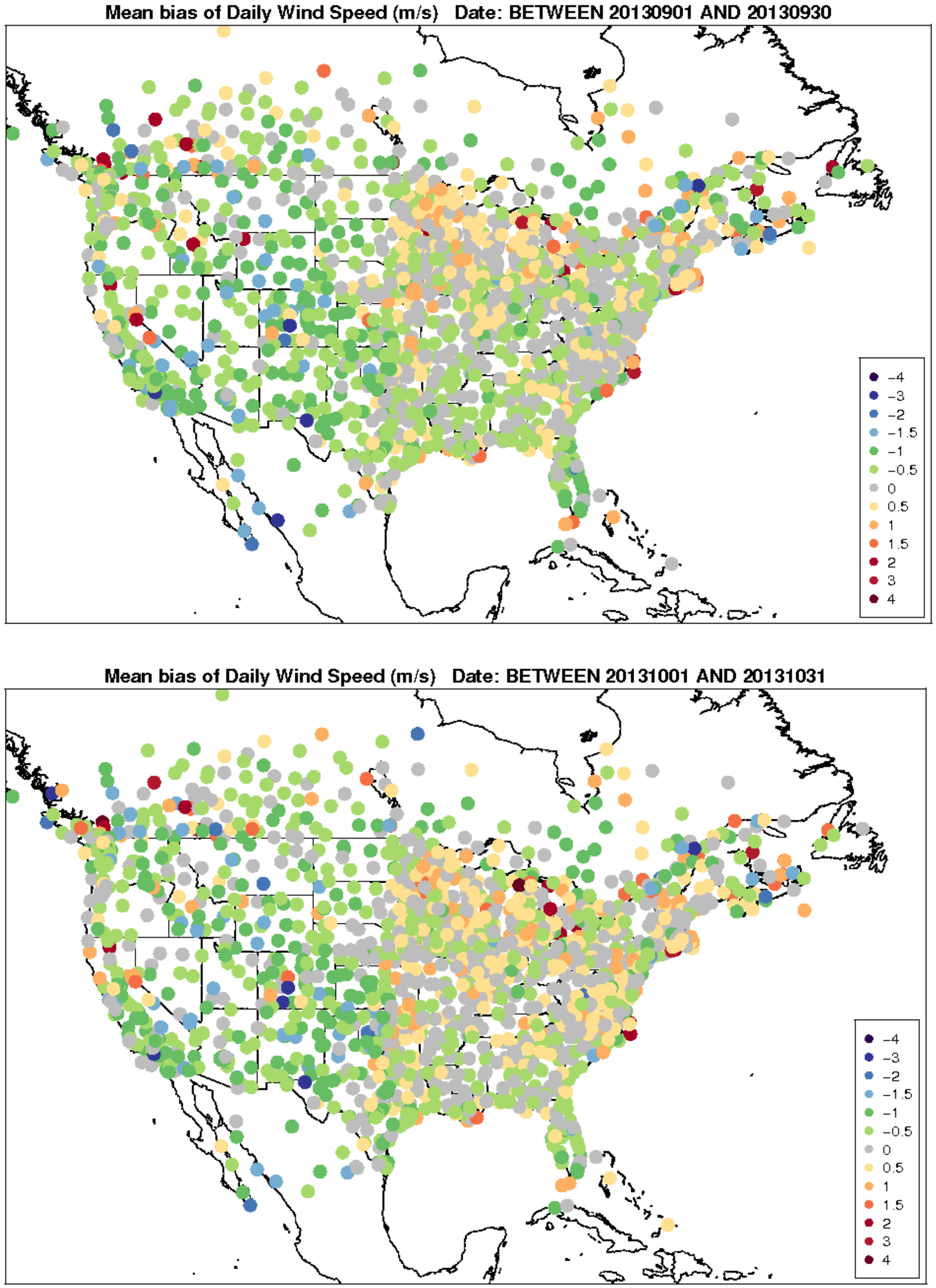

Figure 4-23. Spatial distribution of 10-m wind speed bias (m/s) within the 12-km CONUS domain for September (top) and October (bottom).

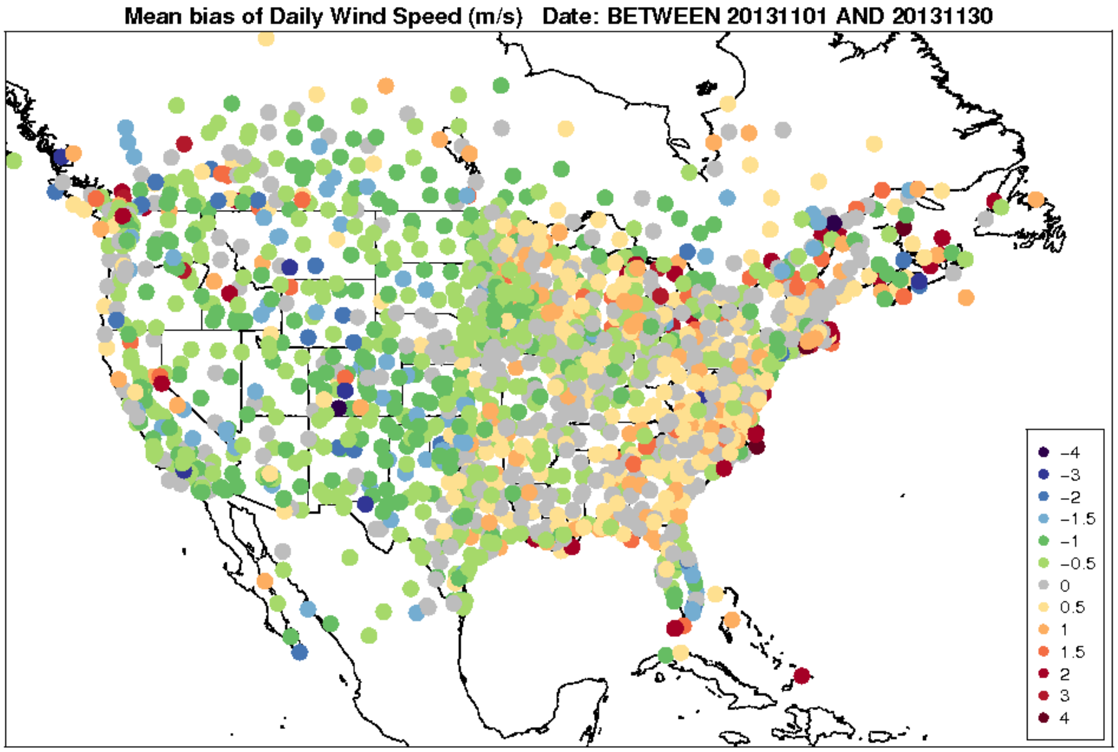

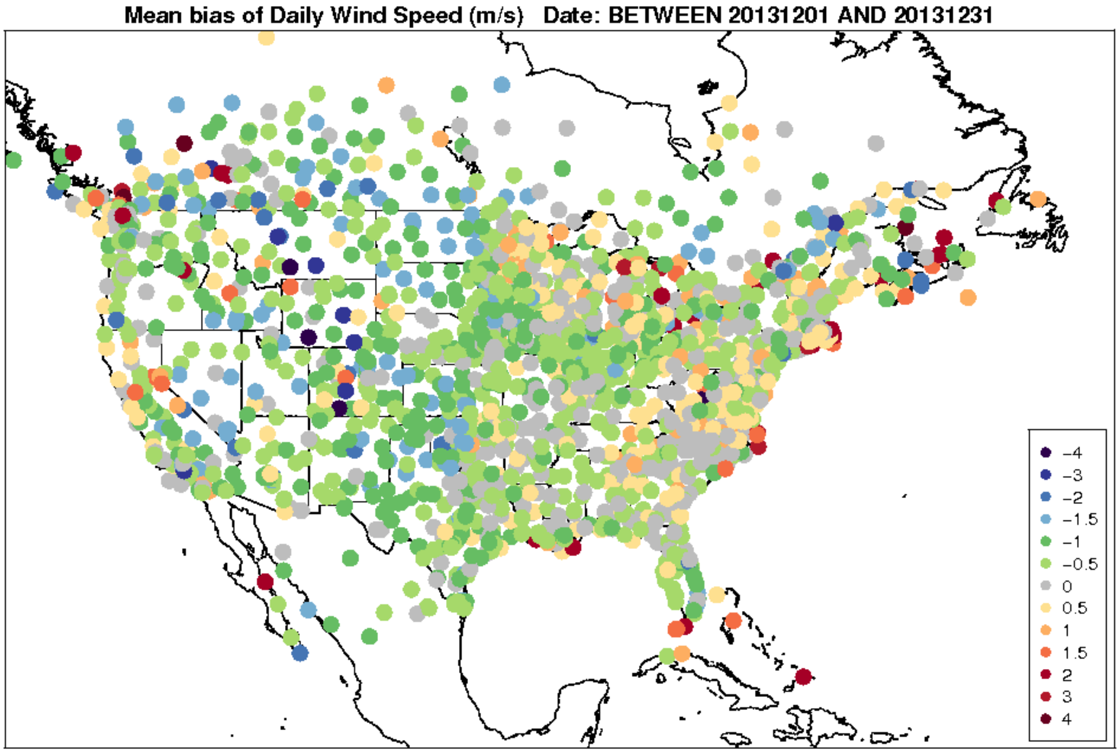

Figure 4-24. Spatial distribution of 10-m wind speed bias (m/s) within the 12-km CONUS domain for November (top) and December (bottom).

Model Evaluation Results for 10-m Wind Direction

The 10-m wind direction error for the CONUS is less than 60 degrees for all months, as shown in Figure 4-25. The largest wind direction bias and errors occur during the summer (June, July, August). The bias and error statistics are similar for the other seasons. Outside of the summer months, the bias and error statistics are similar.

Figure 4-26 illustrates the diurnal statistics for January (winter) and July (summer) and confirms that the average error increases during the summer, by approximately 5 degrees. Diurnally, the bias is fairly consistent throughout the day during January; however, in July the bias and errors increase overnight and during the early morning hours.

In prior analyses, we illustrated the spatial bias for station locations within the CONUS. For wind direction, we focused on the mean absolute error rather than bias because wind direction is a vector field. (Please refer to Section 5 for additional plots including the spatial bias plots of wind direction.) During the winter months (January, February), the mean absolute error is largest (>50°) for locations throughout the western states within the CONUS, Figure 4-27. The large errors over the western states within the CONUS are likely a result of the model's inability to resolve the complex topography and can be found in all months. During the winter months, the mean absolute errors are also large (>40°) for locations within the southeast U.S., especially during January. The locations with the best performance for wind direction error (<20°) occurred within Plains and Midwest U.S. In the spring months (March, April), the errors generally improved with many locations having wind direction errors smaller than 20°; however, large errors continue to exist throughout much of the western states, Figure 4-28. Moving into the late spring and early summer (May/June), the wind direction errors become larger (>40°) for the northern Plains, Great Lakes, and northeast U.S. and continue to be large for western states within the CONUS, Figure 4-29. The large wind direction errors in the northern Plains and northeast U.S. are reduced during the summer, but the errors become larger (>40°) for locations within the southeast U.S., Figure 4-30. Additionally, we find a reduction in the wind direction bias for locations within southern California during the summer months. The large errors (>40°) remain during the fall season for most of the southeast U.S. and portions of the Mid-Atlantic to the Northeast with improvements in the wind direction errors (<20°) for locations within the Plains and Midwest, Figure 4-31. By December, there is an improvement in the wind direction errors relative to the fall for much of the Mid-Atlantic and Northeast, but large errors remain for much of the Southeast, from Texas to the Carolinas, Figure 4-32.

Wind vector displacement (km) on average for the CONUS domain is shown in Figure 4-33. The top panel illustrates the hourly wind displacement and the bottom panel the monthly wind displacement. The mean wind displacement for both hourly and monthly is approximately 5-km. The hourly data illustrates that the mean wind vector displacement increases during the afternoon and early evening hours. However, the monthly wind vector displacement is similar throughout the entire year. Overall, the mean wind vector displacement is around 5-km and smaller than the model horizontal resolution of 12-km; thus, negligible impacts due to wind displacement are expected.

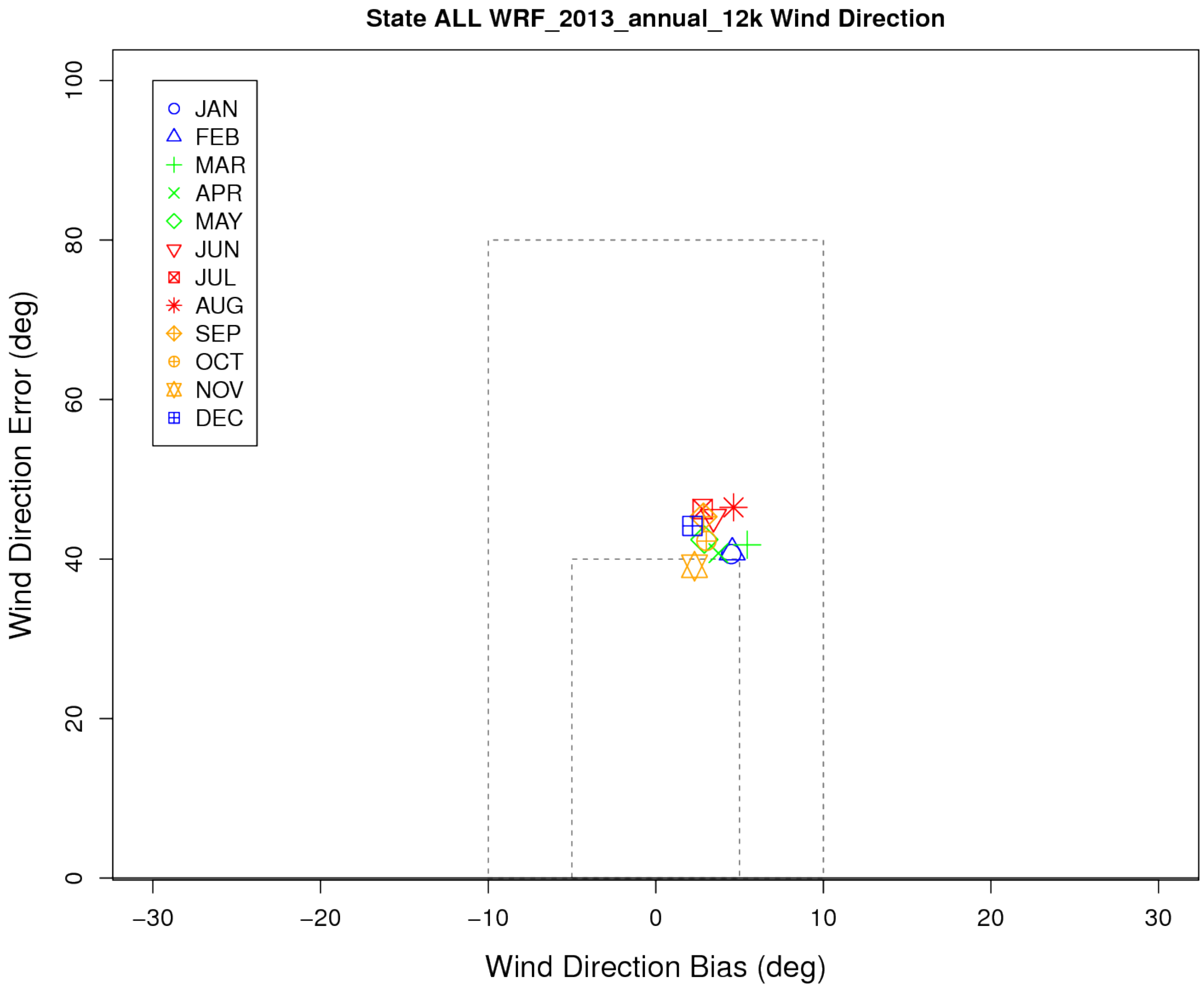

Figure 4-25. Soccer plot of monthly 10-m wind direction error and bias averaged over the 12-km CONUS domain for the 2013 calendar year.

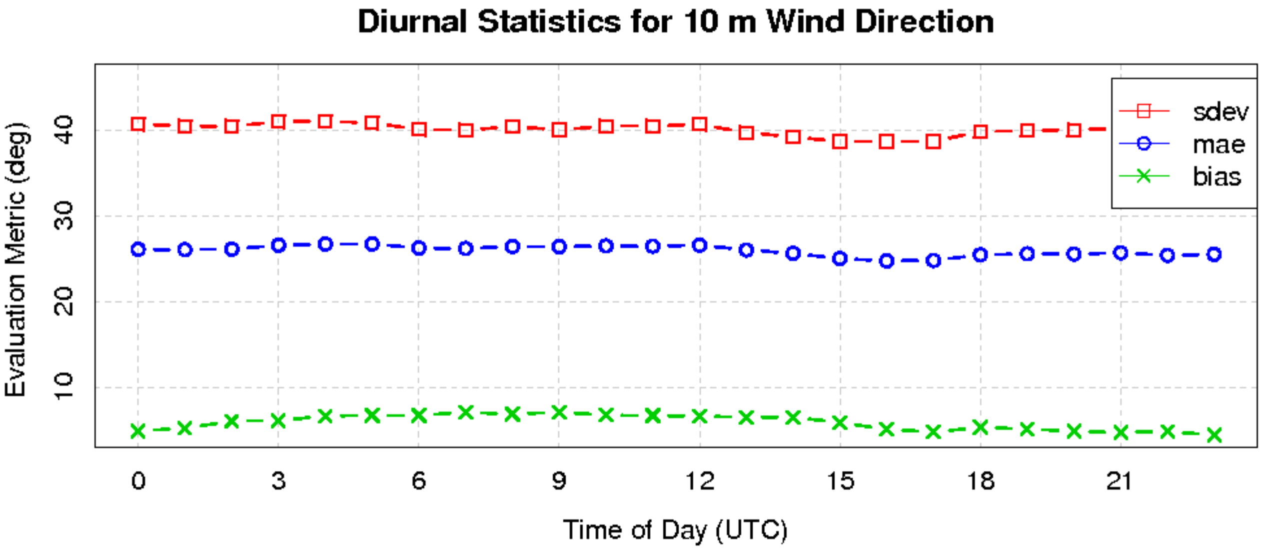

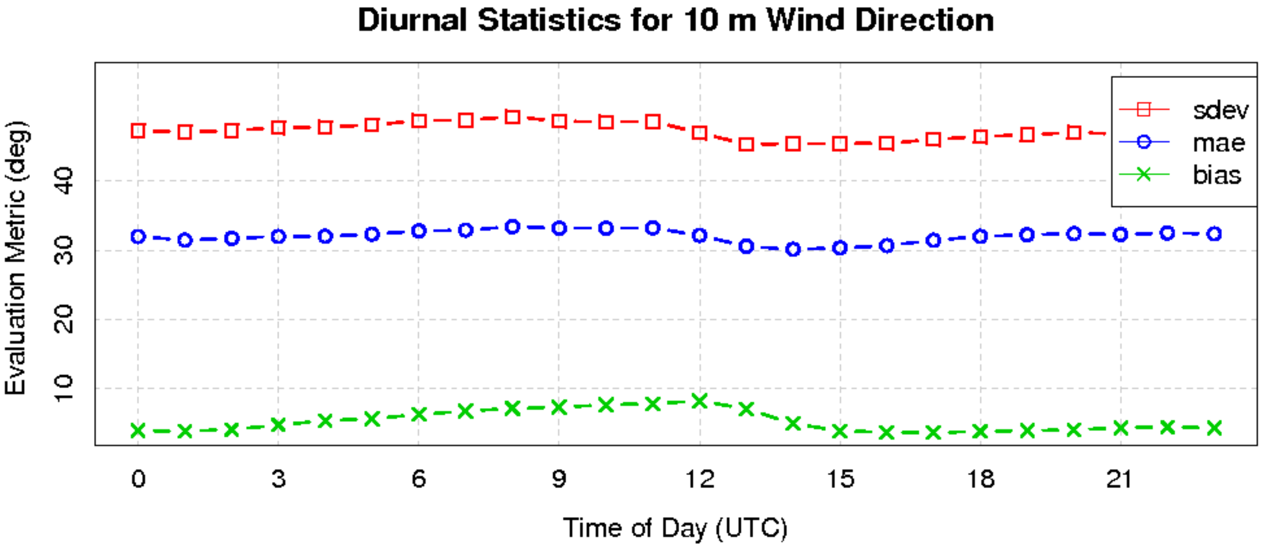

Figure 4-26. Diurnal 10-m wind direction error and bias (m/s) averaged over the 12-km CONUS domain for January (top) and July (bottom) 2013.

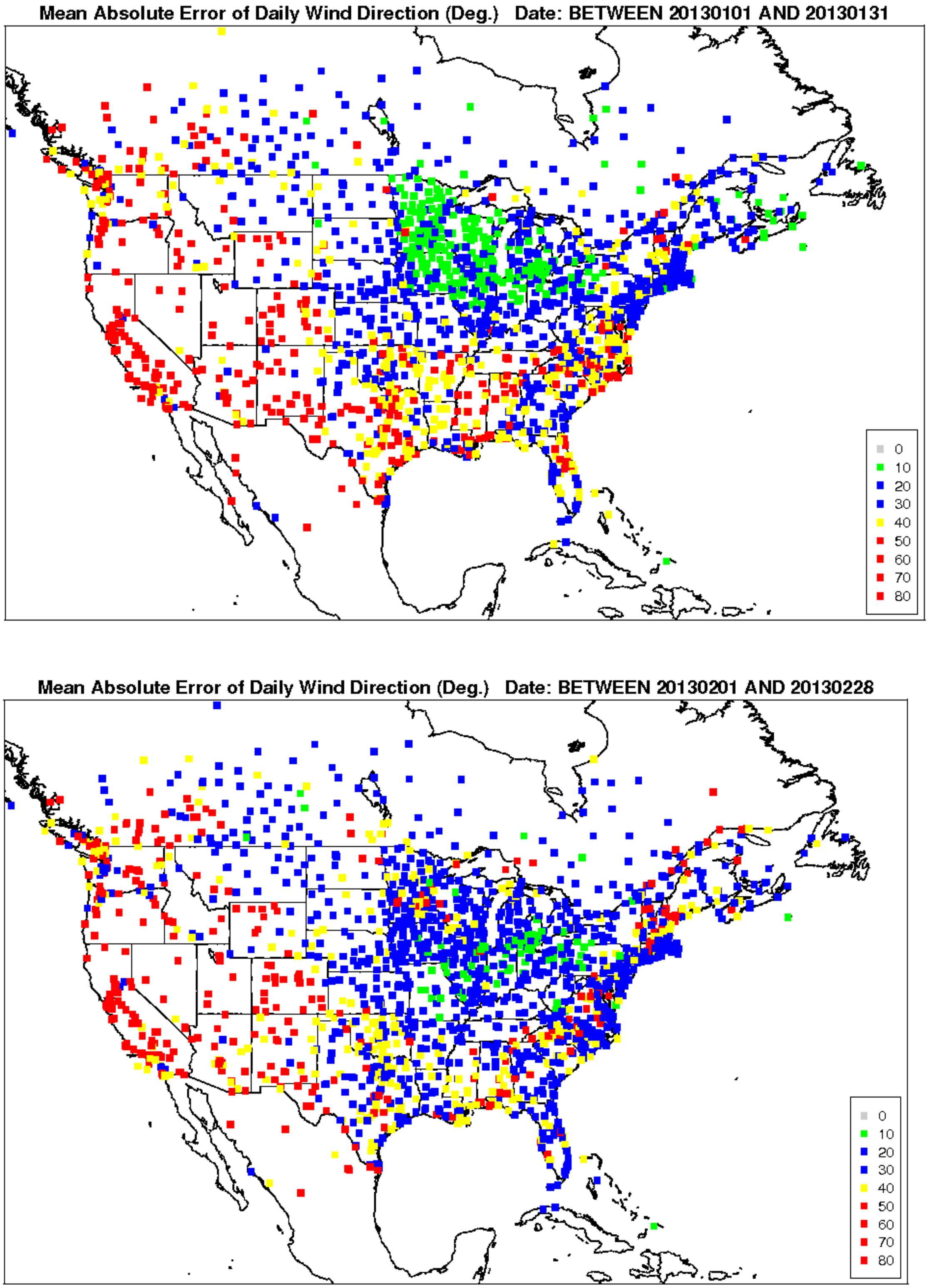

Figure 4-27. Spatial distribution of 10-m wind direction mean absolute error within the 12-km CONUS domain for January (top) and February (bottom).

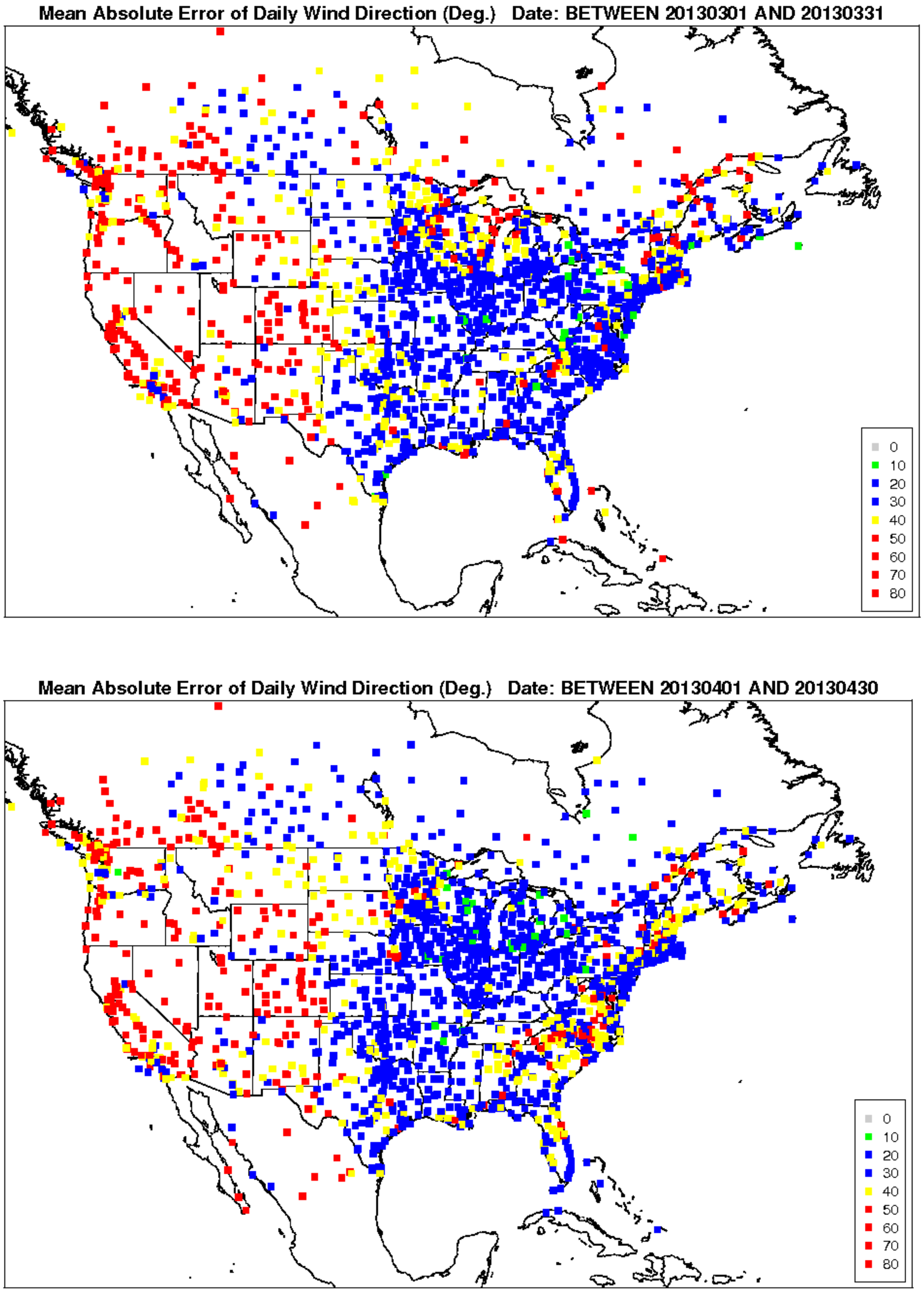

Mean Absolute Error of Daily Wind Direction (Deg.) Date: BETWEEN 20130301 AND 20130331

Mean Absolute Error of Daily Wind Direction (Deg.) Date: BETWEEN 20130401 AND 20130430

Figure 4-28. Spatial distribution of 10-m wind direction mean absolute error within the 12-km CONUS domain for March (top) and April (bottom).

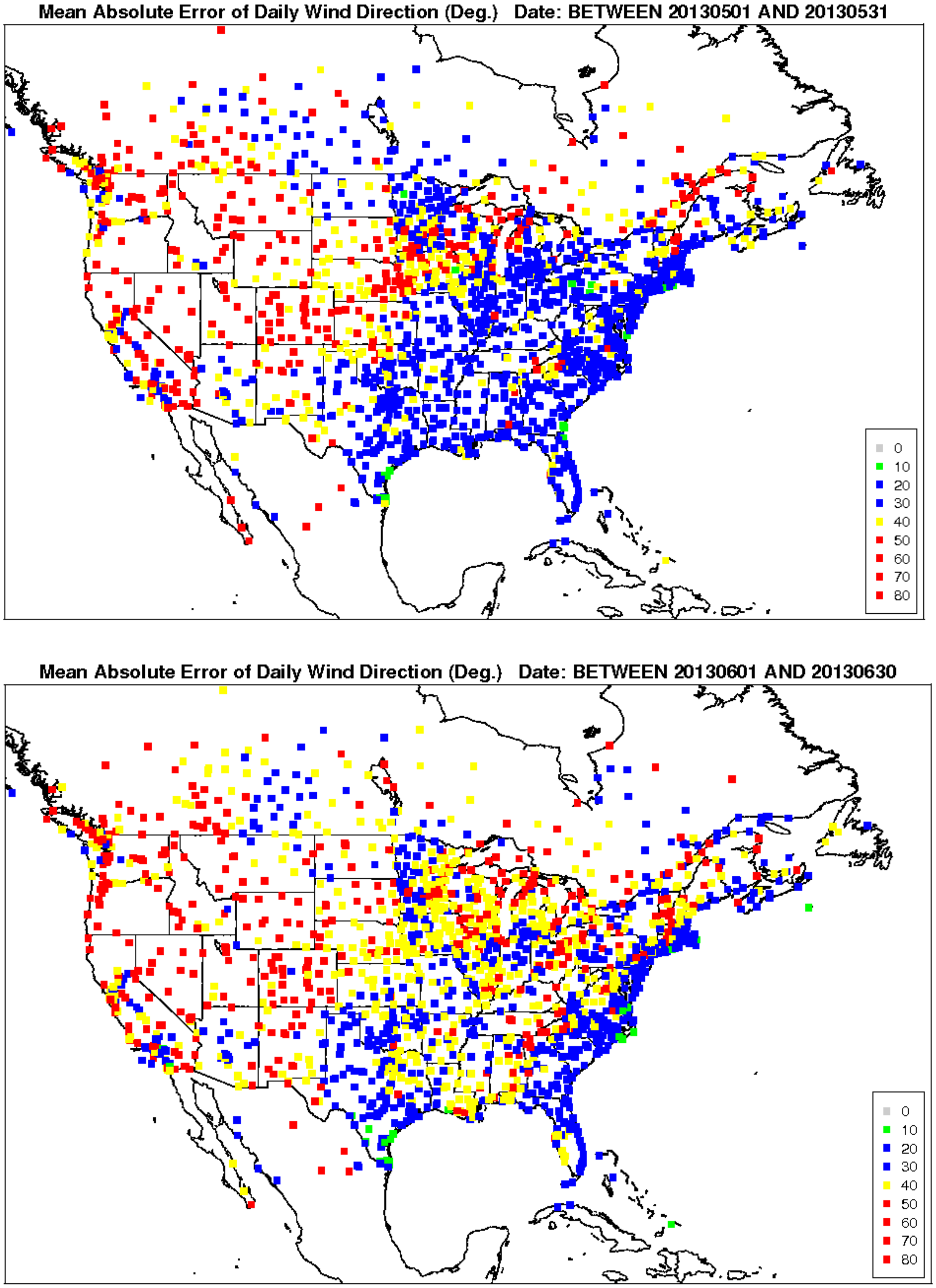

Mean Absolute Error of Daily Wind Direction (Deg.) Date: BETWEEN 20130501 AND 20130531

Mean Absolute Error of Daily Wind Direction (Deg.) Date: BETWEEN 20130601 AND 20130630

Figure 4-29. Spatial distribution of 10-m wind direction mean absolute error within the 12-km CONUS domain for May (top) and June (bottom).

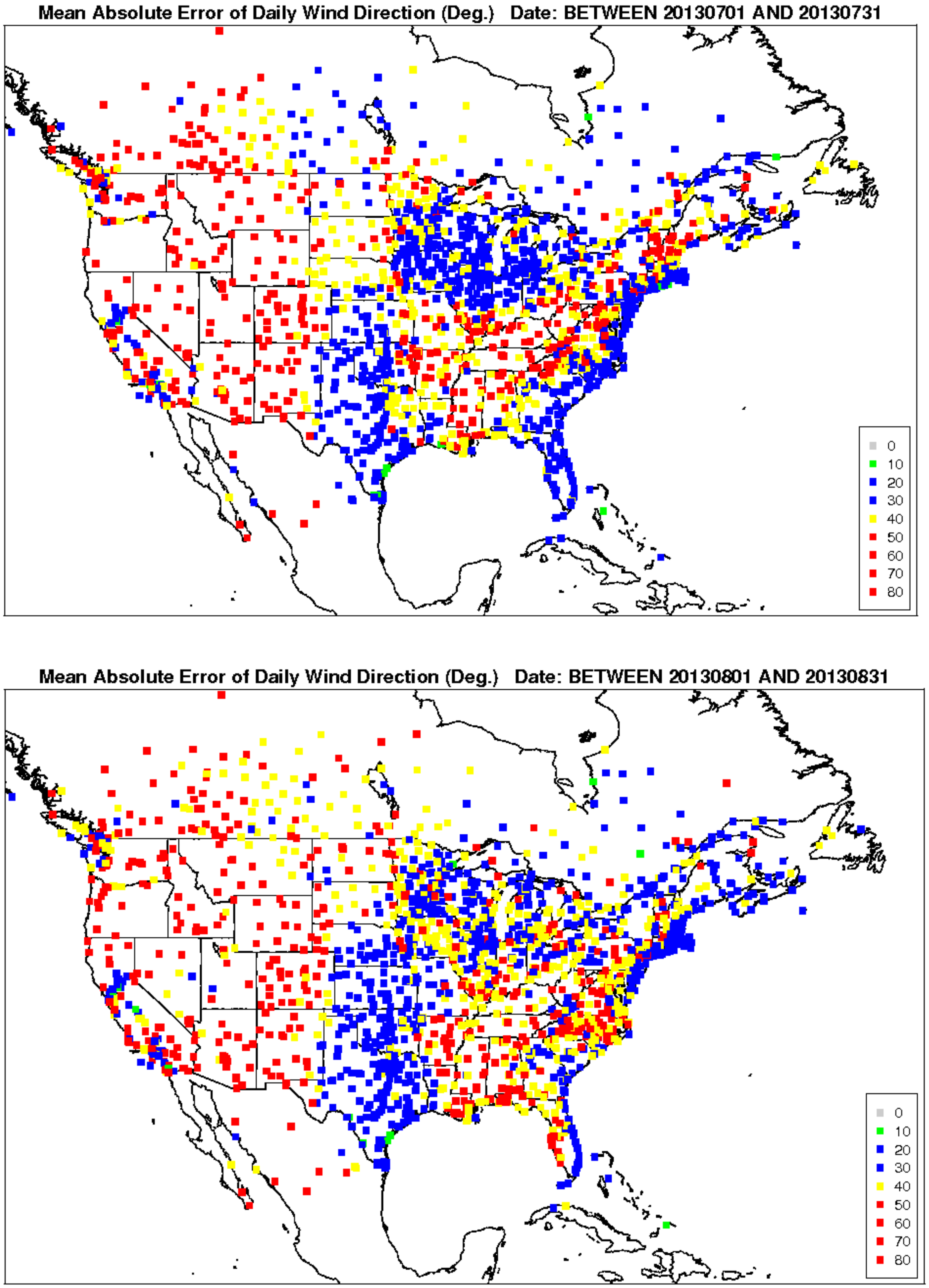

Figure 4-30. Spatial distribution of 10-m wind direction mean absolute error within the 12-km CONUS domain for July (top) and August (bottom).

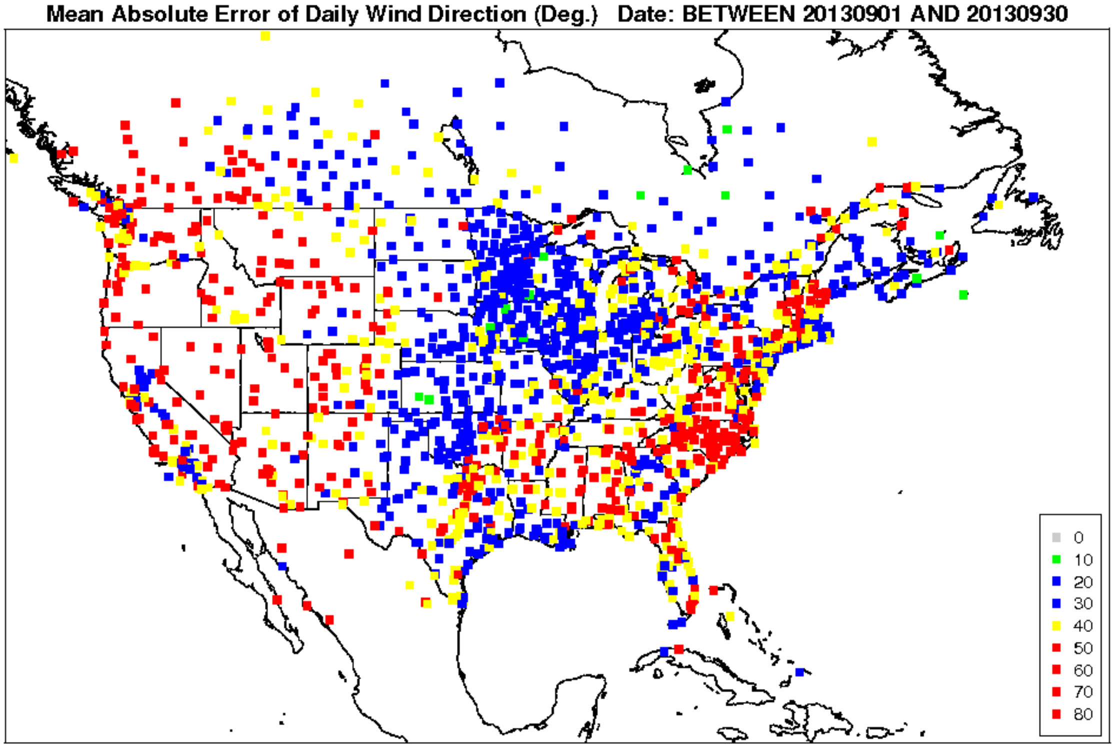

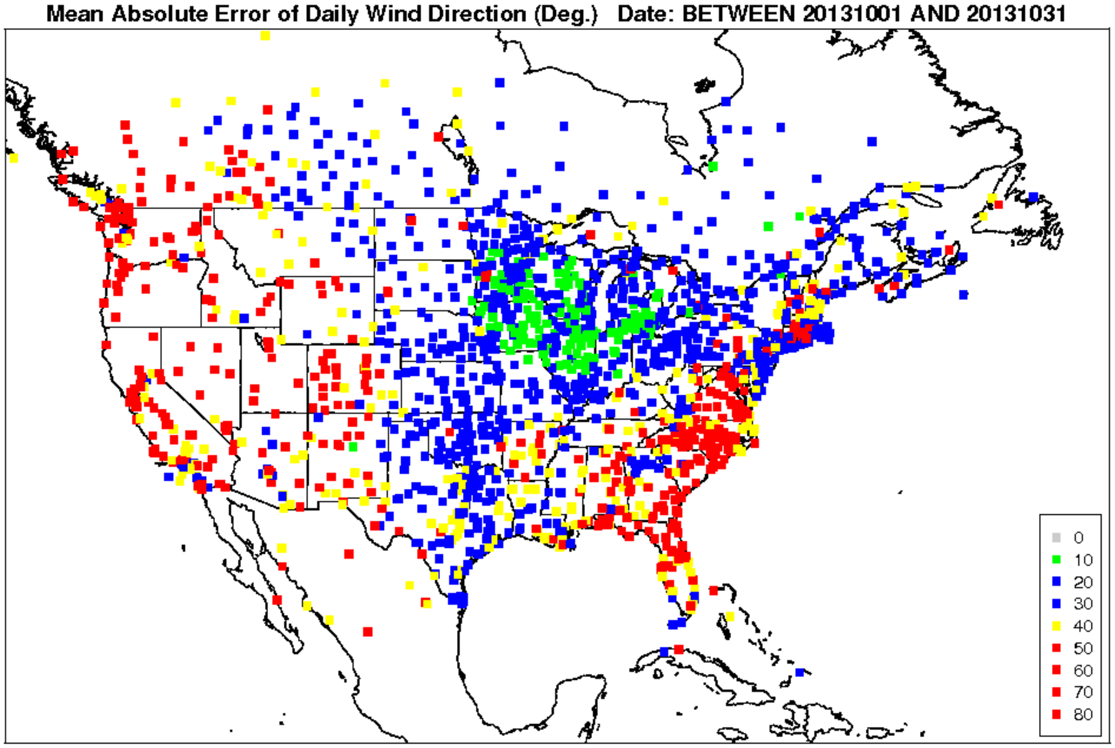

Figure 4-31. Spatial distribution of 10-m wind direction mean absolute error within the 12-km CONUS domain for September (top) and October (bottom).

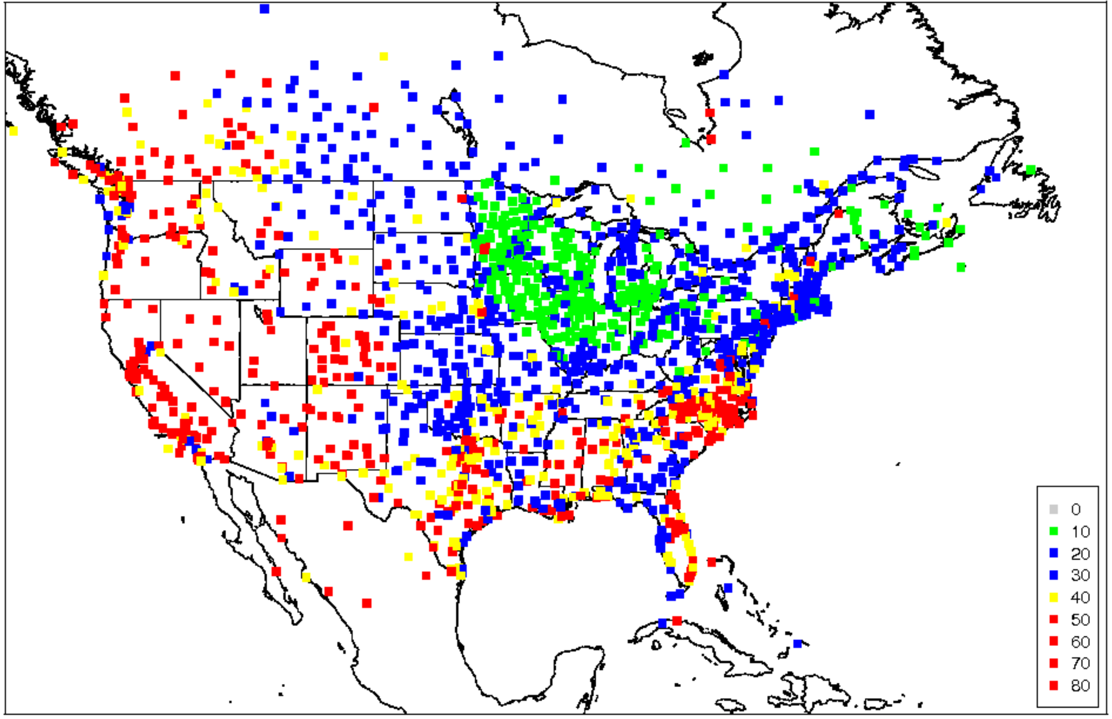

Mean Absolute Error of Daily Wind Direction (Deg.) Date: BETWEEN 20131101 AND 20131130

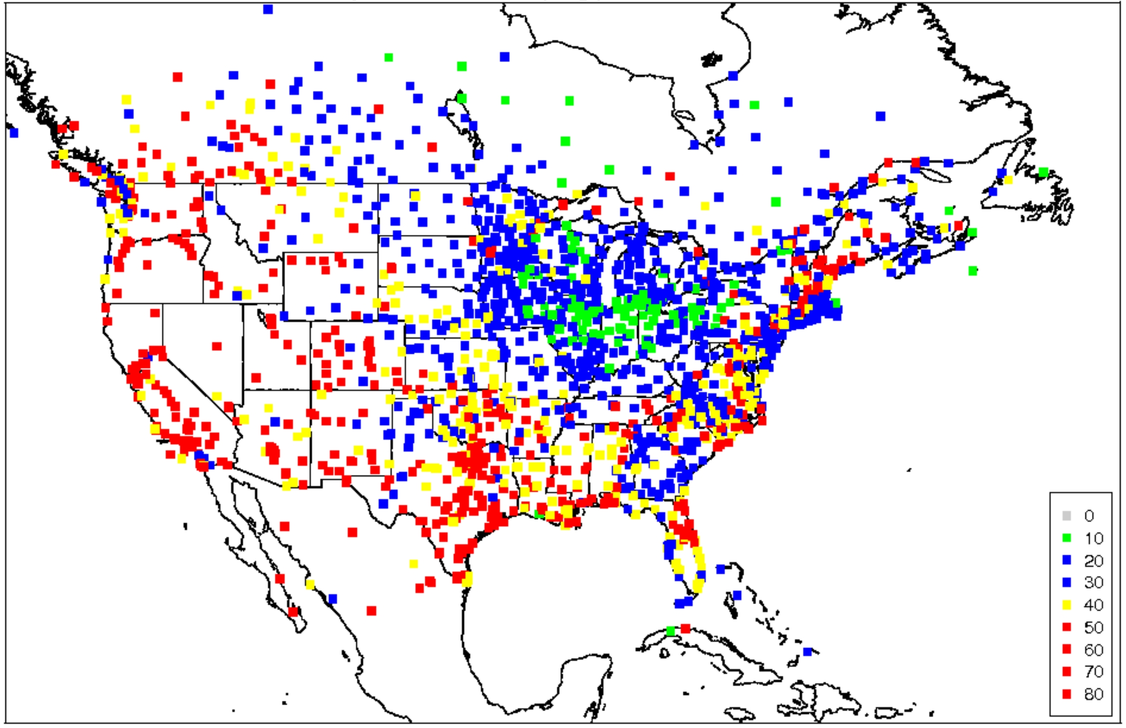

Mean Absolute Error of Daily Wind Direction (Deg.) Date: BETWEEN 20131201 AND 20131231

Figure 4-32. Spatial distribution of 10-m wind direction mean absolute error within the 12-km CONUS domain for November (top) and December (bottom).

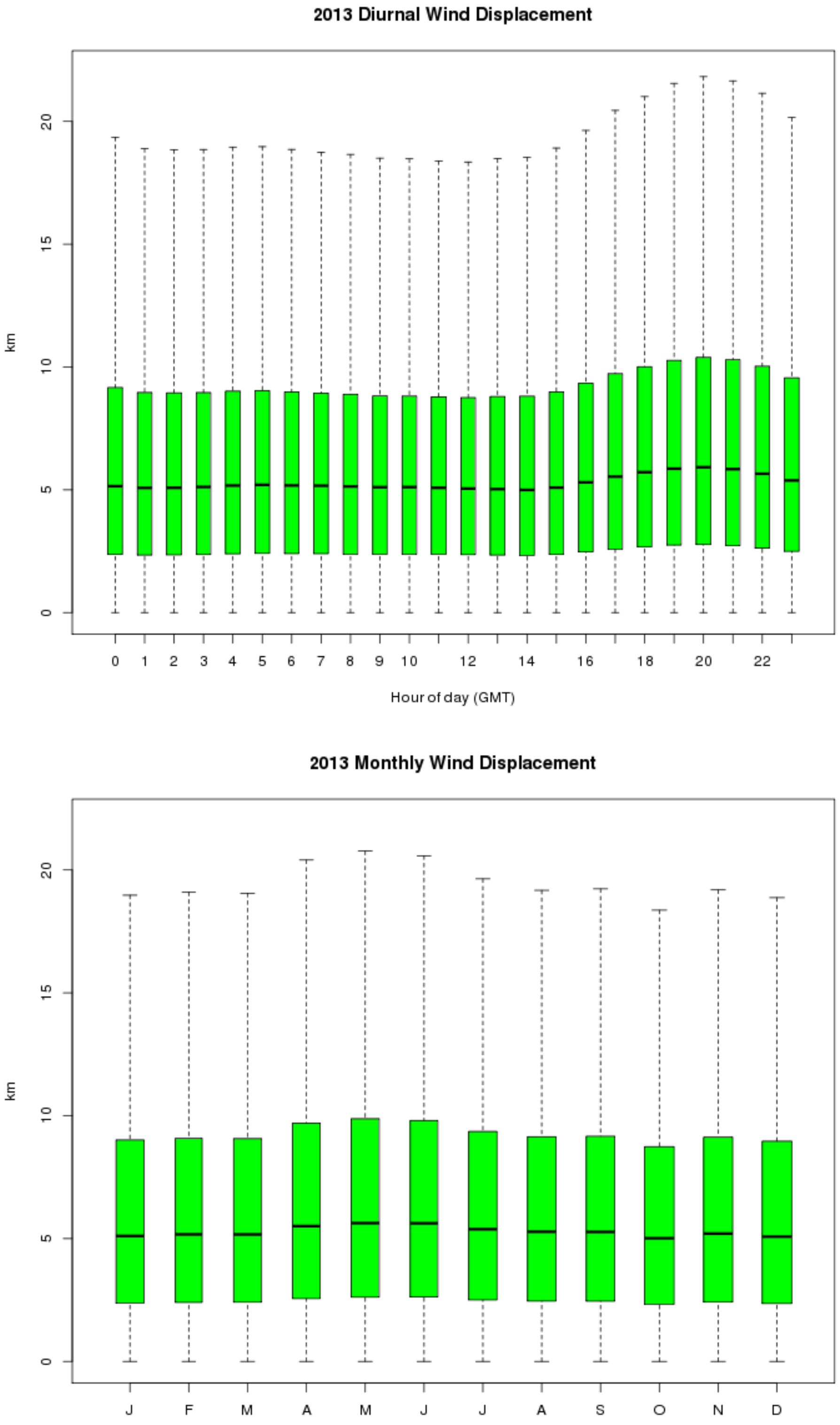

Figure 4-33. Distribution of wind displacement averaged for all stations within the 12-km CONUS domain for each hour (top) and month (bottom).

Model Evaluation Results for Monthly Precipitation

The PRISM-accumulated monthly precipitation was compared to the WRF 12-km domain precipitation amounts for each month of 2013, January through December. The PRISM precipitation was aggregated to the WRF 12-km domain to take a difference in the monthly precipitation totals for each month (WRF minus PRISM). Below is a discussion of the precipitation for each month. Note that PRISM data does not include regions outside of the U.S.

January Precipitation 2013

Figure 4-34 compares the accumulated monthly precipitation from PRISM (top), WRF (middle), and WRF minus PRISM (bottom) for January 2013 within the CONUS. The WRF spatial pattern of monthly precipitation in January 2013 matches the PRISM patterns very well, in areas such as placement of higher rainfall totals for the Pacific Northwest and for areas within the eastern half of the CONUS. Some of the states within the eastern half of the CONUS recorded January precipitation totals ranking among their ten wettest on record including Louisiana, Mississippi, Tennessee, Michigan, and Virginia.[20] WRF simulates larger precipitation totals for each of these states. WRF also reproduces the precipitation gradient within the southeast U.S. with drier conditions found over Florida, eastern Georgia, and the Carolinas, which were all expiring drought conditions during January.

In examining WRF minus PRISM, the largest differences occur for the heavier observed precipitation totals within the southeast U.S., especially Louisiana where rainfall is underestimated by as much as four inches. On the other hand, the precipitation totals are overestimated around the Great Lakes, suggesting that the modeled lake effect may be too strong. Additionally, the higher terrain locations within the Cascades are overestimated within WRF. It is important to note that station density is an important component of the observed precipitation PRISM product; therefore, some caution about the overestimation over the higher terrain, where station density is smaller, must be applied.

February Precipitation 2013

Figure 4-35 compares the accumulated monthly precipitation from PRISM (top), WRF (middle), and WRF minus PRISM (bottom) for February 2013 within the CONUS. The WRF spatial pattern of monthly precipitation in February 2013 matches the PRISM patterns very well. For instance, WRF simulates higher precipitation totals within the southeast U.S extending from Louisiana to South Carolina. South Carolina and Alabama recorded their top 10 wettest Februaries on record and Georgia the wettest February on record.[21] Additionally, heavier precipitation totals are well simulated for coastal New England where precipitation totals were recorded among the top 10 wettest for Massachusetts and Rhode Island. For the western half of the CONUS, precipitation totals are small, excluding the Cascades. Most of the West Coast was abnormally dry during February with California having its 5th driest February on record.

In examining WRF minus PRISM, large differences occur in similar locations to the month of January. Overestimation of rainfall occurs for the higher terrain locations within the Cascades and around the

---

[20] https://www.ncdc.noaa.gov/sotc/national/201301
[21] https://www.ncdc.noaa.gov/sotc/national/201302

Great Lakes. WRF underestimates the rainfall totals within the southeast U.S., as much as 3-4 inches for large area from Louisiana to South Carolina.

March Precipitation 2013

Figure 4-36 compares the accumulated monthly precipitation from PRISM (top), WRF (middle), and WRF minus PRISM (bottom) for March 2013 within the CONUS. WRF simulates the placement of higher rainfall totals within the Northwest including the Cascades and Sierra Nevada and an area from northern Mississippi, Alabama, and Georgia through Tennessee into Kentucky. Overall, most of the CONUS experienced near to below average precipitation.[22] For instance, Louisiana had its fourth driest March on record and is well simulated by WRF despite heavier precipitation totals to the northeast.

In examining WRF minus PRISM, WRF overestimates the precipitation amounts for a majority of the CONUS. An exception is for some locations within the southeast U.S. and coastal locations along the West Coast.

April Precipitation 2013

In April 2013, WRF simulates the correct placement of the largest precipitation totals for locations such as the Cascades and a large area from Louisiana/Mississippi northward into Wisconsin and Michigan, Figure 4-37. Iowa and Michigan recorded their wettest April on record. Additionally, Tennessee, Illinois, Indiana, and Wisconsin each experienced one of their top 10 wettest Aprils on record.[23]

In examining WRF minus PRISM, WRF generally overestimates rainfall for most of the CONUS including the Cascades, Rockies, Plains, Midwest, and northeast U.S. However, rainfall totals for locations within the southeast U.S. continue to be underestimated as in prior months.

May Precipitation 2013

The placement of maximum precipitation in May 2013 was well simulated by WRF over the northern Plains, Midwest, and northeast U.S. from New York to Maine, as shown in Figure 4-38. WRF also simulated the heavier precipitation amounts along the Cascades. In particular, WRF simulates some the location of some of the heaviest rainfall totals, including Iowa, Montana, and North Dakota. For instance, Iowa recorded its wettest April on record while Montana and North Dakota both recorded their top 10 wettest April on record during 2013.[24]

In examining WRF minus PRISM, WRF underestimates precipitation from Louisiana/Mississippi northward into the Midwest. However, the underestimation is more consistent for locations further south. Precipitation totals are also underestimated for coastal New England. On the other hand, the precipitation totals are overestimated, especially for Montana and some states within the southeast U.S. including Florida, Georgia, and the Carolinas. This is the first instance in 2013 where the southeast U.S. experiences a notable wet bias.

---

[22] https://www.ncdc.noaa.gov/sotc/national/201303
[23] https://www.ncdc.noaa.gov/sotc/national/201304
[24] https://www.ncdc.noaa.gov/sotc/national/201305

June Precipitation 2013

In June 2013, WRF simulates the heavy precipitation totals observed for much of the eastern half of the CONUS (Mississippi north to Indiana and areas east), shown in Figure 4-39. Eighteen states from Georgia to Maine recorded precipitation totals that ranked among their 10 wettest on record.[25] On the other hand, much of the western US experienced record dry conditions including Arizona, Colorado, and Wyoming, which had one of their 10 driest Junes on record. WRF reproduces the anomalously dry conditions for most of the western U.S.

In examining WRF minus PRISM, WRF overestimates the precipitation by more than two inches for most of the East Coast. WRF also underestimates precipitation totals in some regions, particularly for large portions of both the Plains and Midwest.

July Precipitation 2013

Figure 4-40 compares the accumulated monthly precipitation from PRISM (top), WRF (middle), and WRF minus PRISM (bottom) for July 2013 within the CONUS. The precipitation associated with the Southwest monsoon is captured in WRF; however, WRF overestimates the amount of rainfall throughout a good portion of the southwest U.S. The difference between WRF and PRISM precipitation shows rainfall totals in WRF are overestimated by three inches or more in July. The monsoonal flow contributed to above average precipitation within the Southwest, with Arizona and California precipitation totals ranking among their ten wettest on record. Additionally, anomalously wet conditions were recorded for the Eastern half of the CONUS, with thirteen states having one of their ten wettest July’s on record.[26] In particular, the southeast U.S. experienced the largest rainfall totals and the location of the largest rainfall totals is reproduced by WRF. However, WRF overestimates the rainfall totals for much of the southeast U.S., with an exception for western North Carolina and southern Florida. The anomalously dry conditions within the Northwest, such those as over Oregon, are reproduced within WRF.

August Precipitation 2013

Like July, WRF estimates higher and more widespread precipitation within the Southwest in August 2013 than PRISM, as shown in Figure 4-41. Again, the results illustrate an issue with WRF simulating the North American Monsoon. Heavy rainfall was also observed within the southern Plains (Oklahoma, Kansas) and portions of the southeast U.S. (Florida, Alabama, Georgia, and South Carolina). Kansas and Georgia recorded rainfall totals that rank among the ten wettest on record.[27] WRF simulates larger precipitation totals for these regions, but the rainfall totals are underestimated. There are some other notable problems with the simulated precipitation totals when compared with PRISM. WRF simulates precipitation that isn’t observed from Tennessee into Kentucky and West Virginia. On the other hand, WRF fails to simulate the observed precipitation around the Great Lakes.

---

[25] https://www.ncdc.noaa.gov/sotc/national/201306
[26] https://www.ncdc.noaa.gov/sotc/national/201307
[27] https://www.ncdc.noaa.gov/sotc/national/201308

September Precipitation 2013

In September 2013, large rainfall totals were observed for much of the western half of the CONUS, including the Northwest, Rockies, and Southwest, as shown in Figure 4-42. Colorado, Oregon, and Washington each had their wettest September on record. Seven additional states from New Mexico to North Dakota recorded precipitation totals that rank among the ten wettest observed. [28] WRF simulates the placement of the largest rainfall totals for the western half of the CONUS but generally overestimated the rainfall. This overestimation included the southwest U.S., illustrating a systematic issue with simulating rainfall totals associated with the North American Monsoon. An exception is the overestimation of precipitation for coastal Oregon and Washington. Large rainfall totals were also observed along the coast of states within the Gulf Coast, Mississippi to Tennessee and Kentucky, and northern New England. The precipitation totals along the Gulf Coast and the areas from Mississippi to Kentucky are underestimated in WRF. However, the precipitation totals are overestimated in northern New England, especially Maine. WRF also reproduces the anomalously dry conditions for large portions of the Great Lakes, Mid-Atlantic, and south Atlantic Coast.

October Precipitation 2013

In October 2013, the heaviest rainfall totals were observed for portions of the northern Plains, around the Great Lakes, and from eastern Texas/Oklahoma/Kansas to Louisiana/Arkansas, shown in Figure 4-43. Much of the central U.S. was wetter than average, especially for the northern Plains where Nebraska, North Dakota, South Dakota, and Wyoming each had one of their top ten wettest Octobers. [29] WRF does an excellent job at simulating the placement and rainfall amounts for areas within the northern Plains. However, WRF underestimates the precipitation for the areas from eastern Texas to Arkansas and overestimates the precipitation totals around the Great Lakes. WRF also fails to simulate the observed precipitation within the Mid-Atlantic.

November Precipitation 2013

In November 2013, the heaviest rainfall totals were observed for portions of the Northwest, Southwest, Great Lakes, and southeast/northeast U.S., seen in Figure 4-44. Above average precipitation was recorded for each of these regions except the Northwest. For instance, Michigan had its seventh wettest November on record.[30] WRF simulates the placement of the heaviest rainfall but the totals are overestimated for much of the Northwest/Southwest and underestimated for the Great Lakes and southeast/northeast U.S. There is an exception to the underestimation of rainfall for some portions of the southeast U.S., such as for eastern North Carolina and southern Florida where rainfall totals are overestimated by WRF. WRF also reproduces the dry conditions throughout much of the northern Rockies and Plains are reproduced by WRF.

---

[28] https://www.ncdc.noaa.gov/sotc/national/201309
[29] https://www.ncdc.noaa.gov/sotc/national/201310
[30] https://www.ncdc.noaa.gov/sotc/national/201311

December Precipitation 2013

In December 2013, the largest precipitation totals occurred within parts of the Pacific Northwest into the northern Rockies and most of the eastern half of the CONUS (east of Texas), as shown in Figure 4-45. States including Alabama, Georgia, North Dakota, Ohio, Virginia, and West Virginia, each had December precipitation totals that ranked among the ten wettest on record.[31] WRF simulates the placement of the largest rainfall totals. However, the rainfall totals are underestimated within most of the southeast U.S. (upwards of four inches) and overestimated (by 1-2 inches) for much of the northern half of the CONUS including portions of the northern Rockies, Midwest, and Northeast. WRF reproduces the drier conditions for much of the central U.S. from Texas to Nebraska and locations along the West Coast, such as California that had its second driest December on record.

---

[31] https://www.ncdc.noaa.gov/sotc/national/201312

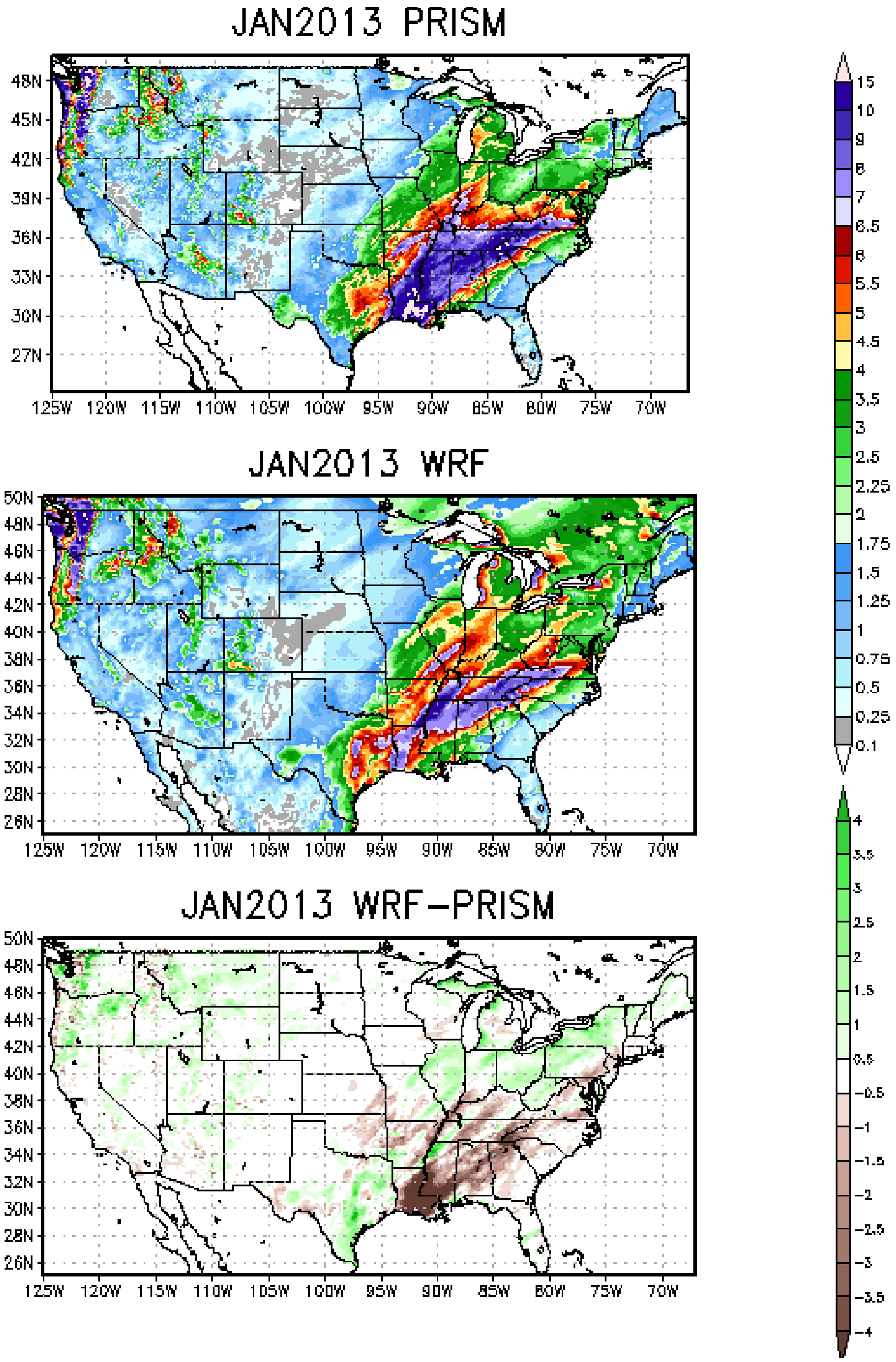
JAN2013 PRISM

JAN2013 WRF

JAN2013 WRF–PRISM

Figure 4-34. Comparison of monthly total precipitation (inches) from PRISM (top) and WRF (middle) and WRF minus PRISM (bottom) for the 12-km CONUS domain in January 2013.

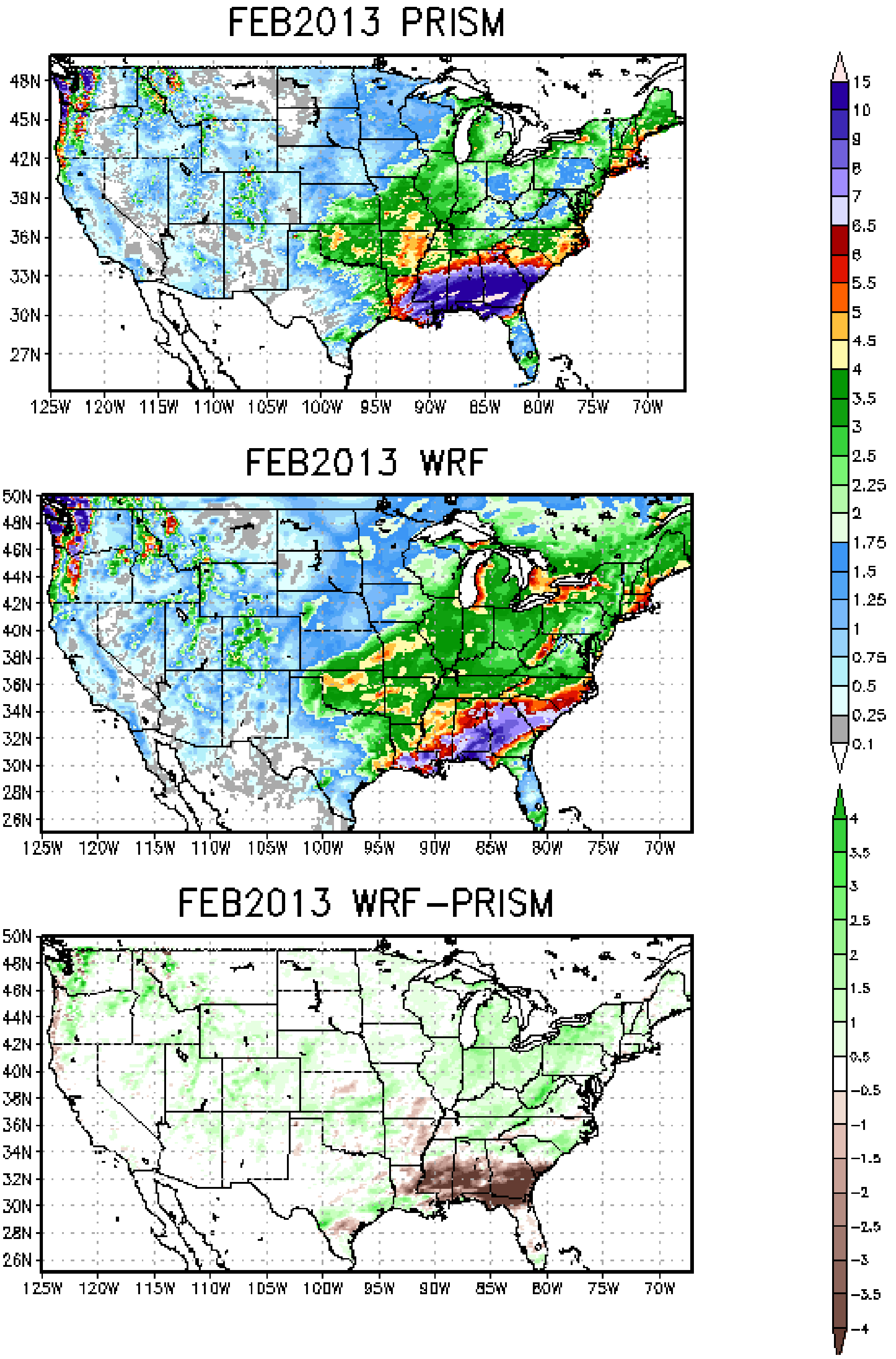

Figure 4-35. Comparison of monthly total precipitation (inches) from PRISM (top) and WRF (middle) and WRF minus PRISM (bottom) for the 12-km CONUS domain in February 2013.

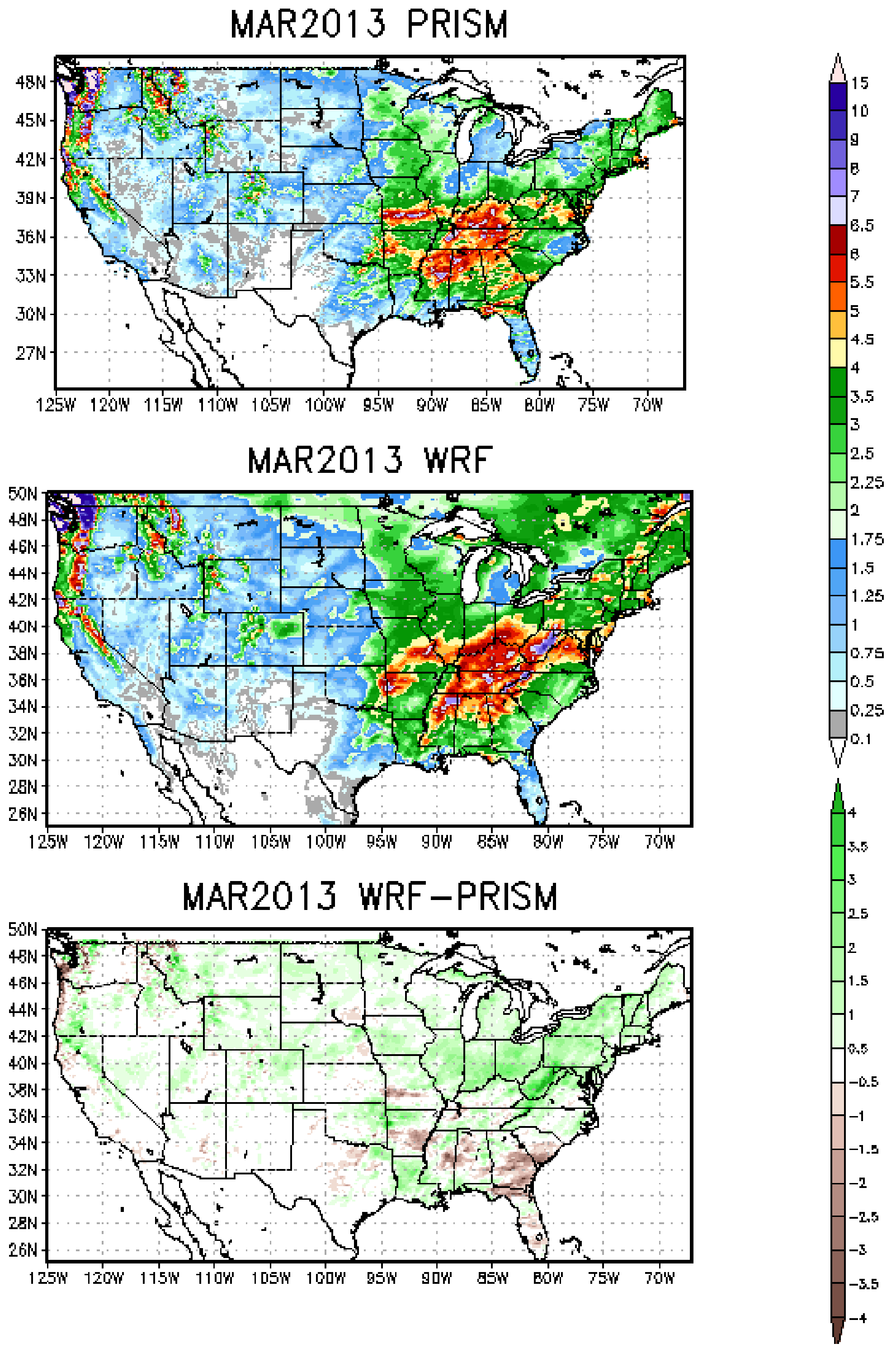

Figure 4-36. Comparison of monthly total precipitation (inches) from PRISM (top) and WRF (middle) and WRF minus PRISM (bottom) for the 12-km CONUS domain in March 2013.

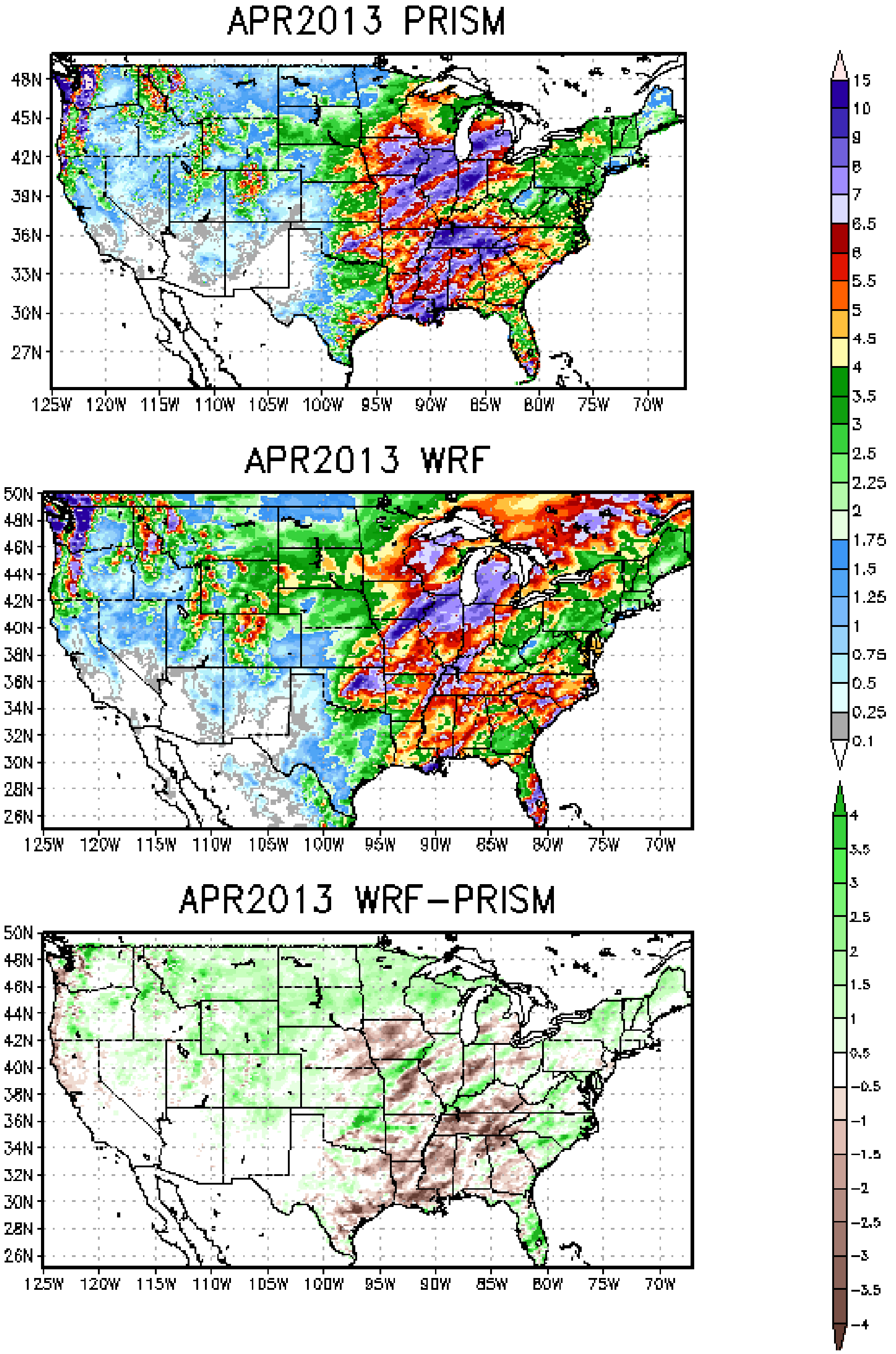

Figure 4-37. Comparison of monthly total precipitation (inches) from PRISM (top) and WRF (middle) and WRF minus PRISM (bottom) for the 12-km CONUS domain in April 2013.

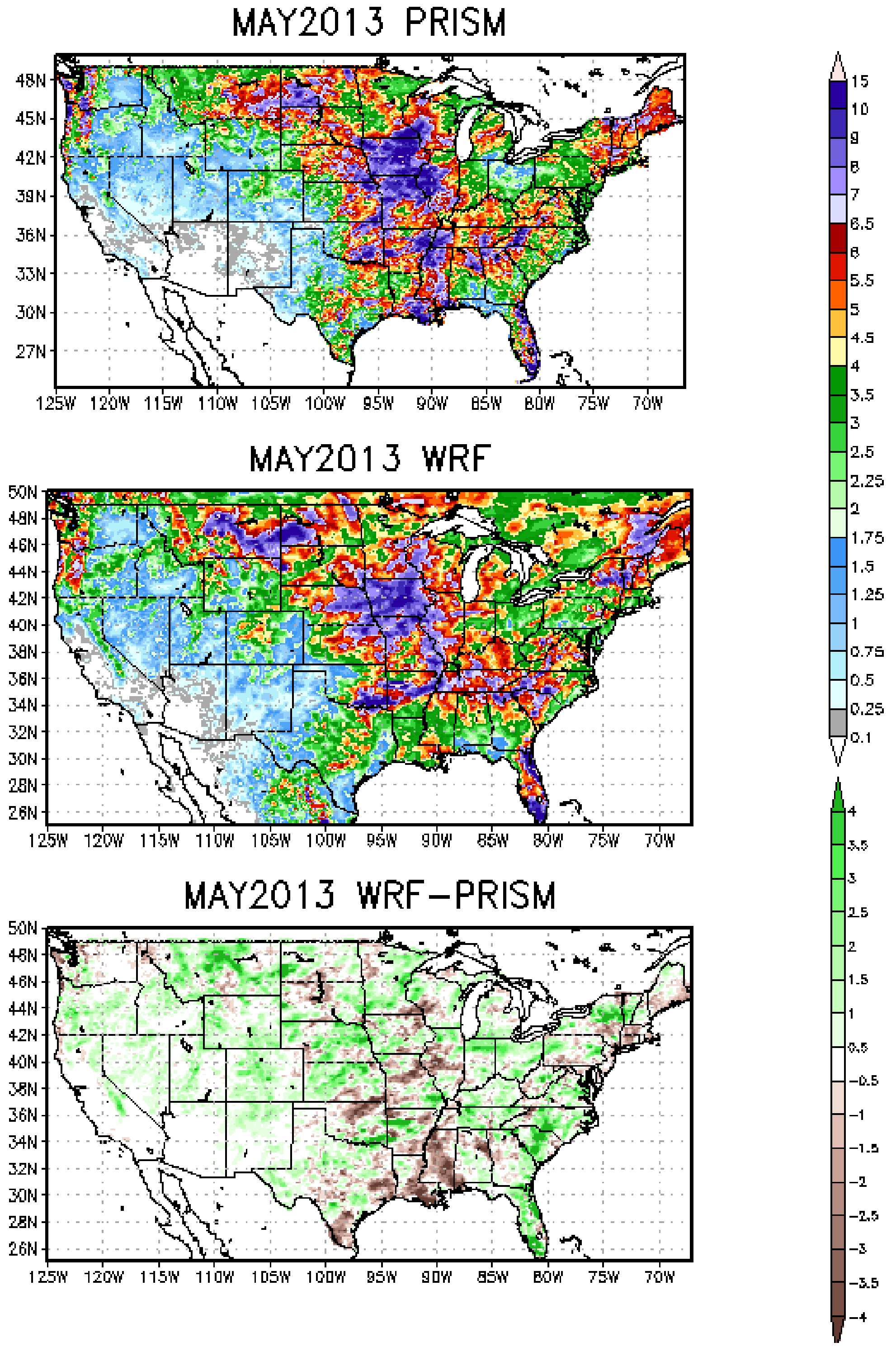

Figure 4-38. Comparison of monthly total precipitation (inches) from PRISM (top) and WRF (middle) and WRF minus PRISM (bottom) for the 12-km CONUS domain in May 2013.

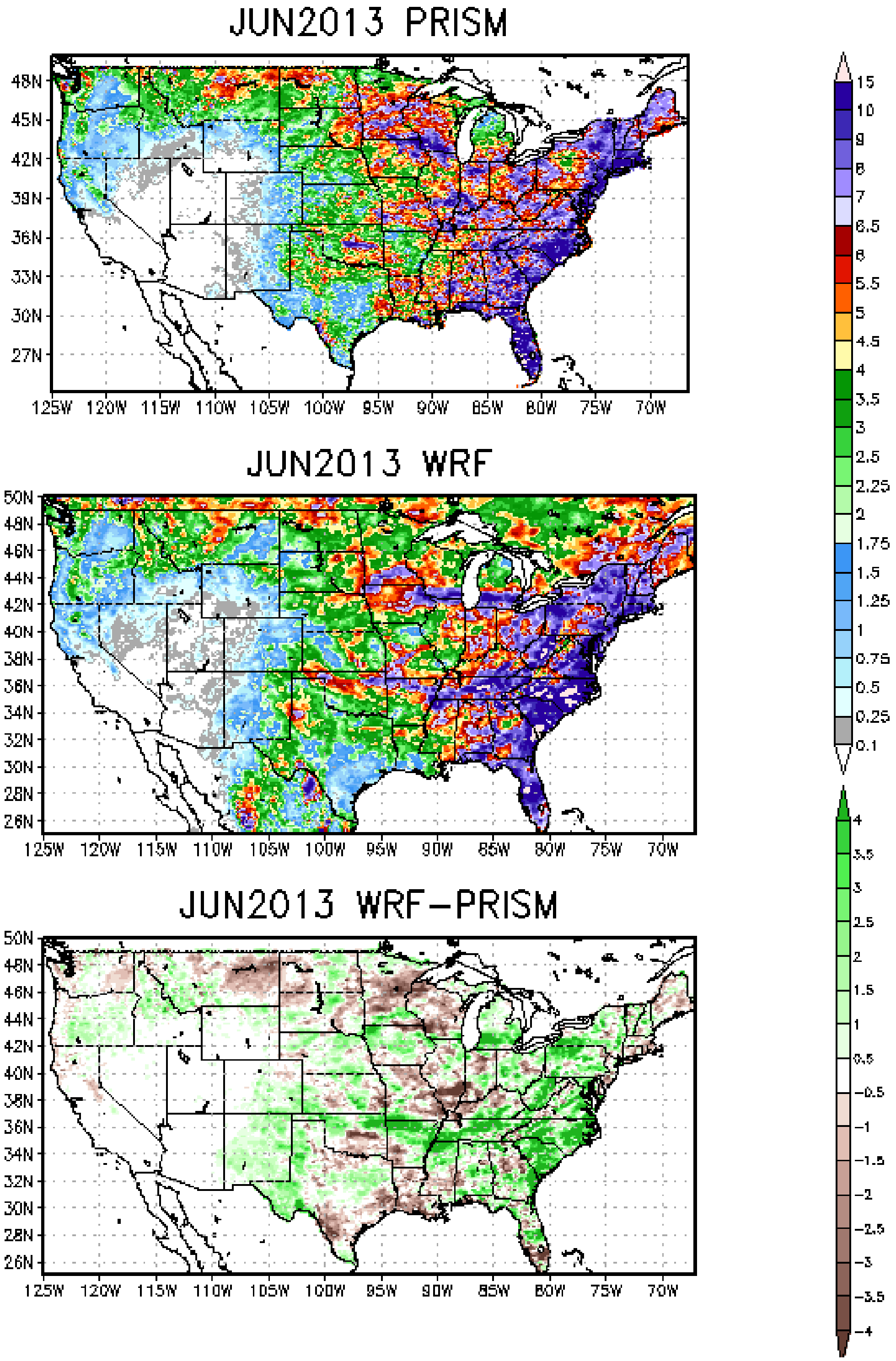

Figure 4-39. Comparison of monthly total precipitation (inches) from PRISM (top) and WRF (middle) and WRF minus PRISM (bottom) for the 12-km CONUS domain in June 2013.

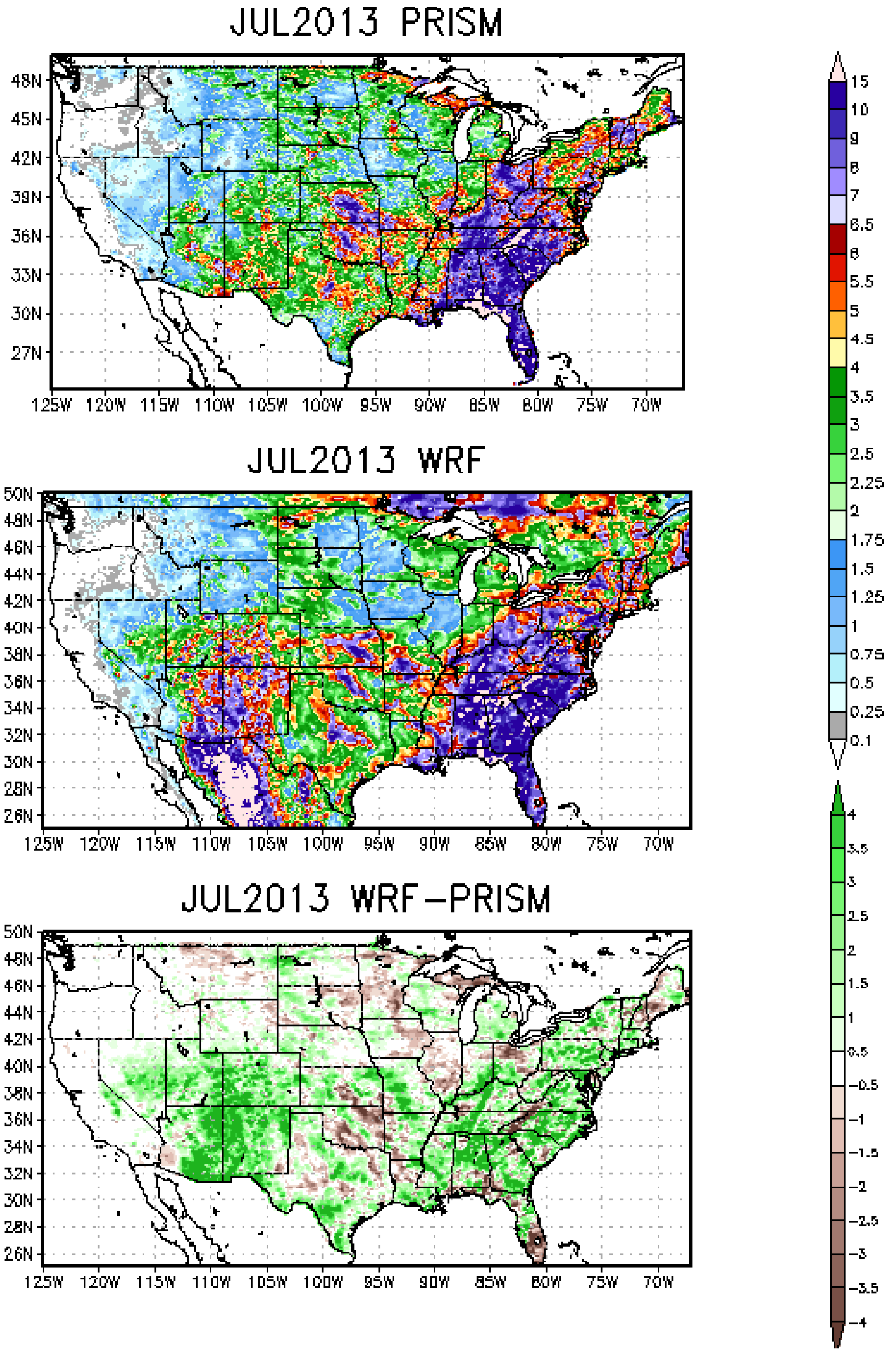
JUL2013 PRISM

JUL2013 WRF

JUL2013 WRF−PRISM

Figure 4-40. Comparison of monthly total precipitation (inches) from PRISM (top) and WRF (middle) and WRF minus PRISM (bottom) for the 12-km CONUS domain in July 2013.

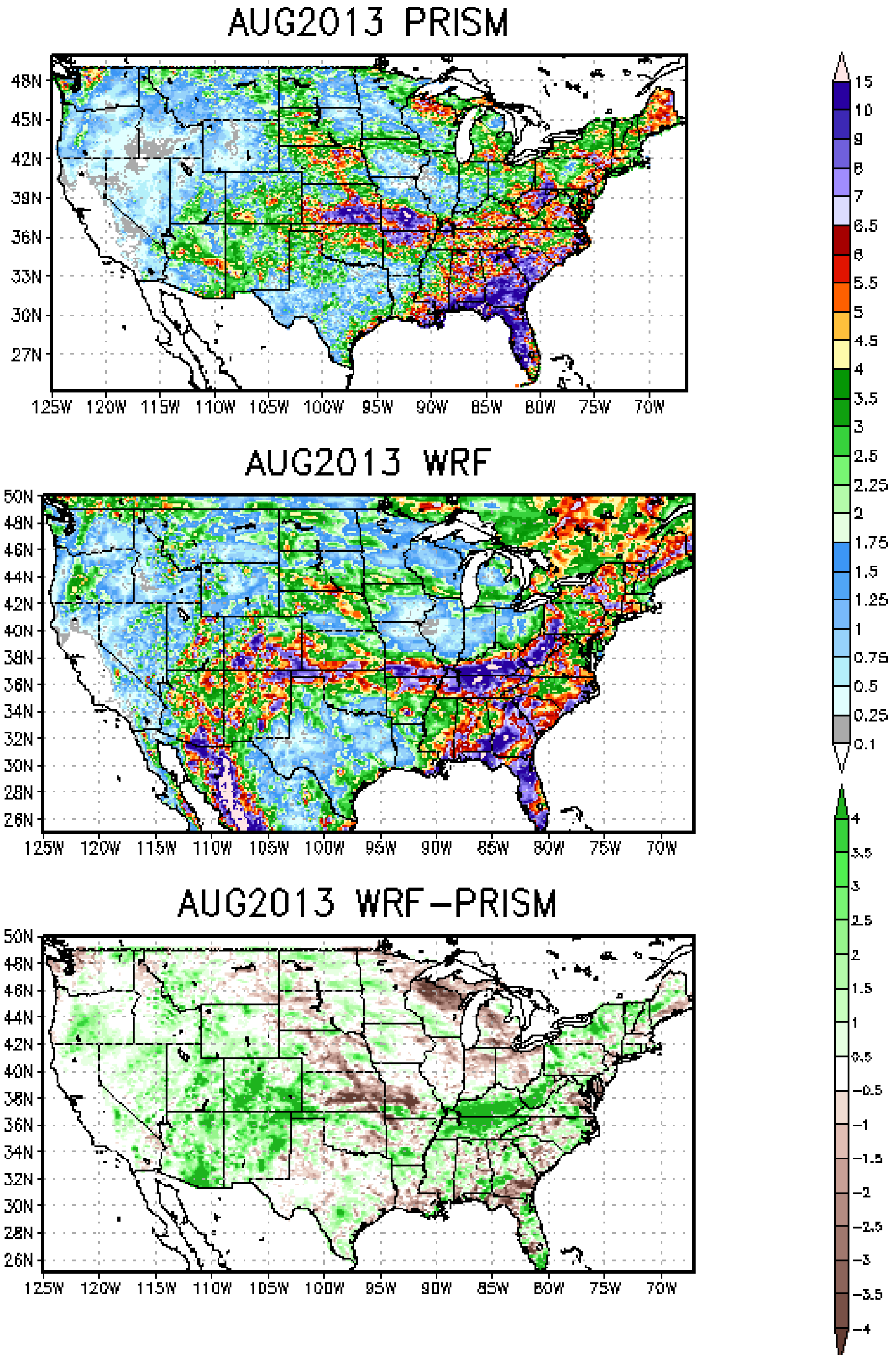

Figure 4-41. Comparison of monthly total precipitation (inches) from PRISM (top) and WRF (middle) and WRF minus PRISM (bottom) for the 12-km CONUS domain in August 2013.

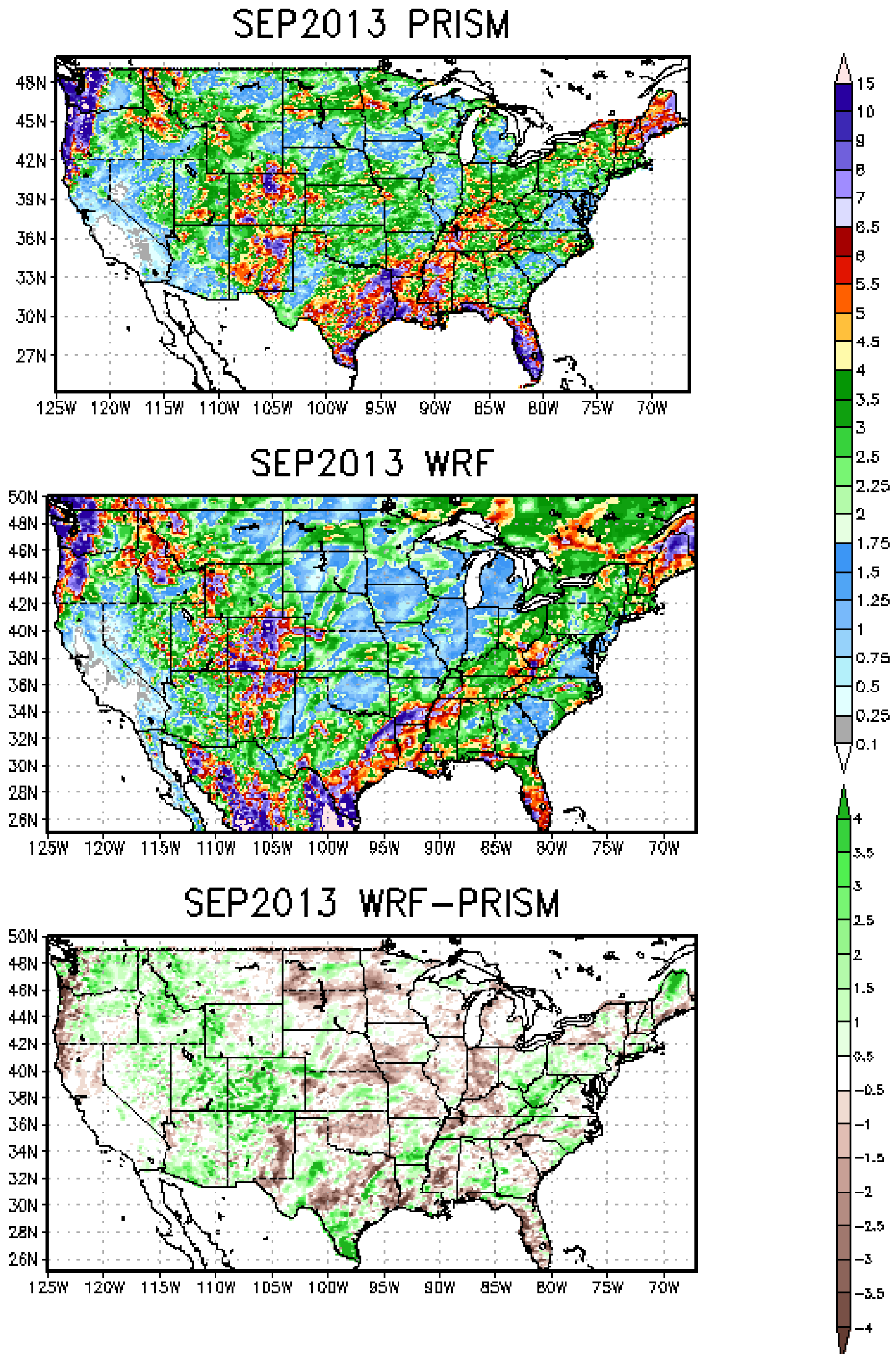

Figure 4-42. Comparison of monthly total precipitation (inches) from PRISM (top) and WRF (middle) and WRF minus PRISM (bottom) for the 12-km CONUS domain in September 2013.

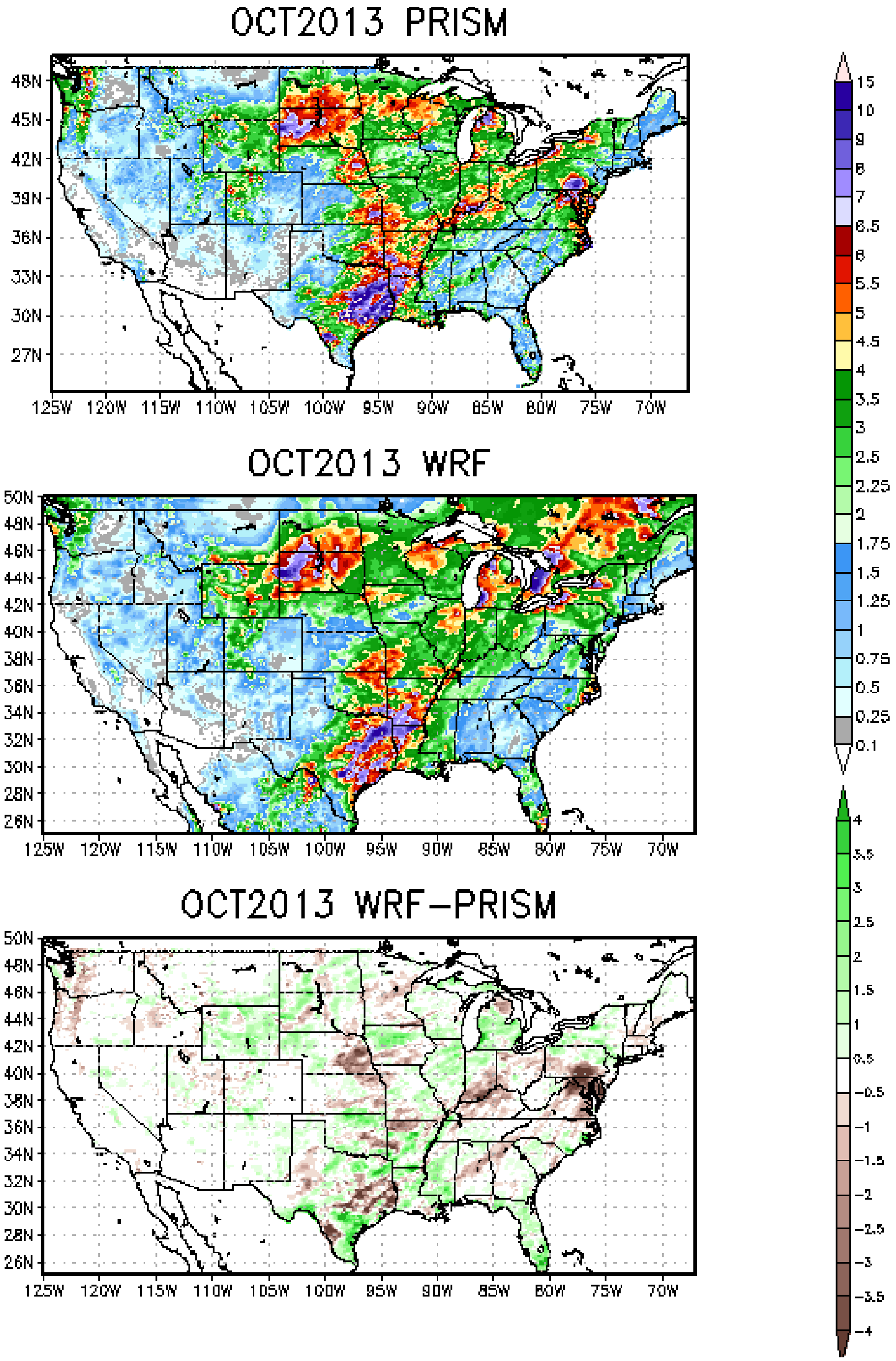

Figure 4-43. Comparison of monthly total precipitation (inches) from PRISM (top) and WRF (middle) and WRF minus PRISM (bottom) for the 12-km CONUS domain in October 2013.

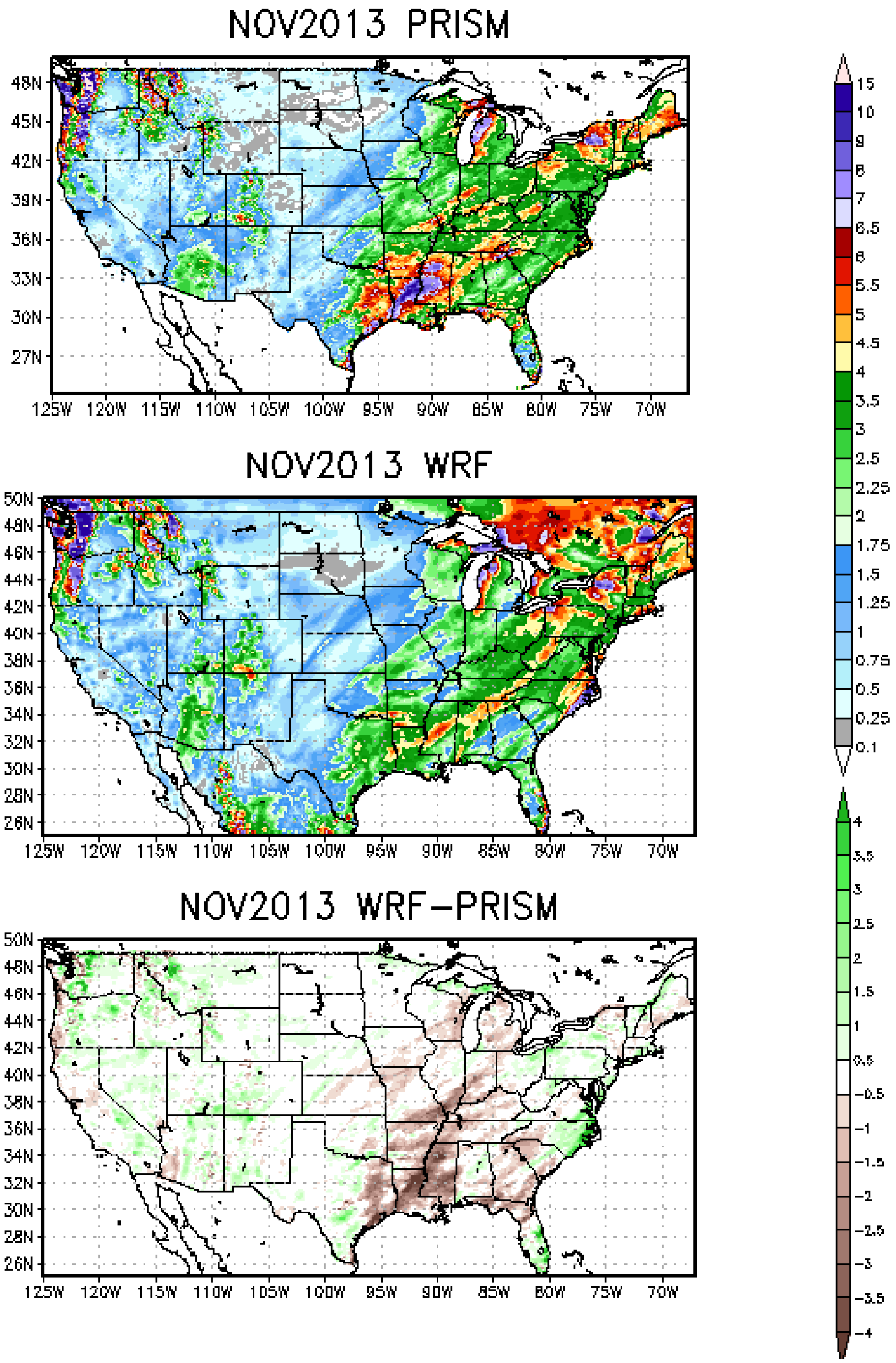

Figure 4-44. Comparison of monthly total precipitation (inches) from PRISM (top) and WRF (middle) and WRF minus PRISM (bottom) for the 12-km CONUS domain in November 2013.

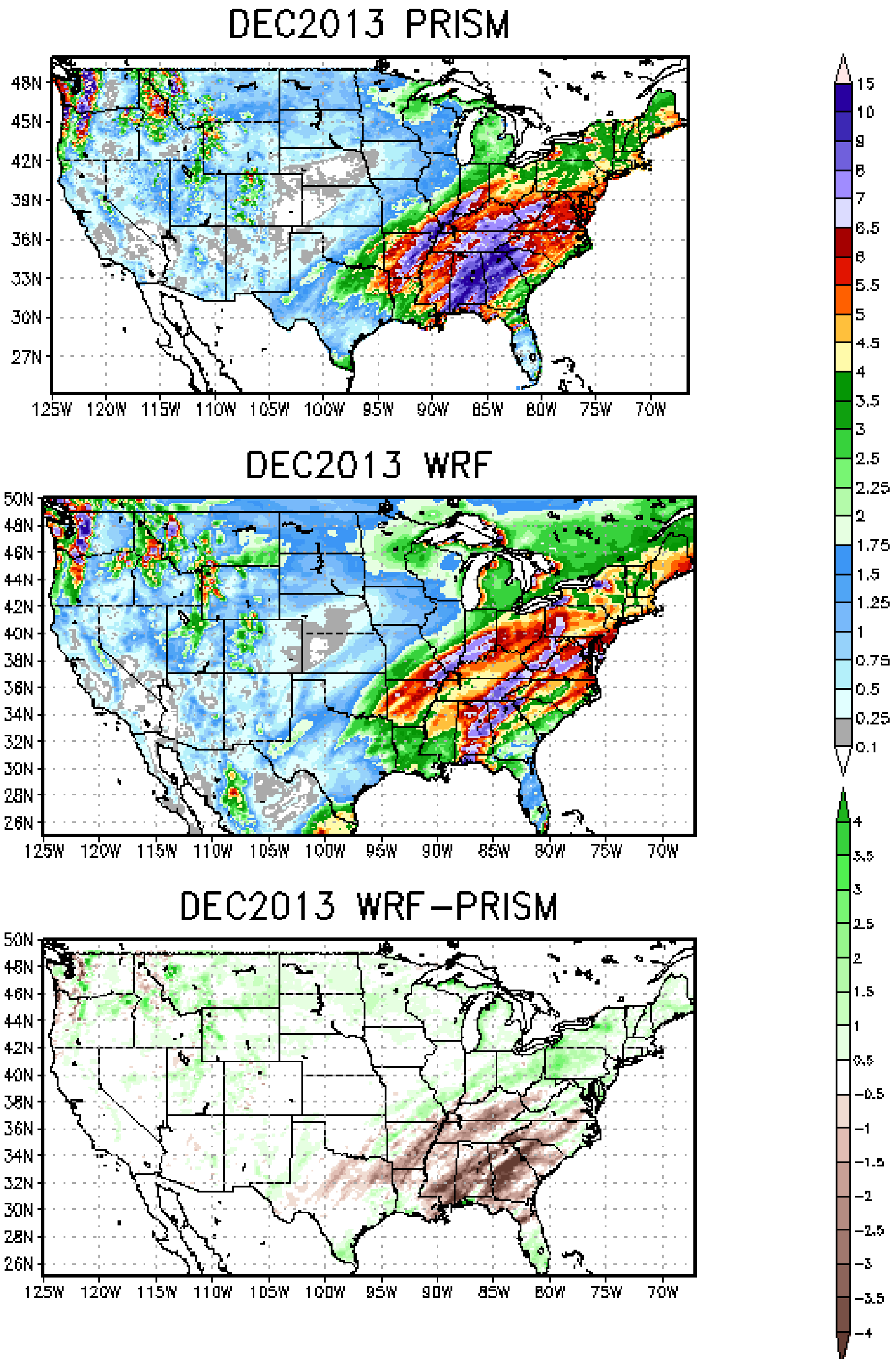

DEC2013 PRISM

DEC2013 WRF

DEC2013 WRF−PRISM

Figure 4-45. Comparison of monthly total precipitation (inches) from PRISM (top) and WRF (middle) and WRF minus PRISM (bottom) for the 12-km CONUS domain in December 2013.

Model Evaluation Results for Solar Radiation

Estimates of modeled biogenic emissions for estimating isoprene emissions are sensitive to the photosynthetically activated radiation, which is a fraction of the shortwave downward radiation.[32] Regional ozone chemistry and the formation of secondary organic aerosols are impacted by changes in the isoprene emissions. Below, we illustrate the model performance of shortwave downward radiation, which has important implications for regional air quality and provides an indirect assessment of how well the model captures cloud formation during daylight hours.

Figure 4-46 is a comparison of the shortwave downward radiation estimates compared to the surface based measurements at SURFRAD and ISIS network monitors averaged for all sites within the CONUS. The top panel is a comparison of the hourly estimates. The model underestimates the shortwave downward radiation during the early to late morning hours and overestimates the amount during the late afternoon into early evening. The over prediction during the afternoon is larger (upwards +100 W/m2) than the under prediction during the morning hours (-50 W/m2). These results hint at problems simulating the relative cloud cover amount during the morning and afternoon. In the bottom panel is a comparison of the monthly radiation estimates. During the late fall through winter into the early spring, the shortwave radiation bias is small. The bias grows by late spring into the summer with a peak in the over prediction of shortwave radiation during the months June and July. The over prediction is generally less than 100 W/m2. The median bias is close to zero for all months.

---

[32] Carlton, A.G., Baker. K.R., 2011. Photochemical Modeling of the Ozark Isoprene Volcano: MEGAN, BEIS, and Their Impacts on Air Quality Predictions. Environmental Science and Technology 45, 4438-4445.

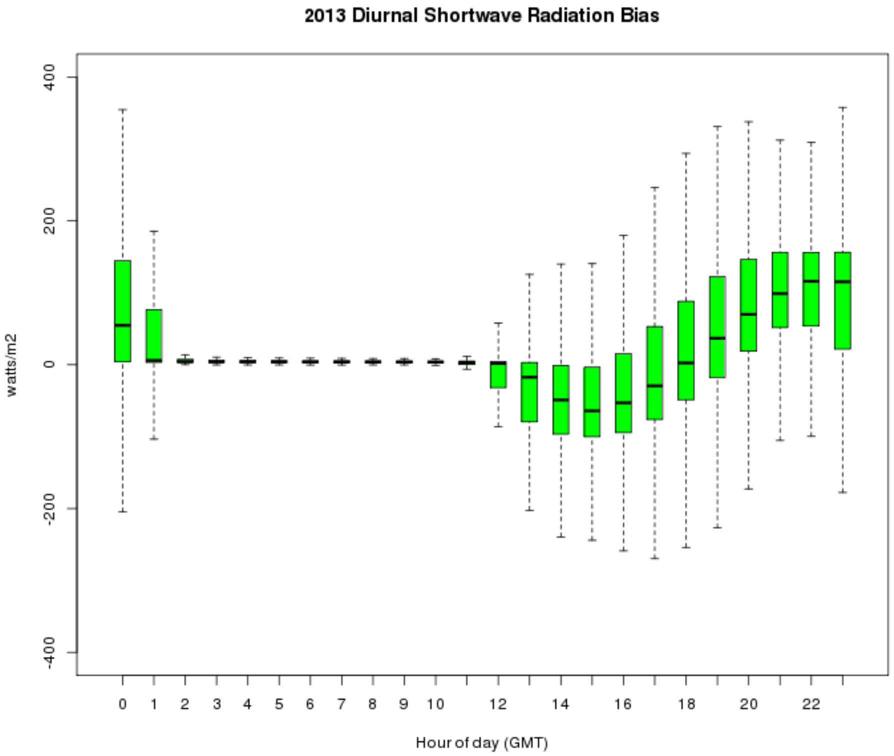

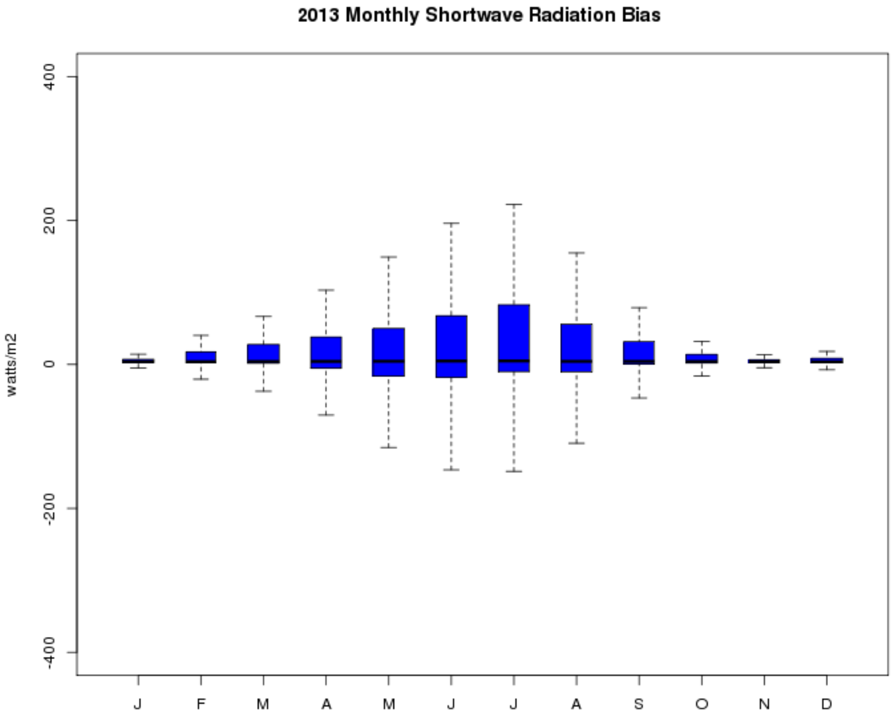

Figure 4-46. Model bias of shortwave radiation averaged over all SURFRAD and ISIS network monitors within the 12-km CONUS domain for each hour (top) and month (bottom).

5.0 ADDITIONAL RESULTS

An electronic docket is also included with this report that contains several other plots illustrating the 2013 WRF model performance.

Link to additional model evaluation plots for 2013 can be found at:
https://drive.google.com/folderview?id=0BxAQ24gAklsMSVkyNGZYNkVOMXc&usp=sharing